理學博士學位論文

*Dictyostelium discoideum*의 ABP34의 구조와 기능

Structural and functional characteristics of ABP34 in *Dictyostelium discoideum*

2015年 8月

서울大學校 大學院

生命科學部

金　智　惠

Dictyostelium discoideum 의 ABP34의 구조와 기능

指導敎授 姜 思 旭

이 論文을 理學博士學位論文으로 提出함

2015年 6月

서울大學校 大學院

生命科學部

金 智 惠

金智惠의 理學博士學位論文을 認准함

2015年 6月

委 員 長 이 광호

副委員長 姜 思 旭

委 員 허 원기

委 員 최 희정

委 員 임 형순

Structural and functional characteristics of ABP34 in *Dictyostelium discoideum*

by

Ji-Hye Kim

Advisor:

Professor Sa-Ouk Kang, Ph. D.

A Thesis Submitted in Partial Fulfillment

of the Requirements for

the Degree of Doctor of Philosophy

August 2015

School of Biological Sciences

Graduate School

Seoul National University

ABSTRACT

ABP34, 34 kDa actin binding protein of *Dictyostelium discoideum* is one of the calcium regulated actin binding protein that crosslinks actin filaments into bundles in the presence of low concentration of calcium. The ABP34 protein contributes to formation of actin filament bundles in filopodia of *Dictyostelium* amoebas. To investigate the biological roles of F-actin bundling protein in *D. discoideum*, mutant strains that underexpress ABP34 were generated by RNA interference mutant (RNAi). The ABP34 RNAi cells grew more slowly in axenic medium and showed decrease cell size. During developmental, they showed fast rate culmination and final fruiting body was also small size. ABP34 was also shown by fluorescence microscopy to associate with the actin cytoskeleton of cells during growth and development. Under dark condition, they showed short period slugger migration stage and fast formed fruiting body.

To identify actin binding proteins from *D. discoideum*, ABP34 recombinant protein was overexpressed in *Escherichia coli* and purified and crystallized. Gel filtration of ABP34 protein indicates monomeric structure of the native protein and molecular weight of ABP34 was estimated to be 32,836 Da. The crystal structure of the ABP34 from *D. discoideum* was solved by Ca^{2+}/S-SAD phasing and refined at 1.89 Å resolutions. F-actin binding and bundling activities are confirmed by co-sedimentation assay and transmission electron microscopy. The electron microscopy data provides direct evidence for binding activity to F-actin. The overall structure of ABP34 adopts a two-domain structure with EF-hand containing N-domain and actin-binding C-domain. The EF-hand is occupied by calcium ion with pentagonal bipyramidal coordination likely with the canonical EF-hand. C-domain structure resembles

three-helical bundle which is well superposed into the rod-shaped helical structures of several cytoskeletal proteins. The residues 216–244 in C-domain is a part of the most strong actin binding sites (193–254) and has conserved sequences with the actin binding region of α-actinin and ABP120. The crystal structure of the C-terminal helix reveals a conserved surface exposed hydrophobic residues surrounded by positive charged group that is correspond to actin binding surface. Thus, C-terminal structure is supposed to be crucial for its actin binding. F-actin binding model suggests that ABP34 binds to the side of actin and the residues 216–244 fit into a pocket between actin subdomains 1 and subdomain 2 by hydrophobic interactions. These studies provide insights into the calcium coordination in the EF-hand and F-actin binding site in C-domain of ABP34 which are associated through inter-domain interactions. The structure of ABP34 is a novel type of actin bundling protein in cytoskeletal protein structures, which could provide valuable structural insights into the efficient actin bundling of actin binding domain. These results suggerst that *Dictyostelium* actin bundling protein ABP34 may be important for growth and developmental process, especially migrating slug to fruiting body by regulating actin cytoskeleton.

Key words: *Dictyostelium discoideum*, ABP34, actin bundling protein, RNAi, X-ray crystal structure, EF-hand

CONTENTS

LIST OF FIGURES

LIST OF TABLES

LIST OF ABBREVIATIONS

ABP	actin binding protein
ATP	adenosine triphosphate
BCIP	5-bromo-4-chloro-3-indoyl phosphate
bp	base pair
DAPI	4′,6-diamidino-2-phenylindole
DEAE	diethylaminoethanol
DEPC	diethypyrocarbonate
DTT	dithiothreitol
EDTA	ethylenediaminetetraacetic acid
EGTA	ethylene glycol tetraacetic acid
FPLC	fast protein liquid chromatography
GFP	green fluorescent protein
HEPES	4-(2-hydroxyethyl)-1-piperazineethanesulfonic acid
IPTG	isopropyl-β-D-thiogalactopyranoside
kDa	kilodalton
LB	Luria-Bertani
NBT	nitro blue tetrazolium
MW	molecular weight
PAGE	polyacrylamide gel electrophoresis
PCR	polymerase chain reaction
PEG	polyethylene glycol
PIPES	1,4-piperazinediethanesulfonic acid
PMSF	phenylmethylsulfonyl fluoride
RNA	ribonucleic acid
rpm	revolutions per minute
SAD	single-wavelength anomalous dispersion
SDS	sodium dodecyl sulfate
TRITC	tetramethylrhodamine-5-(and 6)-isothiocyanate

I. INTRODUCTION

1. Actin cytoskeleton

1.1. Actin and actin filament

Actin filaments, also referred to as F-actin, are composed of highly conserved globular protein molecules found in all eukaryotes (Pollard and Cooper, 1986). The 42 kDa actin monomer (G-actin) has a bound nucleotide (ATP or ADP) and can be polymerized into double-helical actin filaments (F-actin). Upon polymerization of ATP-G-actin, ATP-F-actin filaments are formed transiently and in this state the bound ATP is hydrolyzed rapidly and irreversibly to yield ADP-P_i-F-actin, and eventually ADP-F-actin.

Most actins consist of 375 amino acid residues. Actin molecule consists of two domains, called large and small, although they are similar in size. These two domains can be subdivided further into two subdomains each, the small domain being composed of subdomains 1 and 2, and the large domain of subdomains 3 and 4. The four domains are held together and stabilized mainly by salt bridges and hydrogen bonds to the phosphate groups of the bound nucleotide and to its associated divalent cation localized in the center of the molecule. Because subdomain 2 has significantly less mass than the other three subdomains, the actin molecule appears distinctly polar in the direction of the pronounced cleft separating its two domains. Other structurally prominent features include the 'DNase I-binding loop', the 'hyrophobic loop', the α-helix 222-233 in subdomain 4, the amino terminus and the two carboxyl-terminal α-helices (residues 358-372) in subdomain 1 (Egelman *et al.*, 1982; Bremer and Aebi, 1992). The filaments of actin have polarity and the addition of G-actin to filament depends on two events; generation of free barbed ends and increasing the free monomer pool (Otto

and Kessin, 2001). The barbed ends grow rapidly and are the site of actin assembly in vivo. The con concentration of monomeric G-actin is also controlled by series of sequestering proteins. If it were not for the restraining action pf these proteins, almost all actin would exsit as filaments. The G- and F-actin are found in approximately equal amounts in resting cells, but chemotactically stimulated cells, the amount of F-actin increases by 50-60% within a few seconds (McRobbie and Newell, 1985). It is the generation of barbed ends that is thought to be the most critical event.

There filamentouse state provides the cell with networks of structures that are highly dynamic as well as highly stable. These networks give the cell internal scaffold for maintaining and modelling cell shape and provide routes for inter- and intracellular traffic and signaling (Franzot *et al.*, 2005). The components of the microfilament system are acin and a variety of accessory proteins, the actin binding proteins throught to regulate the actin network (Stossel *et al.*, 1985; Pollard and Cooper, 1986; Witke *et al.*, 1992).

1.2. Micro filament system in *Dictyostelium discoideum*

The cytoskeleton is composed of three major classes of filaments, the microtubules, the intermediate filaments, and the microfilaments.

Microfilaments are built by reversible assembly of monomeric actin, which is ubiquitous in eukaryotes and one of the most highly conserved proteins in evolution (Pollard *et al.*, 1994; Pollard and Cooper, 2009). Actin represents approximately 8% of the total cellular protein in *D. discoideum*, corresponding to an average concentration of about 100 μM. As has been shown also for other orgarnisms, in resting *Dictyostelium* cells approximately half of the actin is in the filamentous state (F-actin), and the

other half os present as monomer (G-actin) (Podolski and Steck, 1990). Since the ionic condition s in the cytoplasm strongly favours polymer formation, one would expect to find more than 99% of actin incorporated in filaments. After receiving an external stimulus *D. discoideum* are able to rearrange their actin cytoskeleton within seconds (McRobbie and Newell, 1985; Schleicher and Noegel, 1992). This fast response requires immediate changes in the regulation of the microfilamentous network. *D. discoideum* harbours a multitude of actin-binding proteins, most of which have been isolated due to their activity. *Dictyostelium* cells respond to local stimulation by extending a newly formed leading edge towards a chemoattractant within less than a minute, thereby changing their polarity. The leading edge is formed by the recruitment of soluble proteins from the cytoplasm and their coassembly with actin into a complicated framework of microfilaments (Gerisch *et al.*, 1993). It plays important roles in processes such as migration, cytokinesis, endocytosis, and establishment and maintenance of cell polarity (Pikzack *et al.*, 2005).

2. F-actin cross-linking proteins

2.1. Overview of actin cross-linking proteins

A large of proteins acts on the filament of actin, either to cross-link them or to cap and sever them. Because of the low tensile strength of an individual actin filament, many of the effects of actin are mediated by the creation of a three-demensional cortical network of many filaments. F-actin cross-linking and bundling proteins are stabilsers of the three-dimensional cortical actin network. Actin filaments orgarnize by actin-binding proteins

into densely packed bundles such as actin cables, the intestinal and renal brush border microvilli or the stereocilia of auditory sensory cells (Furukawa & Fechheimer, 1997).

Important family of cytoskeleton proteins are cross-link or bundle actin filaments (α-actinin, filamin, and fimbrin, fascin, 34 kDa actin binding protein) or link the actin filaments to the cell membrane (β-spectrin, dystrophin and utrophin) or other filamentous systems (plectin). The common functional domain of these proteins is the actin-binding domain (Franzot *et al.*, 2005). They are usually abundant, large, and elongated cytosolic proteins. These proteins can bind actin filaments into orthorgonal or into parallel arrays (Eichinger *et al.*, 1999; Otto and Kessin, 2001). In order to connect neighboring actin filaments into a gel or a bundle, F-actin cross-linking proteins must have at least two actin-binding sites, one site for each filament. The two actin-binding site are either arranged in tendem on one polypeptide chain as in fimbrin or they are located on separate polypeptide chain that form parallel or antiparallel dimers as in α-actinin or gelation factor (Winder, 2003). The members of the α-actinin/ spectrin superfamily of proteins share a homologous F-actin-binding domain of about 250 amino acids. They are composed of distinct modular units that mediate filament binding, oligomerisation, regulation by Ca^{2+}, or membrane binding. The spatial arrangement of the two actin-binding sites in conjunction with the flexibility of the spacer elements determines whether the cross-linking protein induces bundling of actin filaments or network formation (Matsudaira, 1991; Eichinger *et al.*, 1999).

2.2. Actin cross-linking proteins in *Dictyostelium*

Actin binding proteins (ABP) contribute to the generation of cell shape and distinct morphological changes associated with essential physiological functions of cells. In the cellular slime mold *D. discoideum*, these processes include chemotaxis, cytokinesis, locomotion, morphogenesis, and phagocytosis (Schleicher and Noegel, 1992; Condeelis, 1993; Noegel and Luna, 1995). Cells lacking several of actin binding proteins created through gene replacement mediated by homologous recombination exhibit phenotypes which vary in type and severity.

A number of F-actin cross-linking proteins have been identified in *Dictyostelium* including a filamin or ABP240 (Hock and Condeelis, 1987) fodrin or ABP220 (Bennett and Condeelis, 1988), a 120 kDa gelation factor (Noegel *et al.*, 1989), α-actinin (Noegel *et al.*, 1987), elongation factor 1α, comitin, a 34 kDa actin binding protein (ABP34), cortexillins I and II (Faix *et al.*, 1996), and fimbrin (Prassler *et al.*, 1997) and interaptin (Rivero *et al.*, 1998) belong to the α-actinin/spectrin superfamily of proteins (Rivero *et al.*, 1999). Knock-out mutants for several of these cross-linkers have been isolated and characterised in detail. Only subtle changes could be detected for single knockout mutants while double mutants were severely impaired in either cytokinesis or development (Schleicher *et al.*, 1988; Brink *et al.*, 1990; Eichinger *et al.*, 1996; Faix *et al.*, 1996; Rivero *et al.*, 1996). These findings led to the provocative notion that the cytoskeletal network is composed of redundant activities that could functionally compensate one another. Central to this redundancy concept is the assumption that the viscoelastic network is self-stabilised over a wide range, and elimination of a single actin-binding protein at least under laboratory conditions can be counterbalanced by other activities. However, removing more proteins from

the system destroys the balance and results in distinct defects (Witke*, et al.*, 1992).

α-Actinin

α-Actinin is calcium regulated the major F-actin crosslinking protein in both muscle and non-muscle cells. α-actinin is a functional antiparallel homodimer and is composed of an N-terminal actin binding domain, followed by a rod domain consisting of four spectrin-like repeat and a C-terminal calmodulin-like domain. The actin binding domain (ABD) consists of two consecutive calponin homology (CH) domains. Several α-actinin isoforms exist, which are regulated differently: actin binding in the non-muscle isoforms is Ca^{2+}-sensitive, whereas in muscle α-actinin it is not. The calmodulin-like domains consist of two EF-hand motifs. The EF-hands regulate the actin-binding domain of the adjacent subunit. *Dictyostelium* α-actinin 100-LVGIGAEELVDKNLKMTLGMlWTllLR-126, amino acid sequence is actin binding site. This domain is highly homologous to similar size domains in other cross-linking proteins including dystrophin, spectrin, 120 kDa gelation factor from *D. discoideum*, fimbrin and filamin. α-Actinin is known to localize to pseudopods of rapidly moving cells, phagosomes, and contractile vacuoles (Brier *et al.*, 1983; Furukawa and Fechheimer, 1994). *Dictyostelium* cells lacking α-actinin show growth impairments under osmotic conditions, motility defects, and orientation defects (Witke *et al.*, 1993; Eichinger *et al.*, 1996; Rivero *et al.*, 1996).

ABP120

ABP120 (filamin, gelation factor) is homodimer contains the globular two

CH domain followed by an extended rod of six filamin repeats in *D. discoideum* (Condeelis *et al.*, 1984). Two such rods dimerize in antiparallel fashion thereby cross-linking the actin strands with their globular heads into highly viscous, orthogonal networks. A tandem pair of CH1 and CH2 domains (ABD), or the variants found in fimbrins are fully functional actin-binding modules (Friedberg and Rivero, 2010). ABP120 have actin binding residues 89-115. This 27-mer sequence is directly involved in the binding of ABP120 to the sides of actin filaments and represents the major actin-binding site. Very similar sequences are present in the ABDs of *Dictyostelium* a-actinin, human dystrophin, β-spectrin, fimbrin and plastin (Vandekerckhove and Vancompernolle, 1992).

ABP120 are localized to the cell cortex, lamellipods, phagocytic cups, and pseudopods of motile cells (Stendahl *et al.*, 1980; Carboni and Condeelis, 1985; Stossel *et al.*, 2001; Feng and Walsh, 2004). *Dictyostelium* mutants lacking ABP120 exhibit reduced frequency and size in psuedopod formation, decreased motility, chemotaxis, and phagocytosis, possibly as a result of reduced cross-linking of actin filaments (Brink *et al.*, 1990; Cox *et al.*, 1992).

Fimbrin

Fimbrins are modular proteins consisting of a pair of α-actinin like actin binding domains each composed of two CH domains and two EF-hand calcium-binding motifs. Fimbrin is calcium regulated actin bundling protein that contains the actin-binding domains (Korenbaum and Rivero, 2002). Fimbrin localizes to the cell cortex, leading edge, phagosomes, and macropinosomes of *Dictyostelium* (Prassler *et al.*, 1997). *Dictyostelium* null mutants of fimbrin show decreased cell size (Prassler *et al.*, 1997; Pikzack *et*

al., 2005).

2.3. Actin bundling protein ABP34

The *Dictyostelium* ABP34 (the 34 kDa actin binding protein) is one of the F-actin bundling proteins that play dynamic distribution during cell shape changes, cell movement and phagocytosis, and cortical architecture. This protein is located at the leading and trailing edges of locomoting cells, the phagocytic cup, pseudopodia and filopodia in motile cells, and cell to cell contact sites (Fechheimer and Taylor, 1987; Fechheimer *et al.*, 1991; Fechheimer *et al.*, 1994; Lim *et al.*, 1999; Rivero *et al.*, 1999). ABP34 protein contributes to formation of actin filament bundles in the filopodia of *Dictyostelium* amoebas. Previously, alignment of the *Dictyostelium* ABP34 protein sequence identified partially homologous regions to other F-actin binding proteins (Fechheimer and Furukawa, 1991). Moreover, antigenic homologs of the ABP34 protein have been reported in *Physarum polycephalum*, *Schistosoma mansoni*, *Chara Carolina and Drosophila melanogaster*. Mammalian homologs identified in the Lewis lung adenocarcinoma epithelial cell and MDCK cell culture, which is E-cadherin on intracellular junctions during the induction of monolayer formation (Johns *et al.*, 1988; Furukawa and Fechheimer, 1990). This suggests that ABP34 protein is not restricted to lower eukaryotes. In actin associated proteins are regulated the activity by variety of mechanisms. The ABP34 is one of the calcium regulated actin binding protein that include α-actinin, fimbrin, and villin (Bretscher and Weber, 1979; Bretscher *et al.*, 1981; Fechheimer and Taylor, 1984; Pikzack *et al.*, 2005).

In *D. dicoideum*, mutants lacking the ABP34 protein exhibited growth and

development normally, but showed abnormal filopodia formation, increased persistence of motility, lost bits of cytoplasm during locomotion, and represented cold-sensitive for growth (Rivero *et al.*, 1996; Rivero *et al.*, 1999). Double mutation of the ABP34 protein and other actin cross-linking proteins in *D. dicoideum* results in more pronounced aberrant phenotypes suggesting some redundancy among the F-actin crosslinking proteins (Ponte *et al.*, 2000). Several proteins might share similar activities or take overlapping fuctions. Reversible cross-linking of actin filaments by the ABP34 protein may contribute to regulation of the consistency and contractility of cytoplasm in *Dictyostelium* (Fechheimer and Taylor, 1984).

The ABP34 protein has a high affinity calcium binding region which residues are belonged to second one in two putative EF-hand regions on 295 amino acids of the protein (Furukawa *et al.*, 2003). The ABP34 is actin bundling protein that crosslinks actin filaments and promotes formation of actin bundles in the presence of low concentration of free calcium but not formation of bundles in micromolar, high concentration of free calcium ions in vitro (Fechheimer and Taylor, 1984; 1987; Fechheimer and Furukawa, 1993). Previously report, purified ABP34 revealed three actin binding sites located at amino acids 1 to 123, 193 to 254, and 279 to 295. Among the sites, amino acids 193 to 254 are the most contribution for actin binding. And terminal located amino acids 279 to 295 are important for formation of actin bundle (Lim *et al.*, 1999).

2.4. The relationship between ABP34 and Hbx4

Hbx4, homeodomain-containing protein in *Dictyostelium*, possessed a highly conserved homeodomain. In Hbx4-overexpressing cells, $Hbx4^{OE}$,

show the defects in growth rate and cytokinesis. Hbx4^{OE} show reduced transcription level of cadA encoding DdCAD-1, Ca^{2+}-dependent cell-cell adhesion molecule. Constitutively expressed DdCAD-1 in Hbx4^{OE} rescues the defects that Hbx4^{OE} showed in cytokinesis and development. Hbx4^{OE} modulates the expression of DdCAD-1, which regulates cytokinesis during growth and cell-type proportioning during development. In Hbx4^{OE}, RhoGDI1, Rho GDP dissociation inhibitor 1 (encorded by *rdiA*), and ABP34 are reduced. Rho GTPase regulates several pathways controlling cell motility, cytokinesis, phagocytosis, pinocytosis and development. RhoGDIs modulate the cycling of Rho GTPase between active GTP-bound and inactive GDP-bound states. In *Dictyostelium*, RhoGDI-null cells exhibit defects in cytokinesis and actin cytoskeleton. ABP34 is an F-actin bundling protein that crosslink actin filaments in Ca^{2+}-dependent manner and functions in regulating growth and cell size. DdCAD-1 regulated by Hbx4, modulates the transcription levels of *rdiA* and *abpB*. DdCAD-1 regulates the localization of ABP34 in dividing cells (Kim, 2011; Kim *et al.*, 2011).

3. *Dictyostelium discoideum*

3.1. *Dictyostelium discoideum* genome

D. discoideum belongs to the social amoebae (*Dictyostelia*). Phylogenetically, *Dictyostelia* form a subbranch in the amoebozoa, one of the six kingdoms into which eukaryotes are currently partitioned. Global protein sequence comparisons, made possible by the genome sequence, showed that *D. discoideum* is evolutionarily closer to animals and fungi than to plants (Eichinger and Noegel, 2005). More recently, the genomes of three

other *Dictyostelia*, *Dictyostelium fasciculatum*, *Dictyostelium purpureum* and *Polyspondylium pallidum*, confirmed this (Heidel *et al.*, 2011; Sucgang *et al.*, 2011).

The *Dictyostelium* genone is composed of 6 chromosomes ranging in size from 4 to 7 Mb that make up for about 34 Mb of DNA, a multicopy 90 kb extrachromosomal element that harbours the rRNA genes, and a 55 kB mitochondrial genome. The estimated number of genes in the genome is 8,000 to 10,000. Many of the kown genes show a high degree of sequence similarities to homologues in vertebrate species (Eichinger *et al.*, 1999; Kuspa and Loomis, 2006).

3.2. *Dictyostelium discoideum* as a model organism

Since its isolation and description about 80 years ago the unicellular amoeba *Dictyostelium* has been established as valuable model orgarnism (Raper, 1935). *Dictyostelium* is readily grown in pure clonal culture either on the surface of nutrient agar plates (in association with bacterial prey-generation time 3 h), or in a nutrient broth (in the absence of bacteria-generation time 9 h). Genetic transformation methods were developed for *Dictyostelium* and have been supplemented by a variety of genetic and biochemical techniques including gene knockout by homologous recombination, knockdown using antisense RNA or RNAi expression constructs, ectopic overexpression of wild type or mutant genes, cell type specific expression, GFP-and epitope tagging of proteins, random insertion mutageneis and genetic suppression analysis (Annesley and Fisher, 2009).

Dictyostelium cells are highly motile throughout their lifetime and their motility characteristics parallel those seen in human leukocytes (Devreotes

and Zigmond, 1988). In contrast to leukocytes, however, *Dictyostelium* is haploid. This intrinsic property is a huge advantage of the *Dictyostelium* system and greatly facilitates the isolation and characterization of mutant phenotypes (Eichinger *et al.*, 1999).

These advantage have led to *D. discoideum* is nonmammalian genetic model system for investigating diverse biochemical, cell biological and genetic approaches, from well-established ones, such as actin cytoskeleton-based cell motility, chemotaxis and the role of actin-binding proteins phagocytosis and endo-lysosomal traffic, collective cell migration during development, and pattern formation, to relatively new roles on stage, such as autophagy and social evolution. (Titus *et al.*, 1989; Mann *et al.*, 1994) (Schleicher and Noegel, 1992). Thus, in biosciences and in particular cell biological and biomedical research, the simple eukaryote *Dictyostelium* will continue to serve as a valuable model with great potential to investigate fundamental biological questions. The molecular genetic techniques that have been continuously expanded over the years and a well curated genome sequence, which is accessible *via* the online database dictyBase (Muller-Taubenberger *et al.*, 2013).

3.3. Life cycle of *Dictyostelium discoideum*

The social amoeba or cellular slime mold *D. discoideum* is the lowest eukaryote able to form multicellular structure. In the vegetative phase of their life cycle, the single-celled amoebae divide by simple mitotic divisions. *D. discoideum* amoebae ingest bacteria by phagocytosis or, in the case of axenic derivates, take up nutrients by pinocytosis. The natural habitat of *Dictyostelium* is forest soil and decaying leaves where the cells feed on

bacteria. Exhaustion of the food source triggers the cells to enter a developmental program, which is completed within approximately 24 hours in the laboratory. When developmental program is initiated, cells begin to signal each other by secreting cAMP and to aggregate by chemotaxis toward this chemoattractant. (Saran *et al.*, 2002; Van Driessche *et al.*, 2002). The resulting multicellular aggregate contains up to a few hundred thousand cells and undergoes further differentiation and morphogenetic changes. After the cells have aggregated, they form the hemispherical mound, tight aggregate. The aggregate develops polarity, creating a protruding tip then forms at the apex of each aggregate. All subsequent movements are regulated by the tips. Under the control of the tip, the aggregate elongates into a finger-like structure or standing slug that falls onto its side and crawls away (Dormann and Weijer, 2001). The slug is phototatic and is also capable of migrating up heat gradients (Fisher, 1997). The cells of the slug become differenciated at an early stage into two types. They arrange themselves by differential movement in a simple axial pattern in the slug (Aubry and Firtel, 1999). The anterior one- third of the slug consists of prestalk cells, the precursors of stalk cells in a fruiting body and the posterior portion of prespore cells, the precursors of spores. Prespore and prestalk cells have different patterns of gene expression and are formed in response to different signals; extracellular cAMP induces prespore differentiation and EIF, a chlorinated hexaphenone, induces prestalk differentiation (Kay, 1997). The transition form slug to the fruiting body occurs by a process called culmination (Bonner and Williams, 1994). When conditions are suitable for culmination, terminal differentiation is initiated resulting in a fruiting body consisting of a spore-containing sorus supported by a rigid, slender stalk. Finally, a fruiting body consists of two

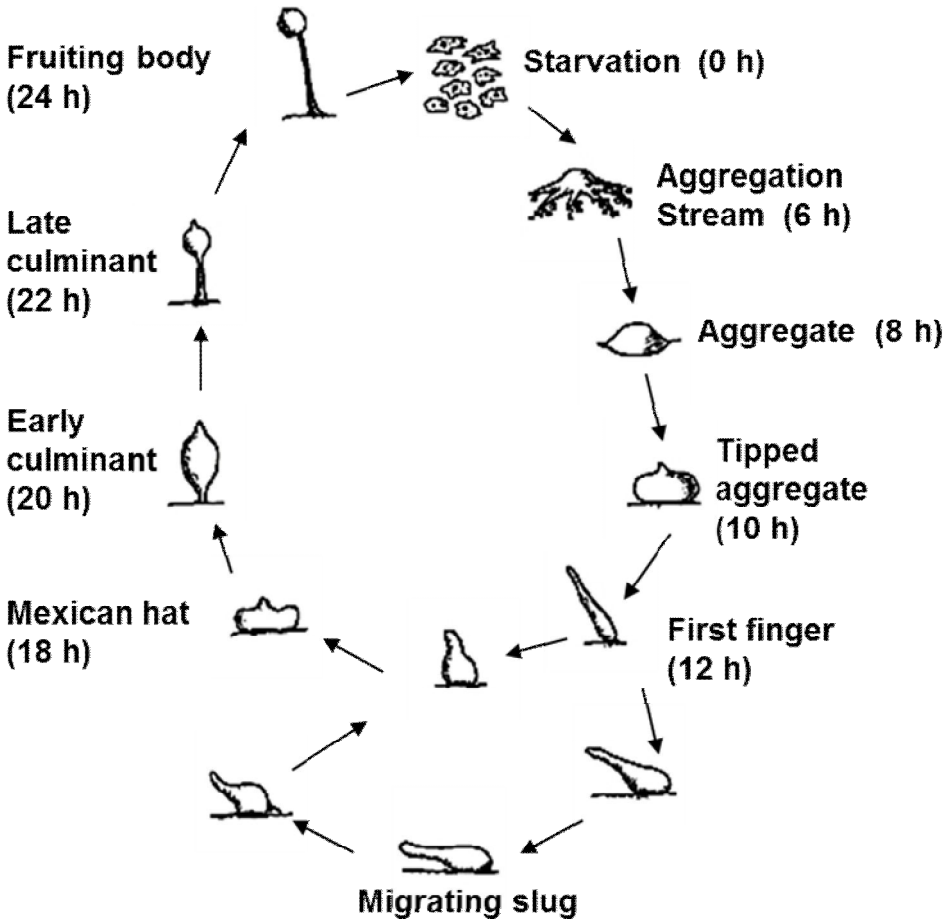

Scheme 1. Developmental cycle of *Dictyostelium discoideum.*

Starved cells aggregate together in response to cAMP pulse, forming a finger-like structure. Falling down on the ground, it can migrate away as a slug. A slug consists of the prestalk cells localizaed to the anterior and the prespore cells to the posterior. The slugs migrate to the favorable place to disperse spores and finally form fruiting bodies consisting of stalk and spore cells (Choi, 2004).

main cell types, spore and stalk cells. The stalk consists of dead vacuolated cells, while the spore cells are resistant to extreme temperatures or drought. More favorable environmental conditions enable the hatching of new amoebae from the spores. The aggregation of thousands of individual cells that build a multicellular organism in this peculiar life cycle, has intrigued scientists for decades since the first description by Kenneth Raper, and is responsible for the addendum 'social' in the name (Raper, 1935; Annesley and Fisher, 2009).

4. Aims of study

The ABP34 is well characterized calcium-regulated actin bundling protein. Several calcium regulated actin binding proteins have been also reported but the structural properties of the ABP34 protein have not presented yet. This study has started from the attempts to understand biochemical properties of actin bundling protein ABP34 and its physiological roles in *D. discoideum*. The biological role of ABP34 identified by using overexpressed cells and RNA interference cells. The recombinant of the protein was identified as functionally in distinguishable form the native protein isolated from *D. discoideum* (Lim and Fechheimer, 1997). Thus, using recombinant protein expression, large quantaities of the recombinant ABP34 protein have been synthesized and purified from *E. coli* for biochemical studies and X-ray crystallography. The crystal structure will lead to further insights into the actin binding regulating mechanisms of ABP34. In this study, cosedimentation of ABP34 with F-actin was used to characterize the activity and cooperativity of the intact protein. In addition, mutant forms of ABP34

were purified and assayed for their ability to interact with actin filament. The analysis of the structural relateness of various binding proteins will give to understanding the mechanism of assembly of actin bundles and their role in the cell.

In previouse study, DdCAD-1 is regulated by Hbx4, modulates the transcription level of *rdiA* and *abpB*. The RhoGDI1 and ABP34 were reduced in Hbx4^{OE} cells. RhoGDI1 induce expression of *abpB* in cytokinesis and actin cytoskeleton. DdCAD-1 is regulated by Hbx4^{OE}, modulates the transcription level of *abpB*. As a result, ABP34 actin bundling protein is regulated by RhoGDI and ABP34 concentrated in cell cortex by DdCAD-1 during cytokinesis (Kim, 2011). For understainding function of ABP34, we identified function in actin cytoskeleton during growth and development the expression and the localization of ABP34. The investigation of structure and function of *Dictyostelium* ABP34 will provide biological insight into the relationship between actin binding protein and actin cytoskeleton system in *D. discoideum* and higher eukaryotic orgarnism.

II. MATERIALS AND METHODS

1. Materials

Enzymes used in DNA manipulations were purchased from Koscochem (Korea), Roche Molecular Biochemicals, or Promega Life Science. Nylon membrane, nitrocellulose membranes, and bacterial alkaline phosphatase were from MBI fermentas. Nitro blue tetrazolium (NBT), BCIP and G418 were from Duchefa. Ampicillin, 4′,6-diamidino-2-phenylindole (DAPI), tetramethylrhodamine-5-(and 6)-isothiocyanate (TRITC)-conjugated phallodin, Diethypyrocarbonate (DEPC), acrylamide, N,N′-methylenebisacrylamide, SDS, sodium acetate, methanol, dimethyl sulfoxide (DMSO), glacial acetic acid, glycerol, ammonium persulfate, bromophenol blue, TEMED, 37% formaldehyde, were purchased from Sigma-Aldrich. Blasticidin and 4-morpholinepropanesulfonic acid (MOPS) were purchased from ICN. All other chemicals used were of the highest quality generally available.

2. Strains and culture conditions

2.1. *Dictyostelium* strains and culture conditions

2.1.1. *Dictyostelium* strains

The axenic *Dictyostelium discoideum* strain KAx3 was used as wild type strain. All mutant strains were derived from KAx3 cells. The *abpB*-overexpressed strain (ABP34^{OE}), *abpB*-RNA interference strain (*abpB* RNAi) and GFP-fusion ABP34 expressed strain (GFP ABP34) were used to examine the role of ABP34 in *Dictyostelium*. For *abpB* overexpression and underexpression, a full length *abpB* cDNA fused behind the constitutively active actin 15 promoter was transformed into KAx3. ABP^{OE} strain and

abpB RNAi strain was used to examine the role of *abpB* during growth and development. GFP-ABP34 (GFP-fusion ABP34) expressed cells was used for subcellular localization.

2.1.2. Growth in liquid nutrient medium

Dictyostelium KAx3 cells and derived transformants were grown in liquid HL5 medium (1.4% thiotone E peptone, 1.4% glucose, 0.7% yeast extract, 3.5 mM $Na_2HPO_4 \cdot 7H_2O$, 4.6 mM KH_2PO4, pH 6.5) containing 200 μg of streptomycin sulfate/ml (Duchefa) and 200 unit of penicillin/ml (Duchefa) and 20 μg/ml G418 (Duchefa) by appropriate selective antibiotics at 22°C in shaking-suspension flasks at 150 rpm (Cocucci and Sussman, 1970; Soll*, et al.*, 1976). For all the cell biological works, cultures were harvested at a density of 2-5 × 10^6 cells/ml. For strain maintenance, stock cells were prepared in HL5 medium supplemented with 5% DMSO and stored at –70°C. For routinely renewal of cell strains, the frozen stock cells was thawed and transferred to a culture dish plate containing 10 ml of HL5 media and used for expriments by a montly interval (Jeong *et al.*, 2006).

2.1.3. Growth on SM agar plates

Dictyostelium cells were plated onto SM agar plates overlaid with *Klebsiella pneumonia* and incubated at 22°C for 5 days until *Dictyostelium* plaques appeared on the bacterial lawns. To obtain single clones of *Dictyostelium*, 10-100 cells were plated onto SM agar plates. Single plaques obtained after incubation at 22°C for 3-5 days were picked up with sterile tooth picks, transferred to separate on culture dish plate with HL5 medium supplemented with appropriated selective antibiotics.

2.2. Bacterial strains and culture conditions

2.2.1. *Escherichia coli* strains

E. coli DH5α was used for DNA manipulation and BL21 (DE3) pLysS was used for overexpression of proteins using pET-3a vector construct. *E.coli* strains were grown at 37°C on Lurea-Bertani (LB, 1% trypton, 0.5% yeast extract, 1% NaCl) medium supplemented, where required, with the following antibiotics at final concentrations: ampicillin (Sigma-Aldrich), 50 μg/ml; chloramphenicol, 34 μg/ml and chemicals at final concentrations: 20 μg/ml 5-bromo-4-chloro-3-indolyl-β-D-galactopyranoside (X-gal from Duchefa).

2.2.2. *Klebsiella pneumoniae* strain

Klebsiella pneumoniae was prepared by sticking on SM plate (1% glucose, 1% bacto peptone, 1% yeast extract, 4 mM $MgSO_4 \cdot 7H_2O$, 14 mM KH_2PO_4, 5.7 mM K_2HPO_4, 2% agar) (Sussman, 1987). Plates were incubated overnight at 37°C and stored at 4°C after sufficient colony growth. Loopful of bacteria cells were harvested from these plates and inoculated for the two-membered cultures with *Dictyostelium*. The *Dictyostelium* and bacterial strains used in this study were summarized in Table 1.

3. Development of *Dictyostelium discoideum*

Development of *Dictyostelium* is induced by starvation. Exponentially growing cell of $2–5 \times 10^6$ cells/ml) were pelleted by centrifugation at 500 g for 5 min at 4°C and were washed twice with non-nutrient cold KK2 buffer

(16.5 mM KH_2PO_4, 3.4 mM K_2HPO_4, pH6.2) and the buffer was removed by centrifugation at 500 g for 5min. Cells were suspended with KK2 buffer and then deposited at a density of $2 \times 10^6/cm^2$ on nitrocellulose filters or KK2 buffered-agar plates (1.5% micro agar). The cells layed plates were air dried and any excess liquid was carefully without disturbing the cell layer. Cells were allowed to develop for desired time at 22°C. To make the dark condition, the KK2 plate was wrapped with aluminum foil.

4. Transformation of *Dictyostelium discoideum*

The transformation of *Dictyostelium* cells was performed according to the protocol (Schlatterer *et al.*, 1992) with some modification (Pang *et al.*, 1999). *Dictyostelium* cells were grown axenically in suspension culture to a density of $2–3 \times 10^6$ cells/ml. The suspension was centrifuged at 500 × g for 5 min at 4°C. Cells were washed twice with an equal volume of ice-cold H-50 buffer (20 mM HEPES, 50 mM KCl, 10 mM NaCl, 1 mM $MgSO_4$, 5 mM $NaHCO_3$, 1 mM NaH_2PO_4, pH 7.0, autoclaved and stored cold or frozen). The washing buffer was removed by centrifugation at 500 × g for 5min at 4°C. After washings, the cells were resuspended in H-50 buffer at a density of 5×10^6 cells/ml. For electroporation, 1–10 μg of plasmid DNA was added to 100 μg of cell suspension and the cell-DNA mixture was transferred to a pre-chilled electroporation cuvette (0.1 cm electrode gap, Bio-Rad) at 0.85 kV/25 μF twice with about 5 sec between pulses. After electroporation, the cells were incubated in the cuvette on ice for 5 min and suspend onto a cell culure dish filled with 10 ml HL5 medium. After 18–24 h incubation at 22°C, the medium was replaced by the seletion medium containing appropriate

Table 1. Bacterial and *D. discoideum* strains used in this study

Strains	Genotypes	References or sources
Bacterial strains		
E. coli DH5α	F- *ΔlacU169(ϕ80lacZΔM15)endA1 rec1hsdR17 deoR supE44 thi-1 λ-gyrA96 relA1*	(Hanahan, 1983)
E. coli BL21(DE3)pLysS	F^- *ompT* $r_B^-m_B^-$(DE)/pLysS	(Studier, 1991)
K. pneumoniae		Microbial resources center, 1997
***Dictyostelium discoideum* strains**		
KAx3	Axenic wild-type strain	Firtel, 1997
$ABP34^{OE}$	KAx3:[pTX FLAG–ABP34], neo^r ABP34-overexpressing KAx3	This study
abpB RNAi	KAx3:[EXP4(+)–RNA interference ABP34], neo^r *abpB*-underexpressed KAx3	This study
GFP–ABP34/KAx3	KAx3:[pTX GFP–ABP34], neo^r	(Kim, 2011)

antibiotics (20 mg/ml of G418 or 10 μg/ml blasticidin S).

5. Genetic manipulation methods

General techniques for isolation and manipulation of DNA in *E. coli* were as previously described (Sambrook and Gething, 1989). pGEM-T easy vector was used for cloning of PCR product and pET-3a vector for overexpression of protein in *E.coli*. Exp4(+), pTX-FLAG and pTX-GFP vectors were used for introducing appropriate genes into *Dictyostelium*. The constructs and plasmids used for this study were summarized in Table 2.

5.1. Isolation and subcloning of *abpB* gene overexpression from *Dictyostelium discoideum*

The *abpB* (888 bp) was amplified by polymerase chain reaction using cDNA as a template. The PCR-primer sequences were as follows: forward 5′-GGATCCATGGCAGAAACAAAAGTTGCAC-3′ and reverse 5′-CTCGAGTTATTTCTTTTGTGGACCGTATCTC-3′. The amplified product was cloned into pGEM-T cloning vector (Promega), yielding pGEM–Teasy–*abpB*. The construct was digested with *Bam*HI and *Xho*I and a construct for constitutive expression of *abpB* was generated by cloning the full-length cDNA *abpB* amplicon into the pTX-FLAG vector for construction of flag fusion protein with ABP34. The constructs were introduced into KAx3 cells using electroporation (Pang *et al.*, 1999), and transformants were selected and maintained in medium containing 20 μg/ml of G418 (Duchefa).

Table 2. Plasmids and constructs used in this study

Plasmids	Descriptions	References or sources
pGEM-Teasy	PCR cloning vector	Promega
pET-3a	Protein expression vector	Amersham
Exp4(+)	Expression vector for *Dictyostelium*	Firtel, 1997
pTX–GFP	GFP-tagged protein expression vector	Egelhoff, 2000
pTX–FLAG	FLAG-tagged protein expression vector	Egelhoff, 2000
pAct15GAL	β-galatosidase expression vector	Firtel, 1997
pGEM–Teasy–ABP34	pGEM–T easy vector containing *abpB* ORF	This study
pET-3a–ABP34	pET–3a vector containing the coding region of ABP34	This study
pGEM–Teasy–*abpB* RNAi	pGEM–T easy vector containing *abpB* ORF	This study
pTX–GFP–ABP34	pTX–GFP vector fused with *abpB* ORF in frame	Kim, 2011
pTX–FLAG–ABP34	pTX–FLAG vector fused with *abpB* ORF in frame	This study
Exp4(+)–*abpB* RNAi	Exp4(+) vector containing *abpB* RNA interference construct	This study

5.2. Cloning of *abpB* RNA interference from *Dictyostelium discoideum*

Full-length of *abpB* (cDNA) amplified into two fragments by polymerase chain reaction (PCR) using complementary cDNA as the template: first fragment (*abpB* RNAi F1) with *Bgl*II and *Spe*I restriction enzyme site, second fragment (*abpB* RNAi F2) with *Xho*I and *Spe*I restriction enzyme site. These two fragments were ligated and cloned into pGEM-Teasy cloning vector (Promega), yielding pGEM–Teasy–*abpB* RNAi. The primer sequences of *abpB* fragment 1 (1 to 888) for PCR were as follows: forward 5′-TACTAGATCTATGGCAGAAACAAAAGTTGAC-3′ and reverse 5′-TACTACTAGTTTATTTCTTTTGTGGACCGTATC-3′. The primer sequences of *abpB* fragment 2 (1 to 300) were as follows: forward 5′-TACTCTCGAGATGGCAGAAACAAAAGTTGCAC-3′ and reverse: 5′-TACTACTAGTGAGAGCAATATCGAAATCCAAATC-3′. The construct was digested with *Bgl*II and *Xho*I and a construct for constitutive expression of *abpB* RNAi was generated by cloning the RNA interference *abpB* into the EXP-4(+) vector containing a constitutively active *Act15* promoter. The constructs were introduced into KAx3 cells using electroporation (Pang *et al.*, 1999), and transformants were selected and maintained in medium containing 20 μg/ml of G418 (Duchefa).

5.3. Cloning of GFP-ABP34 from *Dictyostelium discoideum*

The axenic parental strain KAx3 cells were grown in HL5 medium, which was supplemented with 200 μg/ml of streptomycin sulfate and 200 unit/ml of penicillin and shaken at 150 rpm and 22°C. Construct that GFP-fusion ABP34 were introduced into *D. discoideum* KAx3 using electroporation.

The transformants were selected under G418 (20 μg/ml) containing HL5 medium on tissue culture plate. The expression vector for the ABP34 was constructed by PCR using cDNA from *Dictyostelium* as a template and P1 (5'-GGATCCATGGCAGAAACAAAAGTTGCAC-3') and P2 (5'-CTCGAGTTATTTCTTTTGTGGACCGTATCTC-3') as primers. The PCR product was cloned into pGEM-T easy vector (Promega) and cut by *Bam*HI and *Xho*I. The result fragment was ligated into pTX-GFP vector for the construction of green fluorescent protein (GFP) fusion protein with ABP34. After the selection, GFP-fused ABP34 overexpressed cells were used for subcellular localization.

5.4. Polymerase chain reaction (PCR)

DNA fragment amplification was preformed according to the method recommended by Taq polymerase manufacture (Promega, Madison, WI) with slight modification. For the reactions, 25 pmol of degenerate oligomucleotide primers, 100 ng of DNA or 5 ng plasmid DNA and 0.25 units of Taq polymerase were combined in final volume of 25 μl with reaction buffer (50 mM KCl, 1.2 mM MgCl2, 10 mM Tris-HCl, pH 8.4, 0,01% gelatin) containing 50 μM of each dNTP. The mixture was subjected to 30 cycles of 30 sec denaturation at 94°C, 30 sec annealing at 55°C and 1 min extension at 72°C.

5.5. Site-directed mutagenesis of ABP34

The site-directed mutagenesis method was performed using *pfu* DNA polymerase, which replicated with high fidelity, displacing with the newly designed oligonucleotide primers. Extension was carried at 68 °C for 2 min

for every 1 kb following PCR, and then the product was treated with *Dpn*I for 1 h. The nicked plasmid DNA incorporated with the desired mutation was then transformed into *E. coli* DH5α. The mutation constructs were confirmed by sequencing the purified plasmid. To investigate ABP34 EF-hand, each charged residue of calcium coordination was replaced by alanine. The plasmid containing *abpB* gene was used as template of pET-3a-*abpB* and the following primer pairs were used (mutated sequences are emboldened):

For ABP34 D148A mutant protein,

D148A F: 5-GATGTCAATTTC**GCA**GGTCGTGTCTC-3

D148A R: 5-GAGACACGACC**TGC**GAAATTGACATC-3

For ABP34 D148A mutant protein,

D150A F: 5-CAATTTCGATGGT**GCA**GTCTCTTTC-3

D150A R: 5-GAAAGAGAC**TGC**ACCATCGAAATTG-3

For ABP34 D144A and D148A double mutant protein,

D144A, D148A F:

5-GAGAAAAAGTC**GCA**GTCAATTTC**GCA**GGTCGTG-3

D144A, D148A R:

5-CACGACC**TGC**GAAATTGAC**TGC**GACTTTTTCTC-3

5.6. RNA extraction and Northern blot analysis

Total RNA was isolated using TRIzol reagent according to the supplier's recommendations (Solgent). For Northern blot analysis, 20 μg samples of total RNA were separated on 1% agarose gel containing 0.22 M formaldehyde and transferred to Hybond-N+ membrane filter (Amersham Phamacia Biotech, Buckinghamshire, UK). The coding region of *abpB* was

generated by PCR and labeled with [α-^{32}P]-dATP by random priming. The blot was prehybridized for 1 h, hybridized for 2 h and washed twice for 20 min at 65°C. The signal was visualized by exposing membrane to BAS film.

6. Structural and biochemical analysis of ABP34 protein from *Dictyostelium discoideum*

6.1. Preparation and purification of recombinant ABP34 in *E. coli*

The full-length *abpB* gene coding ABP34 was amplified by PCR using *D. discoideum* cDNA as a template. The amplified gene was inserted downstream of the T7 promoter of the expression plasmid pET-3a (Novagen) and the resulting construct expressed residues 1–295 of the ABP34 protein without additional residues. After verifying the DNA sequence, plasmid DNA was transformed into *E. coli* BL21 (DE3) (Novagen). The cells were grown to OD_{600} of approximately 0.5 in Luria-Bertani media containing 0.1 mg/ml ampicillin and 34 μg/ml chloramphenicol at 37°C and expression was induced by 1 mM isopropyl-β-D-thiogalactoside (IPTG, Duchefa). After 12 h induction at 22°C, the cells were harvested and resuspended in buffer A (100 mM HEPES pH 7.4) containing 1mM phenylmethylsulfonyl fluoride (PMSF). The cells were disrupted by sonication and the cell debris was discarded by centrifugation at 20,000g for 30 min. The supernatant was loaded onto DEAE Sepharose CL-6B (GE Healthcare) column and the ABP34 containing flow-through was collected with buffer A. The protein solution was loaded onto a Superdex 75 HR 16/60 column (GE Healthcare) pre-equilibrated with 10

mM HEPES pH 7.4 containing 100 mM NaCl and 0.1 mM EGTA. The purified ABP34 was concentrated to approximately 40 mg ml^{-1} for crystallization.

6.2. Oligomeric state determination

Purified ABP34 and molecular mass standard (Sigma) were applied on a Superpose 6 10/300 GL column (GE Healthcare) pre-equilibrated with 10 mM HEPES (pH 7.4) containing 100 mM NaCl. A standard curve was generated by plotting the logarithm of molecular mass of standards proteins against their K_{av}, where $K_{av} = (V_e-V_0)/ (V_t-V_0)$: V_e, elution volume; V_0, void volume; V_t, total bed volume. K_{av} of ABP34 determined by using the same column was compared to the profile of protein standards: bovine serum albumin (66 kDa), carbonic anhydrase (29 kDa), cytochrome c (12.4 kDa), aprotinin (6.5 kDa). All samples were allowed to equilibrate at room temperature (25°C) for at least 2 h before use. The calibration curves for the protein standards were determined by linear-squares analysis of the K_{av} vs. log MW. Apparent molecular weight of native ABP34 was estimated to be 32.836 kDa showing that ABP34 behaves as a monomer.

6.3. Circular-dichroism spectroscopy

Circular-dichroism (CD) spectra were recorded at 298 K with a Jasco J-815 CD spectrophotometer using a 0.1 cm path-length quartz cell. Experiments were carried out in 10 mM HEPES buffer pH 7.4 containing 100 mM NaCl with or without EGTA and $CaCl_2$. The protein concentrations in the samples were 6 μM. Random error and noise were reduced for each spectrum by averaging three scans in the wavelength range of 300-190 nm

with 50 nm/min scan speed, 1 nm step resolution, 1 nm bandwidth and 8 s response time. The signal acquired for the buffer used for dilution of the proteins was subtracted from the spectra acquired for the proteins.

6.4. Crystallization and data collection

Crystal screening was conducted by hanging-drop vapour-diffusion method using available screening solutions from Hampton Research and Emerald BioSystems. Droplets composed of 1 μl protein solution and equal volume of crystallization screening solution were equilibrated against 350 μl reservoir solution at 22°C. Rhombus-shaped crystals were produced using 0.2 M Ammonium acetate, 0.1 M sodium citrate pH 5.6, 30% PEG 4K in 3 days. Initial crystallization conditions were optimized by modifying the buffer pH, salt content and PEG concentration. Single crystals of ABP34 were mounted using a nylon loop (50 μm Mounted CryoLoop, Hampton Research) for data collection and were frozen at -173°C using Cryostream cooler (Oxford Cryosystems) without additional cryoprotectant. A 1.89 Å native data set was collected at wavelength of 1.1 Å using an ADSC Quantum 210 CCD on the beamline 6C of the Pohang Light Source, Republic of Korea. A total of 360 frames of 1º oscillation data were collected with the crystal-to-detector distance set to 120 mm (Table. 3). A 2.30 Å SAD data set was collected at wavelength of 1.9 Å using an ADSC Quantum 270 CCD on the beamline 7A of the Pohang Light Source, Republic of Korea. A total of 999 frames of 1º oscillation data were collected with the crystal-to-detector distance set to 120 mm

6.5. Data processing and structure determination

Diffraction data were processed and scaled using *DENZO* and *SCALEPACK* from the *HKL2000* program suite (Otwinowski and Minor, 1997). The structure was determined by Ca^{2+}/S single-wavelength anomalous dispersion (SAD) phasing method. SAD phasing was performed with the *AutoSol* program (Terwilliger *et al.*, 2009) in the *PHENIX* suite (Adams *et al.*, 2010) that is an experimental phasing pipeline that combines *HySS* (Hybrid Substructure Search) (Grosse-Kunstleve and Adams, 2003) for finding heavy-atom sites, *Phaser* (McCoy *et al.*, 2007) or *SOLVE* (Terwilliger, 2002) for calculating experimental phases, and *RESOLVE* (Terwilliger, 2002) for density modification and model-building. The auto-built models from the phasing programs were completed using *COOT* (Emsley and Cowtan, 2004) and refinement was performed with a maximum-likelihood algorithm implemented in *REFMAC5* (Murshudov *et al.*, 2011).

6.6. F-actin co-sedimentation assay

Co-sedimentation assays were performed as described previously (Lim *et al.*, 1999). Actin from rabbit muscle (Sigma) was solubilized by water and then polymerized by addition of equal volume of polymerization buffer (20 mM PIPES pH 7.0, 50 mM KCl, 1 mM $MgCl_2$, 1 mM ATP, 1 mM DTT) containing 5mM EGTA for 1 h at room temperature (25°C). Then, the ABP34 protein (0.25 μM) was mixed with prepared F-actin (5 μM) under actin polymerization conditions (20 mM PIPES pH 7.0, 50 mM KCl, 1 mM $MgCl_2$, 1 mM ATP, 5 mM EGTA, and 0.25 mM $CaCl_2$ for low Ca^{2+} condition) for 24 h at 4°C and centrifuged in ultra-centrifuge (Beckman) at 115,000 *g* for 1 h. The supernatant (S) and the pellet (P) samples were

collected and analyzed by 12% SDS−PAGE. Gel was visualized with Coomassie Blue staining.

6.7. Transmission electron microscopy

The actin filaments and bundles were visualized with energy-filtering transmission electron microscope (LIBRA 120; Carl Zeiss, Germany) operated at an accelerating voltage of 120 kV. Actin (5 μM) was polymerized in F-actin buffer containing 20 mM PIPES pH 7.0, 50 mM KCl, 1 mM $MgCl_2$, 1 mM ATP. F-actin (5 μM) and ABP34 (1 μM) were mixed in buffer containing 0.25 mM $CaCl_2$ and 5 mM EGTA and incubated for overnight on ice. The samples (5 μl) of resulting F-actin preparation mixtures were adsorbed onto carbon-coated copper grids (200 mesh) for 1 min, washed with F-buffer for 30 s, and negatively stained with 2% uranyl acetate (Electron Microscopy Sciences, Hatfield, PA) for 1 min and air dried. All the types of images were recorded with a slow-scan charge-coupled device camera (Ultrascan 4000 SP; Gatan, Pleasanton, CA, USA).

6.8. Protein concentration

The protein concentration was determined according to the method described by Lowry ((Lowry *et al.*, 1951) with bovine serum albumin as standard. Occasionally it was determined by the method proposed by Bradford (1976).

7. Cell biological methods

7.1. Fluorescence labeling of *Dictyostelium* cells

Log-phase cells grown in suspension were diluted at a density of 2.5 x 10^6 cells/ml with HL5 and then fixed on coverslips with cold methanol containing 1% formaldehyde at -20°C for 5 min. To stain F-actin, cells were incubated with 3 μg/ml of tetramethylrhodamin-5-isothiocyanate (TRITC)-conjugated phalloidin (Sigma) for 1 h and washed three times with PBS. Cells were stained with 0.1 μg/ml of 6-diamidino-2-phenylindole (DAPI) and observed under by LSM700 confocal laser scanning microscope (Carl Zeiss) and Axiovert 100 inverted microscope (Carl Zeiss, Inc., Thornwood, NY) as described previously (Kim *et al.*, 2011).

7.2. Slug migration test

The cells washed twice with KK2 buffer were centered on KK2 plate. The plate was wrapped with aluminuim foil in order to make the dark condition and incubated at 22°C for 2 ~ 3 days. The foil was removed and then the trails remaining behind slug during migration were transferred to transparency film and stained with Coomassie blue R-250.

7.3. Chemotaxis assay to cAMP

The chemotactic response of cells to cAMP was determined by the two-drop method (Root *et al.*, 1999) using aggregation competent cells. Drop of 1 μl containing roughly 5000 cells was placed 3 mm of a 1 μl drop of 10 μM cAMP on 1% KK2 agar plates. Drops containing either KAx3 or *abpB* RNAi cells were placed on the opposite side of the cAMP drop as positive controls. Plates were incubated at 22°C and observed from 30 min. Movement of cells toward the drop perimeter nearest the cAMP was indicative of a positive chemotactic response.

III. RESULTS

1. Identification of actin bundling protein ABP34 in *Dictyostelium discoideum*

1.1. Isolation and sequence analysis of *abpB* in *D.discoideum*

The gene (*abpB*) encoding ABP34 was identified by searching in the *Dictyostelium* genome sequencing project (http://www.dictybase.org). The nucleotide sequence of the *D. discoideum abpB* consists of an open reading frame (ORF) of 888 bp that encondes a polypetide of 295 amino acids with a calculated molecular weight of 33,352 Da. The deduced amino acid sequence possessed the conserved EF-hand, characteristic of the ABP34 (Fig. 1).

1.2. The level of mRNA expression of ABP34 during development in *D. discoideum*

According to developmental stage, the total RNA was extracted and Northern blot analysis was carried out using radiolabeled cDNA probe. The amount of *abpB* mRNA was increased to the streaming stage and decreased at final culmination stage (Fig. 2). Under dark condition, the tipped aggregates did not culminate and formed migrating slugs. These slug moved towards an optimal environmental where spore dispersal easily occurred. To examine the mRNA expression of *abpB* in *Dictyostelium*, cells were developed on non-nutrient agar plate under dark condition. Expression of *abpB* decreased at 16 hour, and the level of *abpB* mRNA were constant to 22 hour thereafter *abpB* transcript was elevated up at final development (Fig. 2B). These results suggest that the ABP34 might be role during development.

```
  1   ATGGCAGAAACAAAAGTTGCACCAAATCTTACTGGTATTGAGCAAACCAAGGCAGGTCAA
       M  A  E  T  K  V  A  P  N  L  T  G  I  E  Q  T  K  A  G  Q    20
 61   TCCTTCACTGAAAAATTATCAGCTGAAGCTATGGAATTTTTCTGTAATGTTGCCAAATTA
       S  F  T  E  K  L  S  A  E  A  M  E  F  F  C  N  V  A  K  L    40
121   CCATTCTCACAACAAGCTGTTCACTTTTTGAATGCTTATTGGGCTGAAGTTAGCAAAGAA
       P  F  S  Q  Q  A  V  H  F  L  N  A  Y  W  A  E  V  S  K  E    60
181   GCTGAATTCATCTATTCCGTTGGTTGGGAAACAATCAAATATGCTGATATGCATTGCAAA
       A  E  F  I  Y  S  V  G  W  E  T  I  K  Y  A  D  M  H  C  K    80
241   GGTATCCAACTCGTTTTCAAATACGATGAAGGTAACGATTTGGATTTCGATATTGCTCTC
       G  I  Q  L  V  F  K  Y  D  E  G  N  D  L  D  F  D  I  A  L   100
301   TATTTCTATGAACAATTATGCAAATTCTGTGAAGATCCAAAGAACAAAAACTATGCAACC
       Y  F  Y  E  Q  L  C  K  F  C  E  D  P  K  N  K  N  Y  A  T   120
361   ACCTACCCAATCTCTCAACCACAAATGTTGACTGCTCTCAAACGTAAACAAGAATTAAGA
       T  Y  P  I  S  Q  P  Q  M  L  T  A  L  K  R  K  Q  E  L  R   140
421   GAAAAAGTCGATGTCAATTTCGATGGTCGTGTCTCTTTCCTCGAATATCTCTTATATCAA
       Y  K  D  F  A  N  P  A  D  F  C  T  R  S  M  N  H  D  E  H   160
481   TACAAAGATTTCGCCAATCCAGCTGATTTCTGTACTCGTTCAATGAACCACGATGAACAT
       P  E  I  K  K  A  R  L  A  L  E  E  V  N  K  R  I  R  A  Y   180
541   CCAGAAATCAAAAAAGCTCGTTTAGCTCTCGAAGAAGTCAACAAACGTATTCGTGCTTAC
       E  E  E  K  A  R  L  T  E  E  S  K  I  P  G  V  K  G  L  G   200
601   GAAGAAGAAAAAGCCCGTTTAACCGAAGAATCAAAGATTCCAGGTGTCAAAGGTCTCGGT
       A  T  N  M  L  A  Q  I  D  S  G  P  L  K  E  Q  L  N  F  A   220
661   GCCACAAACATGCTCGCTCAAATTGATAGTGGTCCATTAAAGGAACAACTCAACTTTGCC
       T  T  K  L  H  S  Q  G  K  L  I  P  L  L  Q  E  A  G  L  L   240
721   CTTATCTCTGCTGAAGCTGCTGTTCGTACTGCTTCAAAGAAATATGGTGGTGCTGCTTAT
       L  I  S  A  E  A  A  V  R  T  A  S  K  K  Y  G  G  A  A  Y   260
781   TCAGGTGGTGCTGGTGATGCTGGTGCTGGTTCCTCTGCTGGTGCCATTTGGTGGATGAAT
       S  G  G  A  G  D  A  G  A  G  S  S  A  G  A  I  W  W  M  N   280
841   CGTGATTTAGAAGAAAAGAAAAAGAGATACGGTCCACAAAAGAAATAA
       R  D  L  E  E  K  K  K  R  Y  G  P  Q  K  K  *               295
```

Fig. 1. Nucleotide and deduced amino acid sequences of ABP34 from *Dictyostelium dicoideum*. The nucleotide sequence of the *D. discoideum abpB* consists of an ORF of 888 bp that encodes a polypeptide of 295 amino acids with a calculated molecular mass of 33.4 kDa.

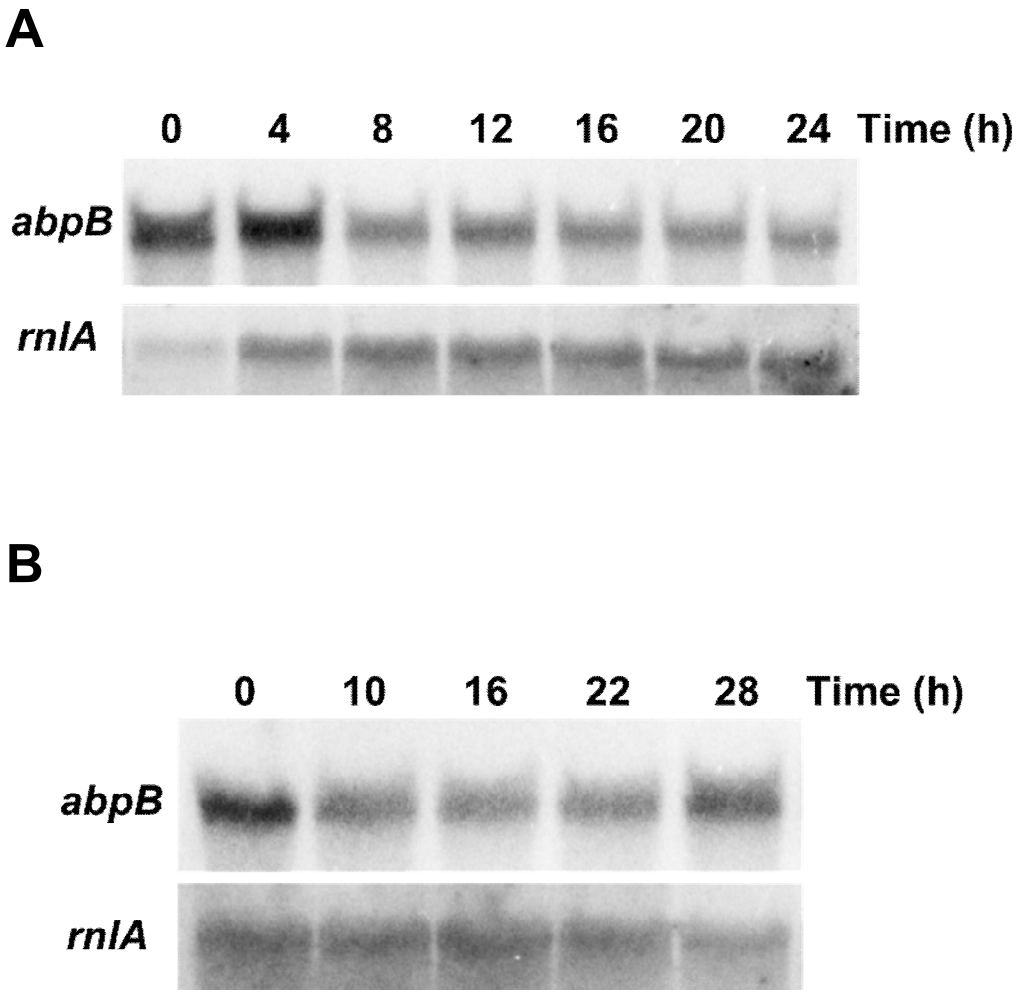

Fig. 2. Determination of expression level of *abpB* during development. (A) in light condition (B) in dark condition. Total RNA samples (20 μg) were isolated from KAx3 wild type strains, and subjected to Northern blot analysis, which used *abpB* probe. The *rnlA* probe was used as a loading control.

1.3. Overexpression and RNA interference-mediated gene silencing of ABP34 in *D. discoideum*

1.3.1 Confirmation of mutant strains

To understand the roles of ABP34 in *Dictyostelium*, we generated ABP34 overexpressing and *abpB* RNAi-silenced mutant strains (Fig. 3). Northernblot assay showed that *abpB* was overexpressed successfully in $ABP34^{OE}$ cells. Despite numerous attemps, it has failed to obtain *abpB*-null cells by homologous recombination by disruption construct including bsr cassett. Using antisence mRNA construct, it also failed to select stable cell lines with reduced expression level of ABP34. So, we generated the *abpB*-underexpressing stain (*abpB* RNAi) by expression *abpB* RNAi-silence (Martens *et al.*, 2002) (Fig. 3). The *abpB* gene of *D.discoideum* which encodes the actin bundling protein ABP34 was silenced by RNAi. RNA interference by double-stranded RNA (dsRNA) has been applied efficiently to silence genes in various organisms ranging from fungi and nematodes to plants. dsRNA has been introduced into organisms by microinjection (Fire *et al.*, 1998), by transformation with gene constructs generating complementary RNAs or fold-back RNA (Wang *et al.*, 2000), or by feeding an organism with *Escherichia coli*-expressing dsRNA (Kamath *et al.*, 2001). Recently, this mechanism (Martens *et al.*, 2002) can be applied to *Dictyostelium* ABP34. To express fold-back RNA in *Dictyostelium*, 5′ 300 bp fragment of *abpB* gene and full open reading frame were ligated into EXP-4(+). We found a variety of silencing levels of *abpB* in different mutant cell lines. Northern blot analysis showed that about 80 to 90% of *abpB* mRNA level was reduced compared to wild type cells and one of these cell lines (*abpB* RNAi) was used for further experiments. Thus, cell lines with strongly reduced

mRNA levels were used in these studies.

To overexpress ABP34, the complete cDNA was cloned into pTX flag vector, and transformed into *D. discoideum*. After selection, indefendent transformants were analysed by western blot for protein expression of ABP34 (data not shown). All of them overexpressed the protein to similar extents, one of these cell lines ($ABP34^{OE}$) was chosen for further experiments. But the phenotype was not different to KAx3.

1.4. Localization of ABP34 in *D. discoideum*

ABP34 has generally found in the filopodia and pseudopodia, and cell-cell contact sites, suggensting participation in diverse cell movements during *Dictyostelium* life cycle (Rivero *et al.*, 1996). The localization of ABP34 and F-actin was also observed in the cell by fluorescence microscopy. GFP-ABP34 was expressed in *D. discoideum* cells (Fig. 5) and F-actin was stained with TRITC-phallodin. As shown in Fig. 5A, ABP34 and actin filaments were co-localized in cell cortex of single cell. Association of ABP34 with F-actin suggests that ABP34 has the binding ability to F-actin *in vivo*.

1.5. Growth properties of ABP34 underexpressing cells

Growth rate were investigated in axenic HL5 medium liquid culture. $ABP34^{OE}$ cells and KAx3 showed similar growth rate in HL-5 medium (Data not shown). However, *abpB* RNAi cells grew more slowly than KAx3 (Fig. 4B). Moreover, when *abpB* RNAi cells were shaken in HL-5 medium, the mutant cells were observed smaller size than wild type cells (Fig. 4A).

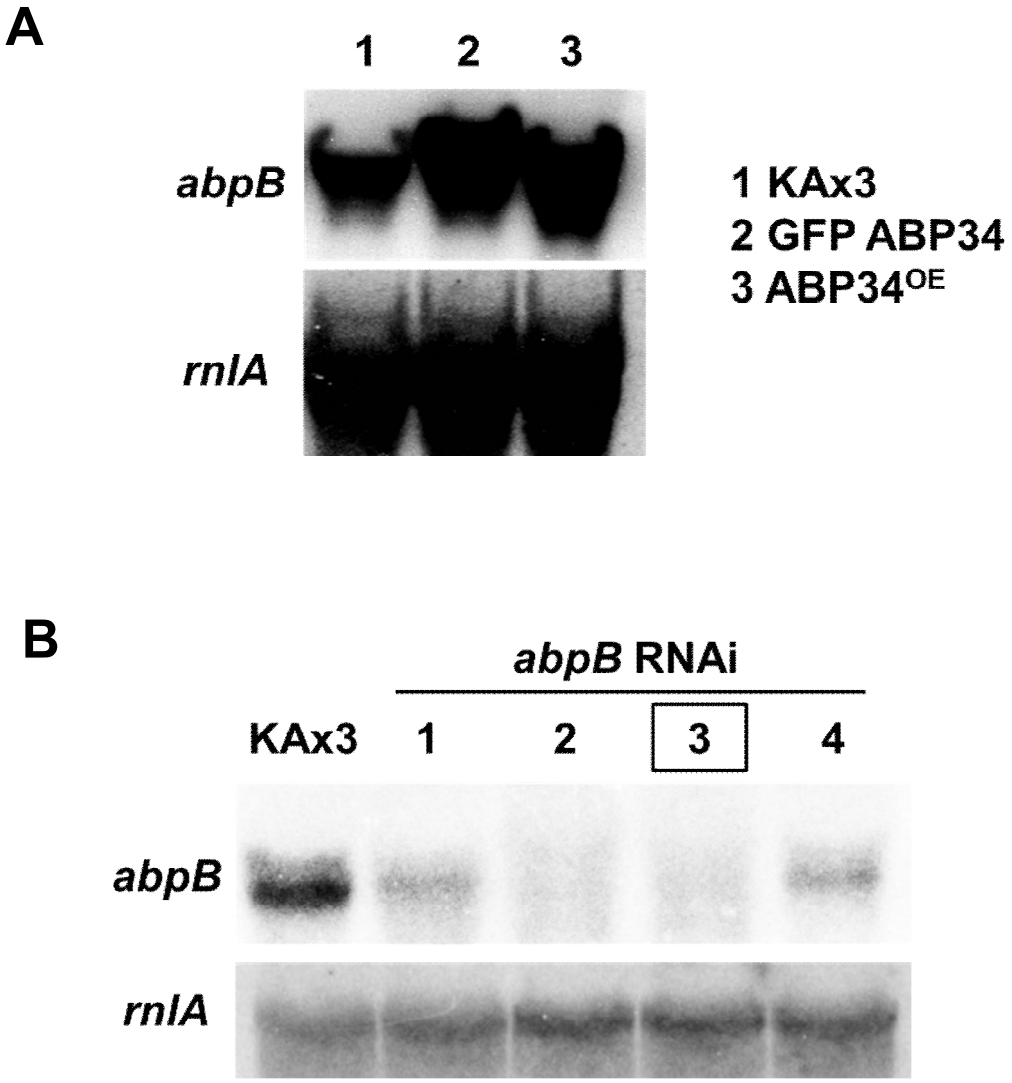

Fig. 3. Production of *abpB* mutant strains in *Dictyostelium discoideum*. (A) Prodcution of *abpB* overexpression strains. (B) Prodcution of *abpB* RNAi underexpression strains. The strain number 3 was selected and used this study. Total RNA samples (20 μg) were loaded from KAx3 and *abpB* mutant strains, and subjected to Northern blot analysis, which used *abpB* probe. The *rnlA* probe was used as a loading control.

1.6. Developmental properties of ABP34 underexpressing cells

When *Dictyostelium* cells starve, they enter a developmental cycle leading from single amoebae to a multicellular fruiting body. About 6 h after starvation is initiated, the amoeba start to aggregate. After formation of tight aggregation a tip appears on top of the mounds and the aggregates elongates and rise into the air.

To examine the developmental phenotype, axenically grown cells were developed on non-nutrient agar plate under light- or dark-condition. When developed, *abpB* RNAi showed smaller size morphological structure of fruiting body (Fig. 8) and displayed the defect in slug migration (Fig. 9). The *abpB* RNAi strains displayed a rapidly developing phenotype (Fig. 7). KAx3 initiated culmination around 20 h under light condition, but *abpB* RNAi cells had begun by 16 h. Moreover, the mutant was shown short abnormal migrating slugs when developed under dark environmental conditions which promote slug formation. The filopodia are slender cellular protrusions that dynamically extend and retract to facilitate directional cell migration.

1.6.1. Developmental gene expression of the mutants

In order to analyse the pattern of gene expression during development, cells were starved on KK2 agar plate and RNA was extracted at time intervals (Fig. 10). To investigate the reason for aberrant phenotype of *abpB* RNAi, we exmined the expression levels of prespore/prestalk-specific genes and genes encoding cell–cell adhesion molecules using Northern blot analysis in KAx3 and *abpB* RNAi mutant strains. In *abpB* RNAi, lower expression of the prespore/spore-specific genes, which included *cotC*, *pspA* and *spiA*, was detected. However, the expression levels of the prestalk-

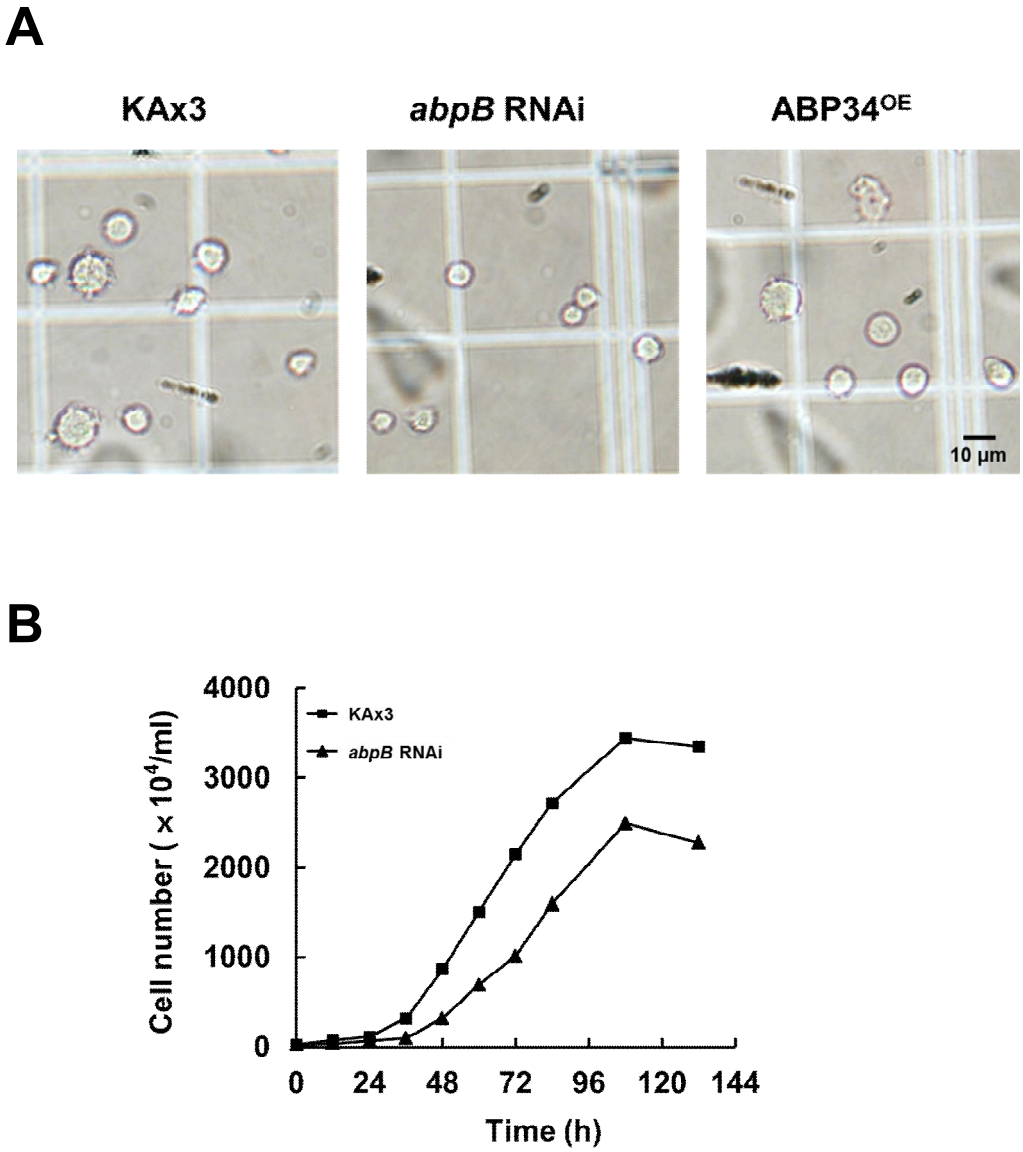

Fig. 4. Comparison of cell size and growth rate KAx3 and *abpB* RNAi strain. (A) Comparision of cell size of KAx3 and *abpB* RNAi**.** Each of the squares is 50 μm ×50 μm. (B) Growth of KAx3 and *abpB* RNAi strain. The cultures were shaken at 22˚C and cell numbers were determined at the indicated times by hemacytometer counters.

A

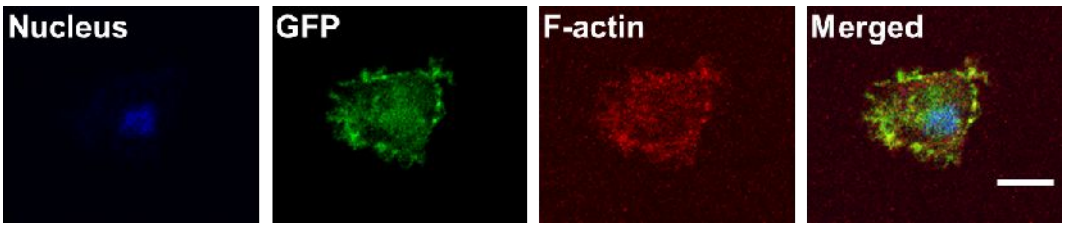

B

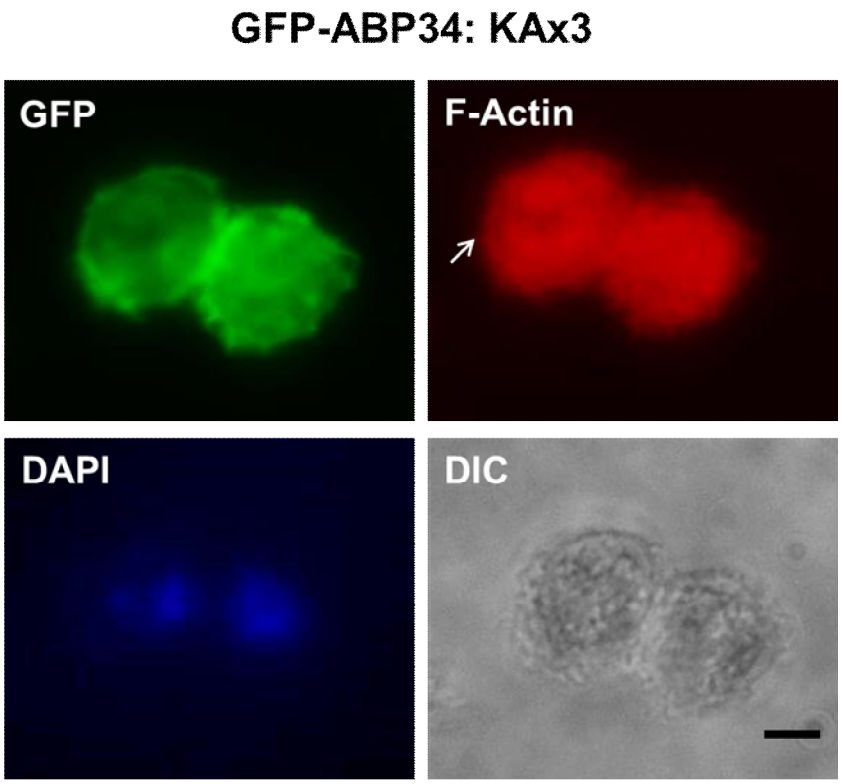

Fig. 5. Localization of F-actin and GFP-ABP34 in KAx3. Cells that express GFP-ABP34 was fixed and F-actin staining was performed using TRITC-conjugated phalloidin, and DAPI was labeled nuclei in cells, The DIC is phase-contrast images. The scale bar represents 5 μm.

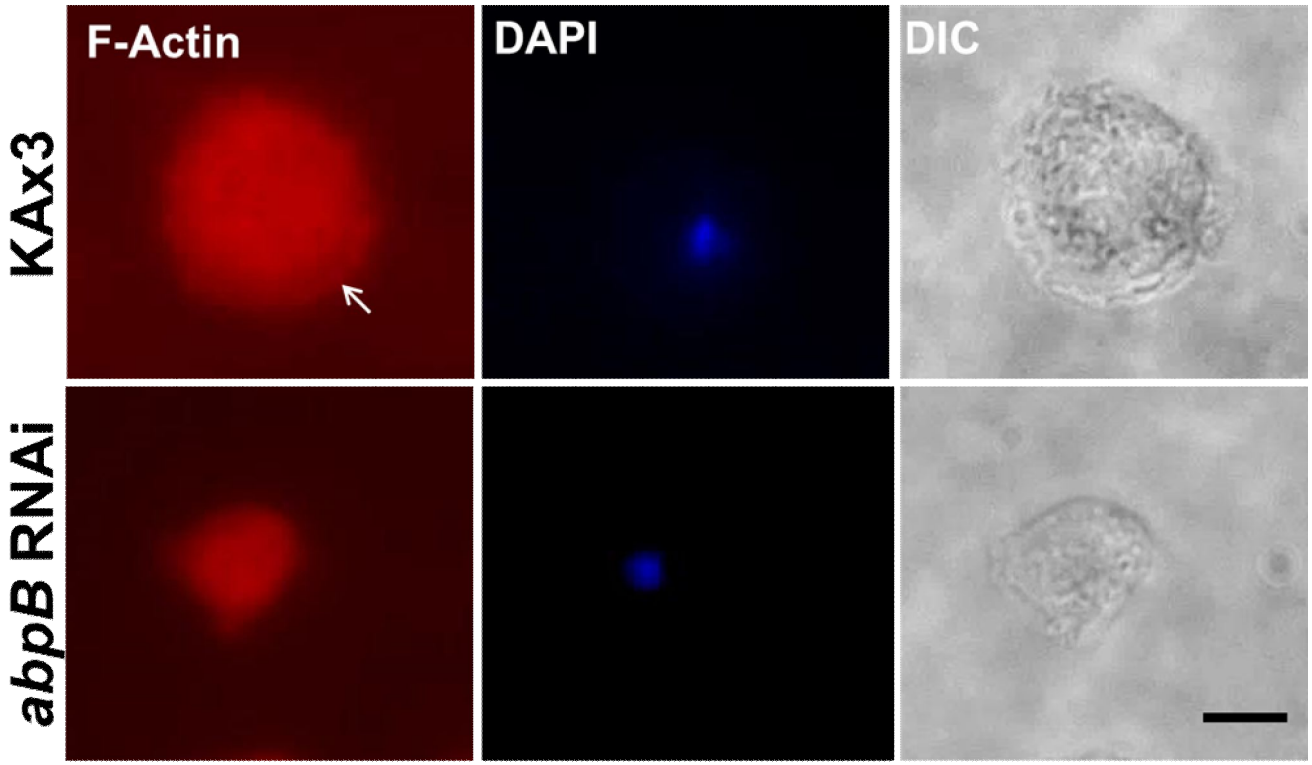

Fig. 6. Distribution of cortical F-actin in KAx3 and *abpB* RNAi strains. Double immunofluorescence staining was performed using TRITC-conjugated phalloidin to label actin filaments and DAPI to label nuclei in cells, which were grown in suspension. The left panels show the staining for actin filaments. The middle panels show DAPI staining. The scale bar represents 5 μm.

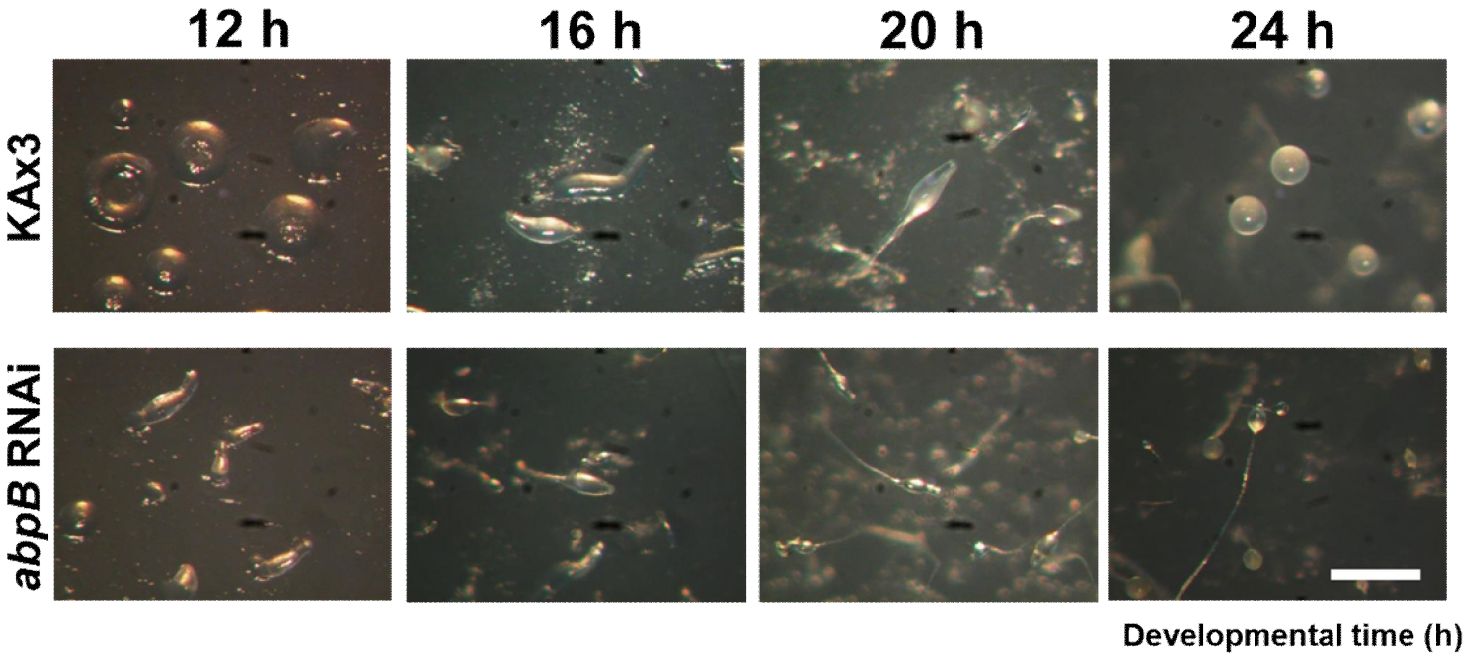

Fig. 7. Developmental morphology of KAx3 and *abpB* RNAi strain under light condition.

Dictyostelium cells were developed on the agar plates under light condition and photographed at the indicated time point. The scale bar represents 0.5 mm.

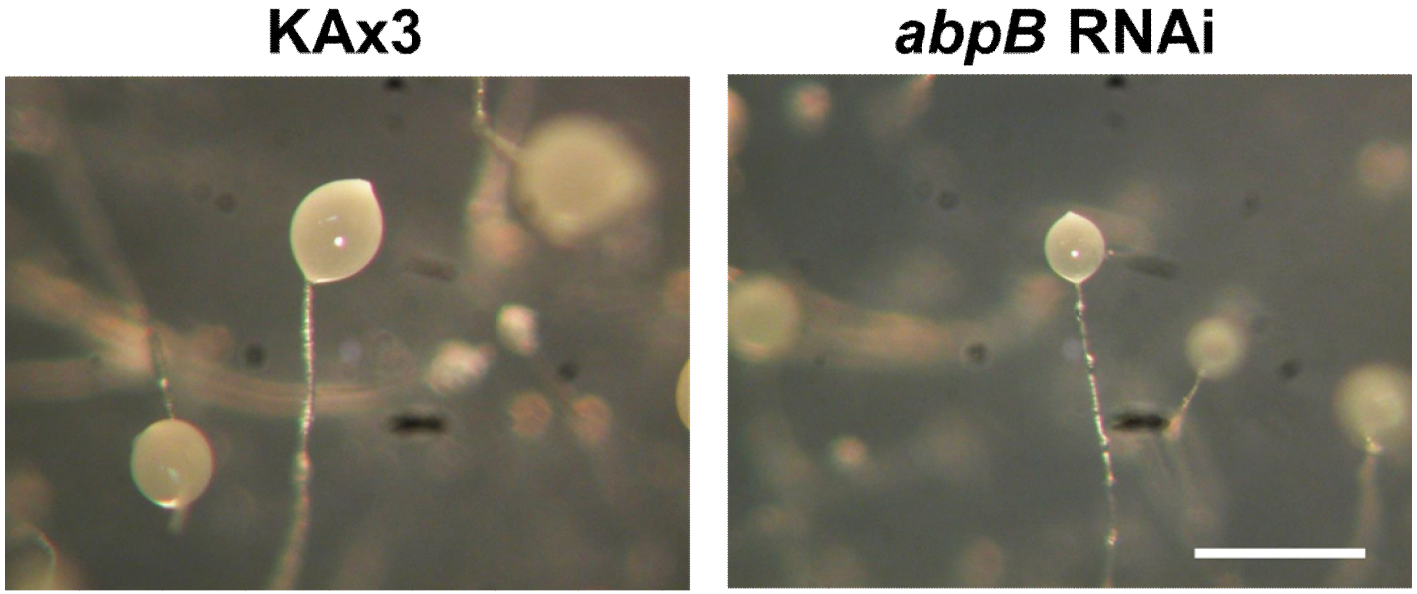

Fig. 8. Developmental morphology of KAx3 and *abpB* RNAi cells.

Cells developed on non-nutrient agar plates was observed fruiting body of KAx3 and abpB RNAi mutant. The scale bar represents 0.5 mm.

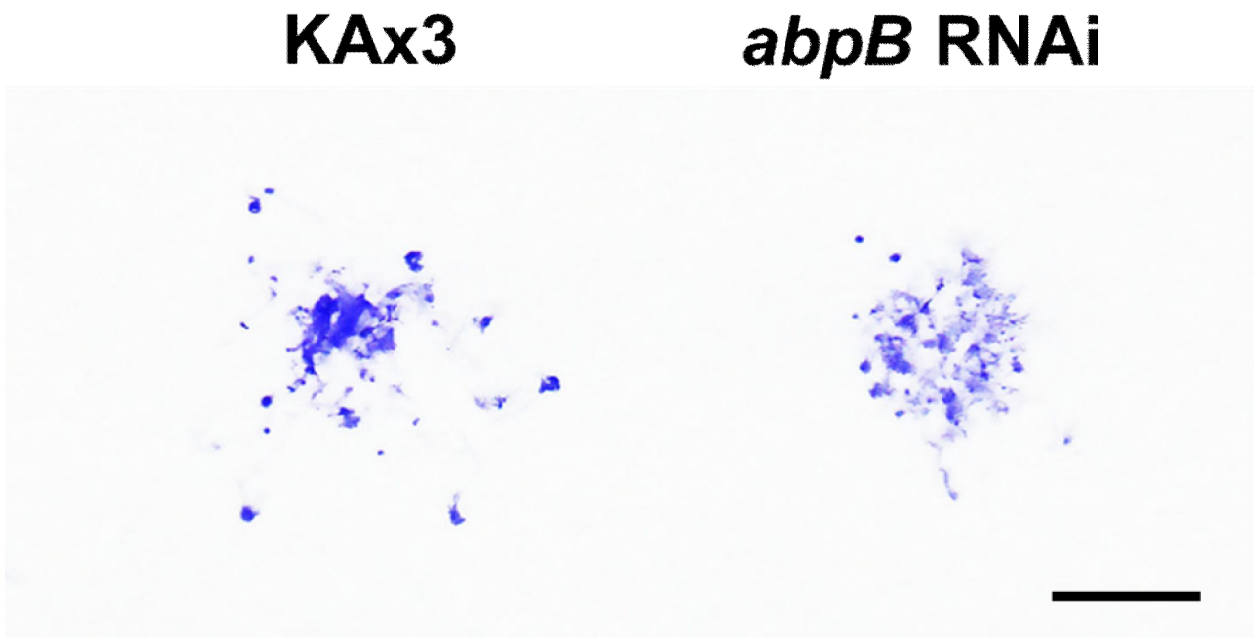

Fig. 9. Migration of slugs under dark condition of KAx3 and *abpB* RNAi strain.
Cells were developed on agar paltes under dark condition and after 40 hours of development, resultant slugs, spores and slime tails were transferred to a transparency film, which stained with Coomassie Blue. The panels show the tracks of slugs migration. The scale bar represents 10 mm.

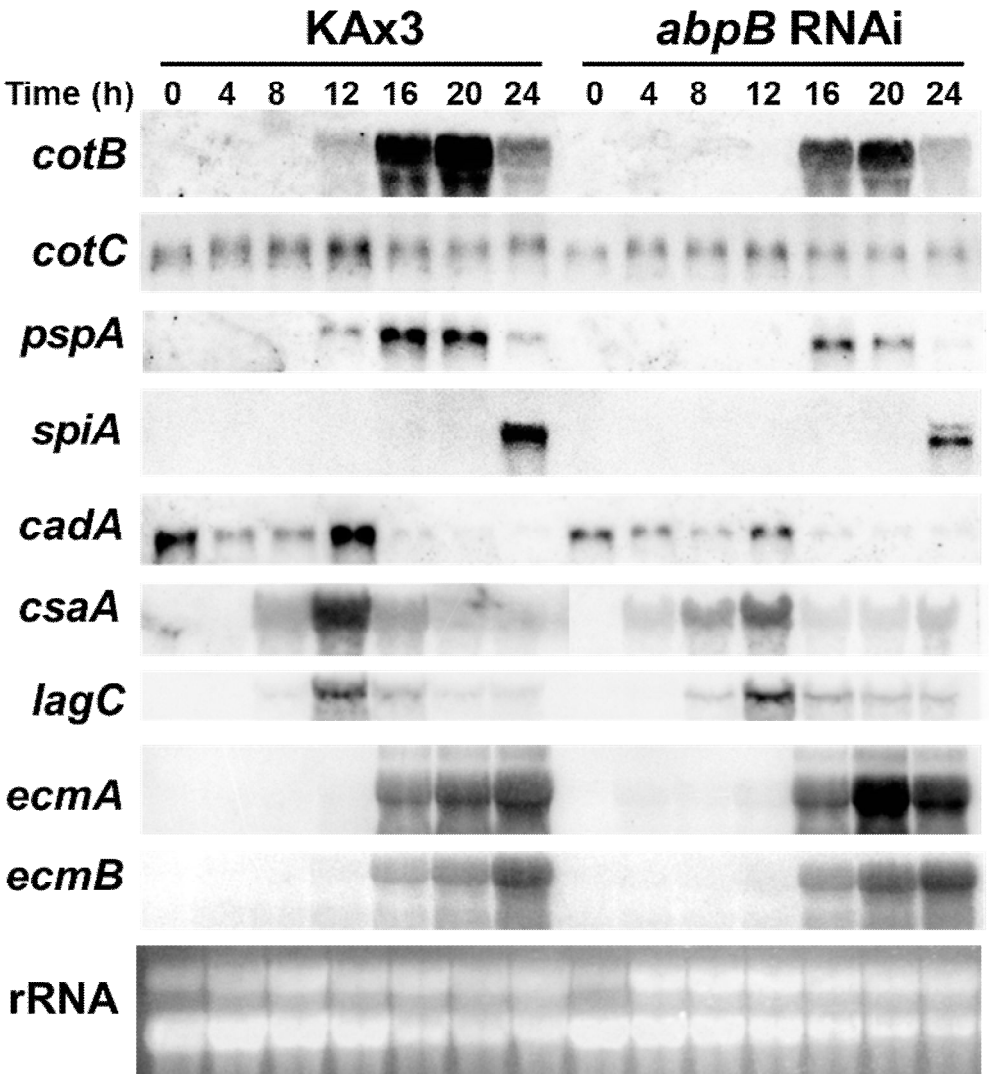

Fig. 10. The expression analysis of genes related to development in KAx3 and *abpB* RNAi strain. Northern blots were performed using fragments of the indicated genes as hybridization probes. *cotB, cotC* and *pspA*, prespore-specific; *spiA*, spore-specific; *cadA* and *csaA*, aggregation-specific; *lagC*, post-aggregative genes; *ecmA* and *ecmB,* prestalk-specific; rRNA was used as a loading control.

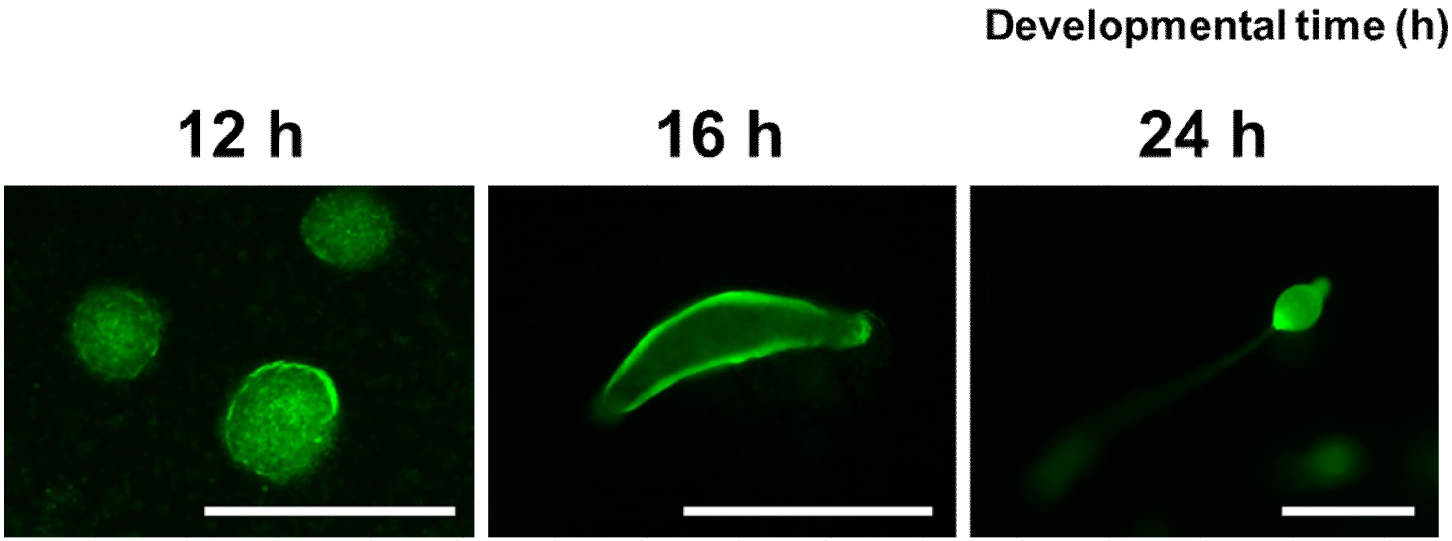

Fig. 11. Localization of GFP-ABP34 in KAx3 cells during development.

Dictyostelium cells were developed on non-nutrient agar plate and images were obtained by Axiovert 200M fluorescence microscope. The left panel is aggregate at 12 hour from development start, middle panel is slug at 16 hour and right panel is fruiting body that is concentrated with GFP-ABP34. The scale bar represents 0.5

specific genes, *ecmA* and *ecmB* were higher than those in KAx3 (Fig. 10). These results are consistent with the morphological analysis. *abpB* RNAi also produced samll fruiting bodies (Fig. 8). These results imply that ABP34 regulates spore size by expression of prespore/spore-specific genes.

1.7. ABP34 associates with spore during development

ABP34 has generally found in the filopodia and pseudopodia, and cell-cell contact sites, suggensting participation in diverse cell movements during *Dictyostelium* life cycle (Rivero *et al.*, 1996). To further characterize the ABP34, we analysed the developemental expression of ABP34 in GFP-ABP34. When wild-type cells expressing act15/GFP (which is uniformly expressed in all type cells) was plated for development. As represented in Fig. 11, ABP34 was found in posterior slug region consisting of prespore cells, while it was detectable weak in the anterior orgarnizer region (prestalk cells) of the slugs and the GFP remained absent during later stages in the upper cup of fruiting bodies as well as mature stalk cells. Most of the GFP-ABP34 cells in slugs were localized to the prespore region and concentrated in spore cells (Fig. 11). These results suggest that ABP34 is required in terminal differentiation and fruiting body formation for efficient spore formation.

2. Identifiction of actin bundling protein ABP34

2.1. Expression and purification of ABP34

To identify actin binding proteins from *Dictyostelium*, ABP34 recombinant protein was overexpressed in *E. coli*. The purification procedure is described in material and methods. The overexpressed cells sonicated to soluble proteins. After centrifugation of cell crude that supernatant was applied to a DEAE-anion exchange column. Most of the proteins found in flow through. Subsequently, the fraction of containing ABP34 protein was concentrated and was applied to a gel filtration column with the application of EGTA containing buffer. Gel filtration of the proteins on Superdex 75 yielded the ABP34 protein and two peak fractions of the contamination proteins which were separated by chromatography on Mono Q Sepharose. The ABP34 was then eluted pure protein by chromatography in this column. The typical purification yielded about 40 mg/ml of the ABP34 protein with purity >95% from 0.5 liter culture of overexpressing *E. coli* cells of total lysate protein.

2.2. Recombinant ABP34 is monomer in solution

We characterized the molecular properties of recombinant purified native ABP34 protein. The native molecular weight was directly determined by the gel permeation chromatography in column of Superose 6. To confirm the oligomeric state in solution, purified native ABP34 proteins was applied to the column with molecular weight standards (Sigma-Aldrich) pre-equilibrated with 10 mM HEPES (pH7.5) containing 150 mM NaCl. (Fig. 13). Standard curve was generated by plotting the logarithm of molecular

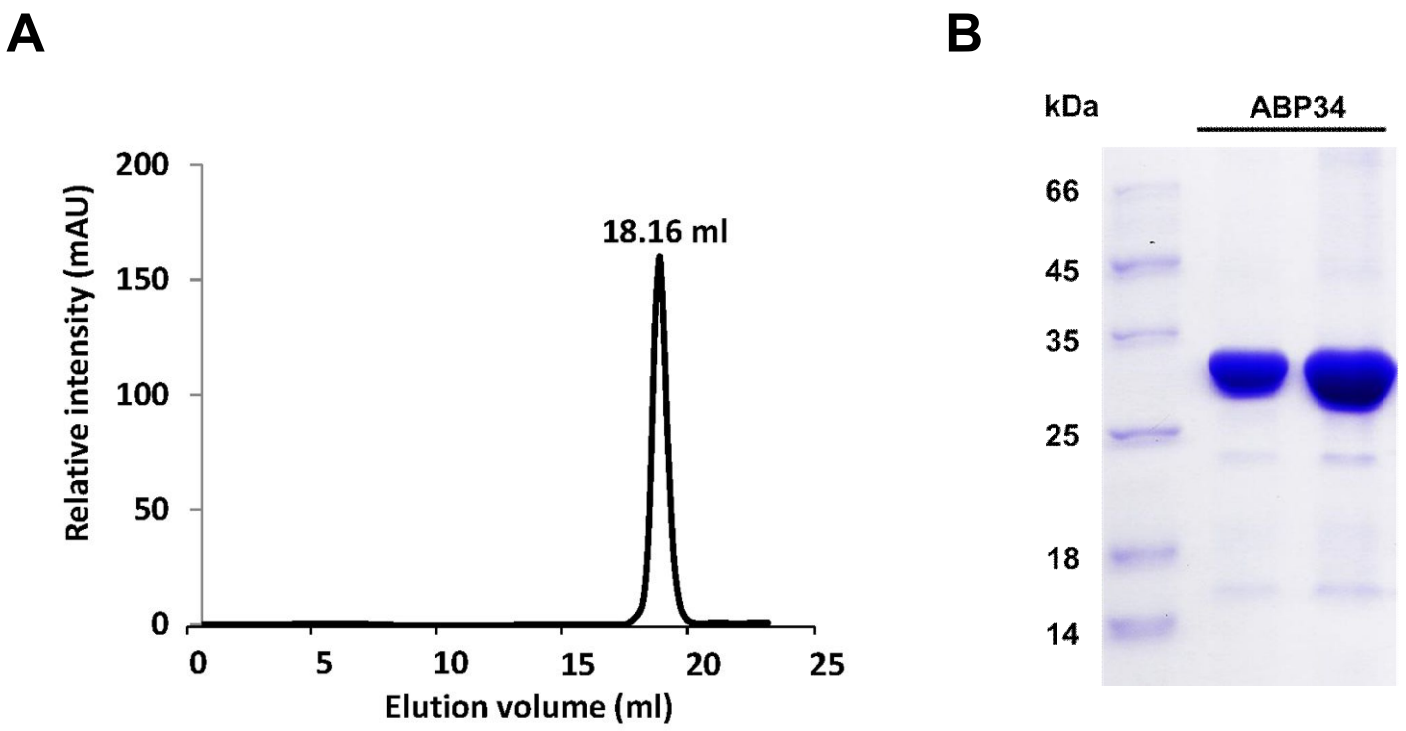

Fig. 12. Size exclusion chromatography of ABP34. (A) The purified ABP34 was loaded on superose 6 gel permeation column. ABP34 peak was eluted at 18.16 ml from injection. (B) Purified ABP34 was confirmed with SDS-PAGE. Lane left, molecular-mass markers, lane right, and purified recombinant ABP34 protein.

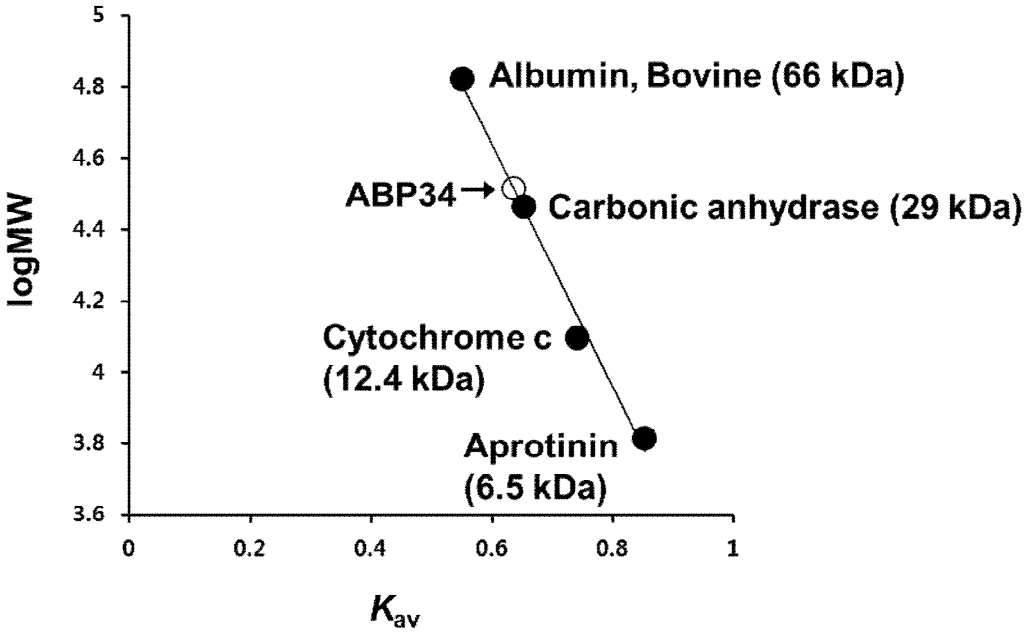

Fig. 13. Determination of oligomeric state of ABP34. Oligomeric state of ABP34 was analysed by gel filtration chromatograhpy. Predicted molecular mass of ABP34 is 32,836 Da (K_{av} = 0.63), indicating that ABP34 exists as a monomer in solution.

mass of standard proteins against their K_{av}, where $K_{av}=(V_e-V_o)/(V_t-V_o)$: V_e, elution volume; V_o, void volume; V_t, total bed volume. K_{av} of ABP34 determined by using the same column was compared to the profile of protein standards; Bovine serum albumin (66 kDa), carbonic anhydrase (29 kDa), cytochrome c (12.4 kDa), aprotinin (6.5 kDa). This calculated molecular weight of native ABP34 was 32,836 Da from the plot of standard proteins (Fig. 13). The measured native molecular weight, therefore indicating that protein existed predominantly as highly soluble monomer in solution. The elution of the ABP34 protein from a column was not significantly affected by changes in the buffer conditions (data not shown). And estimated by gel electrophoresis, apparent molecular mass was also approximately 34 kDa. These results suggested that ABP34 behaves as a monomer in native state. In addition, all of the analysis from chemical crosslinking, analytical ultracentrifugation and gel filtration indicate monomeric structure of the native protein (Fechheimer and Taylor, 1984; Lim *et al.*, 1999). ABP34 was not observed conformational change upon environmental Ca^{2+} concentration changes and Ca^{2+} is bound at crystal structure when ABP34 presence in alone (Fig. 14, 15). These results suggested that ABP34 could act all Ca^{2+} binding conformation when ABP34 bound to F-actin. Possibly, ABP34 could form dimer due to conformational change induced upon binding to actin. ABP34 are unstable at oligomeric forms in solution thus that the proteins are short lived in vitro (Lim *et al.*, 1999).

2.3. Far-UV CD spectra of recombinant ABP34

Circular dichroism (CD) spectroscopy is frequently used technique for evaluation of protein conformation in solution. As predicted by secondary

structures of ABP34, the protein is highly helical structure. The far-UV CD spectra of native ABP34 has the characteristic minima at 210 and 220 nm, showing that the protein has a high contents of α-helical secondary structure (Fig. 15). In *Dictyostelium*, ABP34 has bundling activity that is inhibited by micromolar calcium ion (Fechheimer, 1987). Structural change of ABP34 in calcium induced and absence state was determined. The CD spectra of ABP34 addition of Ca^{2+} were not conformational rearrangement to that of the native ABP34. Addition of calcium up to 5 mM to the assay has no influence on the ABP34 structure. In addition of EGTA, the ABP34 protein was detected almost identical spectra to that of the native ABP34. According to the results, there is no spectral change in ABP34 addition of EGTA or Ca^{2+}, indicating that native ABP34 have a fixed structure in vitro without F-actin. Actually, according to the crystal structure of ABP34, due to tightly Ca^{2+} binding in EF-hand of ABP34 that might not affect conformational change. Furthermore, we generated protein in Ca^{2+} binding EF-hand by site direct mutagenesis. However native protein and mutant proteins show the same secondary structure content as estimated by the far-UV CD spectra (Fig. 16, 17). The CD spectroscopy results give evidence for that the ABP34 construct is a stable, folded molecule, and that it has highly α-helical structure. This suggests that Ca^{2+} binding structure of ABP34 is important for stable folding and may be significant to biological activity. The conformation displayed by ABP34 when bound to F-actin is unknown. The possibility of conformational change could require when ABP34 binds to F-actin in extended conformation.

2.4. Recombinant ABP34 retains actin-bundling activity

2.4.1. F-actin binding of ABP34

To directly measure the actin binding activity of ABP34 protein, we used high speed centrifugation sedimentation assay. The co-sedimentation assay of ABP34 and F-actin was analyzed by ultracentrifugation. When ABP34 protein bound to F-actin filaments are bundled in the pellet after centrifugation. ABP34 and actin filaments were incubated at 4°C for 24 hour and centrifuged at 115,000×g for 30 min. To stoichiometry binding of the ABP34 proteins, F-actin and ABP34 were used 20:1 ratio of concentration (Fechheimer and Taylor, 1984). And F-actin co-sedimentation was performed as established previously (Fechheimer and Taylor, 1984; Lim and Fechheimer, 1997) as function of the ABP34 at low free calcium concentration condition. All assays were performed in presence of low free calcium concentration to attest of actin binding. High speed centrifugation revealed that the presence of ABP34 in pellets indicates F-actin binding, while ABP34 remained supernatant in the absence of actin. ABP34 remaining in the supernatant does not bind F-actin. The mixture of ABP34 and F-actin were existed both ABP34 and F-actin in the pellet (Fig. 18). Mutant proteins of EF-hand bind also F-actin (Fig. 19, 20). This indicates that the ABP34 bound to F-actin in the ABP34 with actin. Therefore, ABP34 protein has ability to bind with actin.

2.4.2 ABP34 induces actin bundling

Next we analyzed the specificity of bundling of purified ABP34 to F-actin. F-actin bundling ability of ABP34 was examined by electron microscopy after negative staining. The reaction mixtures of ABP34 and F-actin were incubated with 0.25 mM $CaCl_2$ and 5 mM EGTA for overnight on.

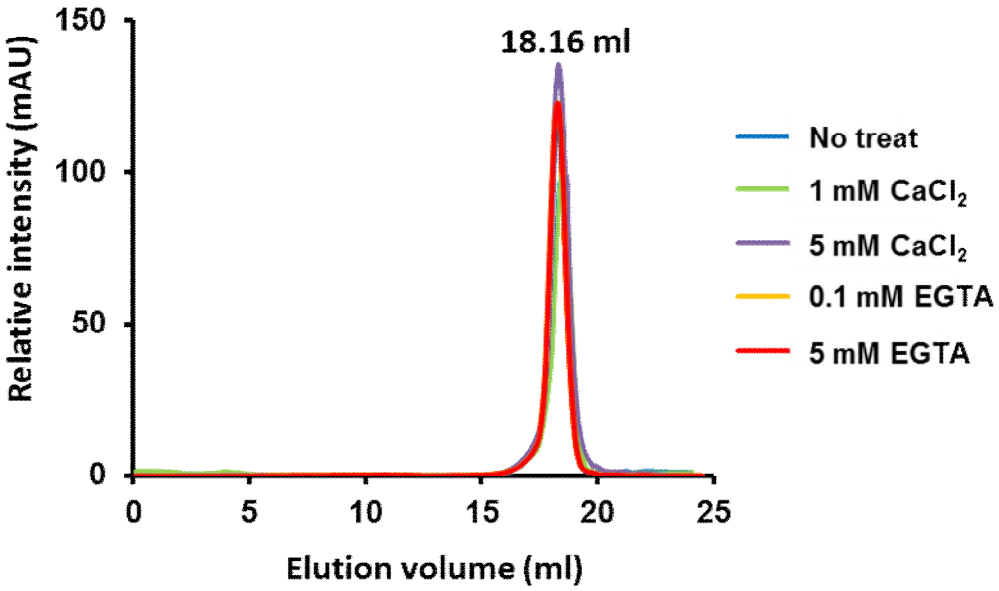

Fig. 14. Analytical gel filtration profile of ABP34. Purified ABP34 was applied onto Superose 6 10/300 GL size-exclusion column. ABP34 peak was eluted at 18.16 ml from injection. Each elution peaks were detected in presence of 1 mM $CaCl_2$, 5 mM $CaCl_2$, 0.1 mM EGTA, 5 mM EGTA, repectively in the buffer containing 10 mM HEPES pH 7.4, 100 mM NaCl. Concentration of ABP34 was approximately 10 μM of each elution peak.

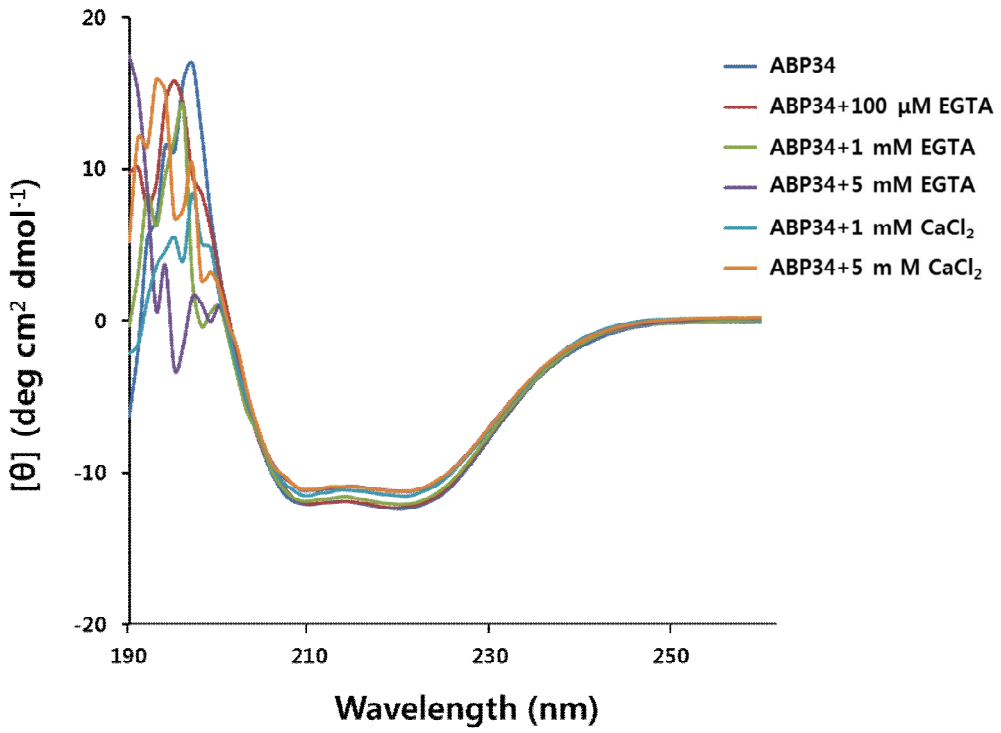

Fig. 15. Far-UV CD spectra of ABP34. The far-UV CD spectrum (190 ~ 270 nm) were recorded on Jasco J-815 spectropolarimeter at 25°C. Protein concentration was approximately 6 μM. Each protein was measured in presence of EGTA or calcium in 10 mM HEPES buffer, pH 7.4, 100 mM NaCl. Measured ellipcities were converted to molar ellipticity [θ], and the quantification of the secondary structure contents were carries out with the self-consistent method.

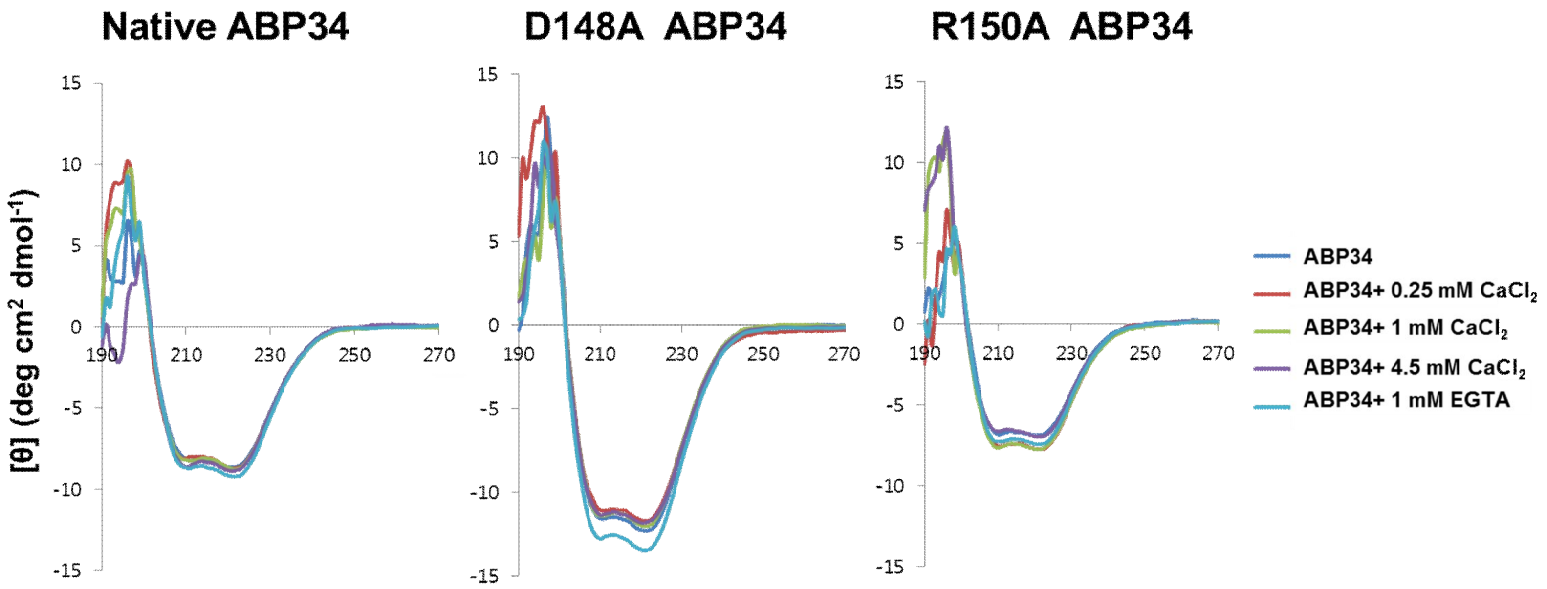

Fig. 16. Far-UV CD spectra of native and mutant ABP34. The CD spectrum (190 ~ 270 nm) were carried out in 10 mM HEPES buffer pH 7.4 containing 100 mM NaCl with or without EGTA and $CaCl_2$. The protein concentrations in the samples were 6 μM.

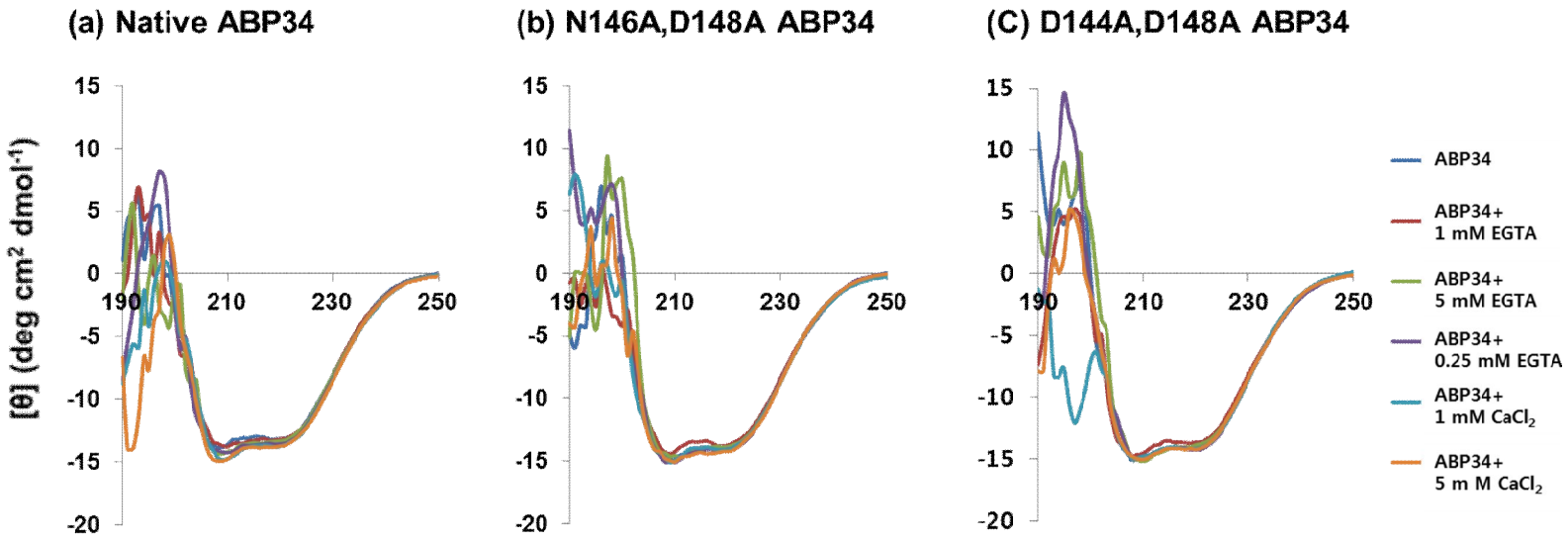

Fig. 17. Far-UV CD spectra of native and double mutants ABP34. The far-UV CD spectrum (190 ~ 250 nm) were recorded on Jasco J-815 spectropolarimeter at 25°C. Proteins concentration was approximately 6 μM. Each protein was measured in presence of EGTA or calcium in 10 mM HEPES buffer, pH 7.4, 100 mM NaCl.

ice to formation of crosslinking structures. The F-actin and ABP34 concentration was used 5 μM and 1 μM respectively. The electron micrographs of the ABP34 bound actin filaments are shown in Fig. 21. The figure shows that the ABP34 induce bundle formation of actin filaments. The bundle is generated when actin was mixed with the ABP34 in a 5:1 ratio (Fig. 21). In contrast, the condition of filamentous actin alone condition, F-actin appears disordered long filaments. This structure was not observed when mixture of actin filament and ABP34 was present large actin bundles under identical condition. Upon higher magnification, ABP34 with F-actin mixture generated highly ordered bundle that contained several fold of parallel actin filaments. Therefore, these results confirmed that purified ABP34 had F-actin bundling activity. These results identify the 34 kDa proteins that contribute to the positive cooperative formation of F-actin bundles.

2.5 ABP34 binds to the actin cytoskeleton *in vivo*.

ABP34 is an F-actin bundling protein that crosslink actin filament in Ca^{2+}-dependent. ABP34 also show diverse distributions in cytoplasm, cell cortex, leading and trailing edges, phagocytic cup and cell-cell contact sites (Fechheimer, 1987; Fechheimer *et al.*, 1994; Furukawa *et al.*, 2003). To determine whether ABP34 localizes with actin in the cell, GFP-tagged recombinant proteins were overexpressed in the wild-type *Dictyostelium* cell AX3. Cells transfected with GFP-tagged ABP34 were assessed by Northern blot analysis and fluorescence microscopy to confirm expression of GFP. The expression level of *abpB* was assayed by Northern blotting using *abpB* probe encoding the ABP34 protein. The C-terminal GFP-tagged cells were

expressed at level higher than *abpB* of wild-type. The localization of the ABP34 protein and F-actin were investigated in wild type cell expressing GFP-fused ABP34 and stained using TRITC-conjugated phalloidin to label actin filaments in *Dictyostelium discoideum* cells (Fig. 23). The subcellular localization of ABP34 relative to actin distribution was observed in cells expressing GFP-ABP34 (Fig. 23). GFP-ABP34 fluorescence was detectable in both the central region and cortical region of the cell. But GFP-ABP34 was enriched almost in filopodia and cell cortex. The ABP34 proteins were selectively incorporated into filopodia as reported previously (Fechheimer, 1987). The regions known to contain actin filament also localized at cell cortex and cytoplasm cytoskeleton. The location of F-actin stained with phalloidin to the GFP labeled ABP34 protein was identical. Overlay image show localization of GFP-ABP34 with cortical F-actin in same region. The enrichment to F-actin relatively in the cortex Thus, ABP34 actin bundling proteins that colocalize with the cortical actin cytoskeleton in *Dictyostelium*. These observations suggest that bundling activity of ABP34 could localize same region with actin filament by cross-linking. Consequently, ABP34 regulates actin crosslinking in cortical structure such as filopodia.

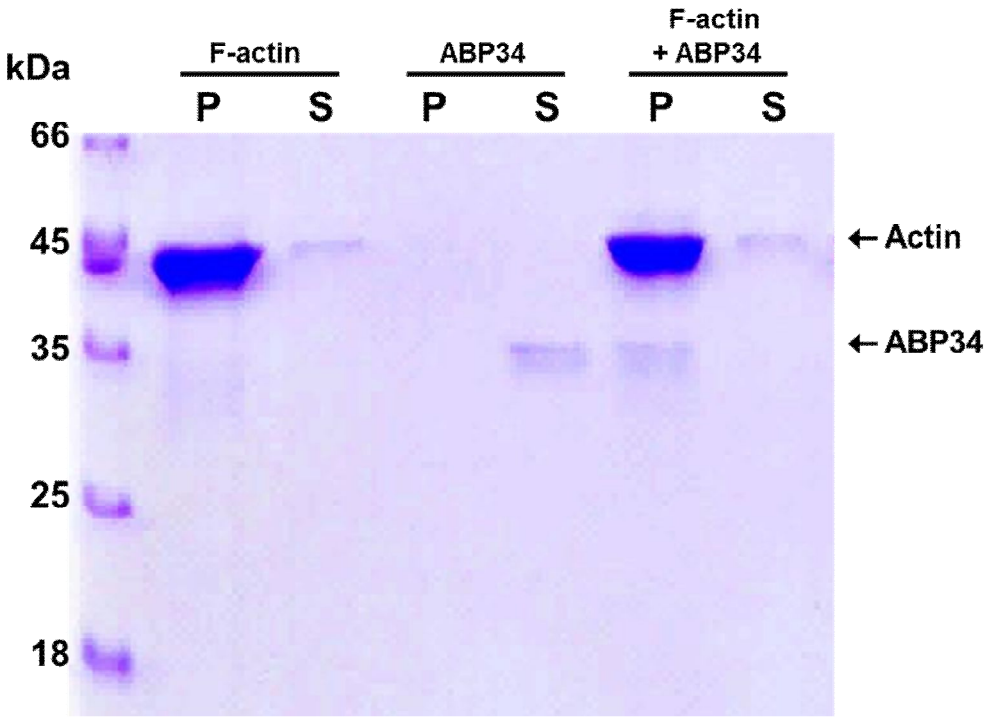

Fig. 18. ABP34 binds actin filaments in vitro. ABP34 and actin filaments were incubated at 4°C for 24hour and centrifugated at 115,000 ×g for 1hour. ABP34 and actin proteins in the pellets (P) and supernatants (S) were separated by 12% SDS-PAGE after centrifugation. Gel was stained with Coomassie blue.

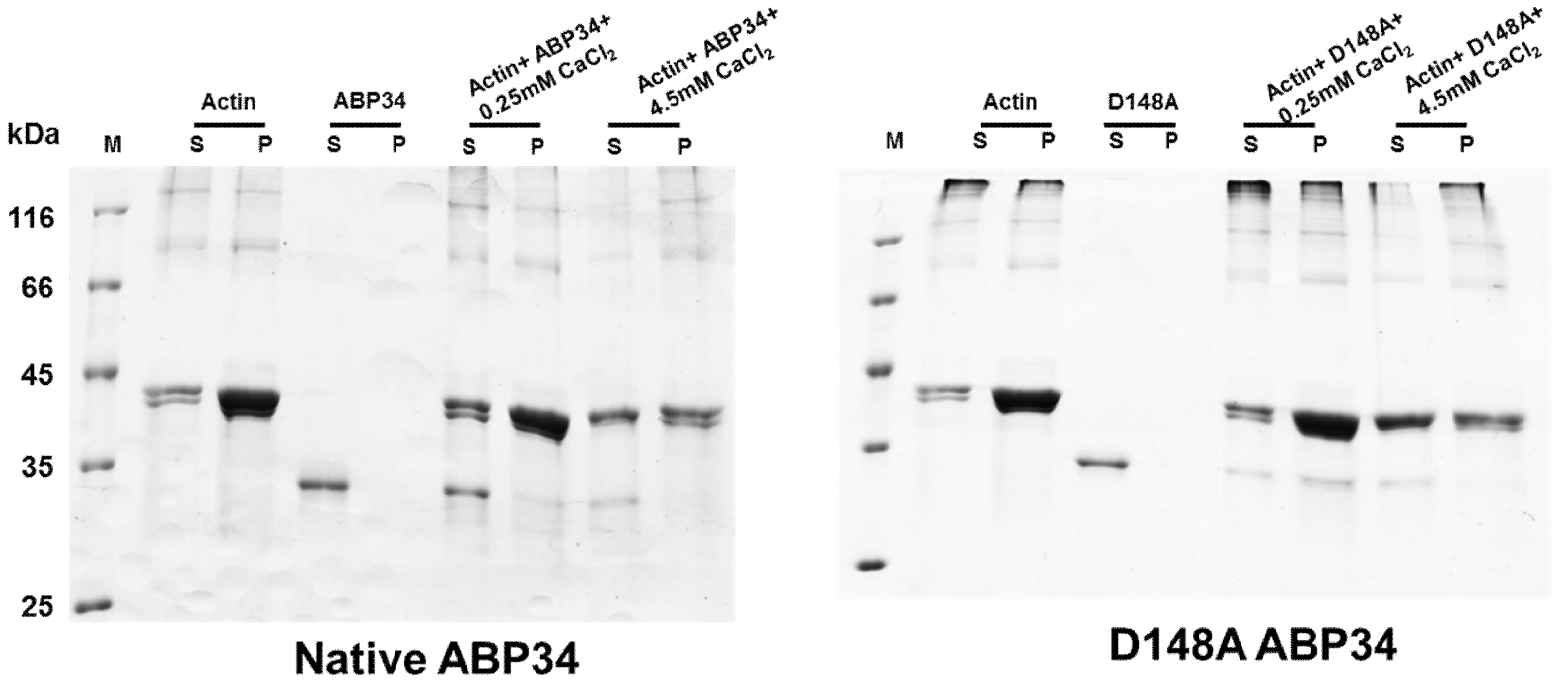

Fig. 19. Actin binding of native and D148A mutant ABP34 protein at low calcium concentration.

ABP34 and mutant ABP34 with actin filaments were incubated at 4°C for 24 hour and centrifugated at 115,000 ×g for 1 hour in low calcium concentration (0.25 mM $CaCl_2$) and high calcium concentration (4.5 mM $CaCl_2$). ABP34 and actin proteins in the pellets (P) and supernatants (S) were separated by 12% SDS-PAGE after centrifugation.

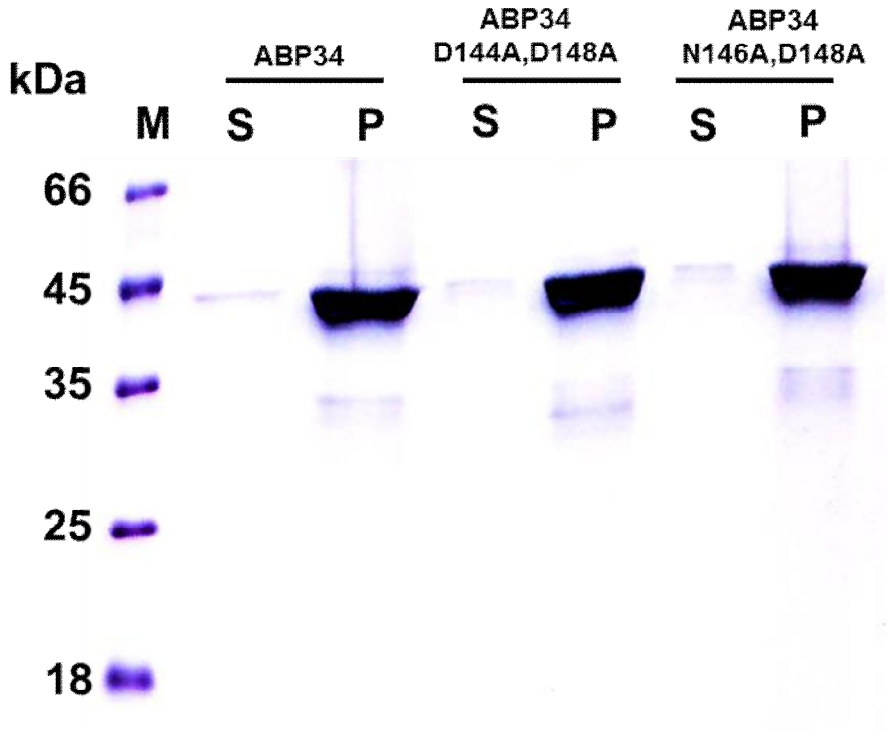

Fig. 20. Actin binding of native and double mutant ABP34 protein at low calcium concentration. ABP34 and double mutant ABP34 with actin filaments were incubated at 4°C for 24 hour and centrifugated at 115,000 ×g for 1 hour in low calcium concentration (0.25 mM $CaCl_2$). ABP34 and actin proteins in the pellets (P) and supernatants (S) were separated by 12% SDS-PAGE after centrifugation.

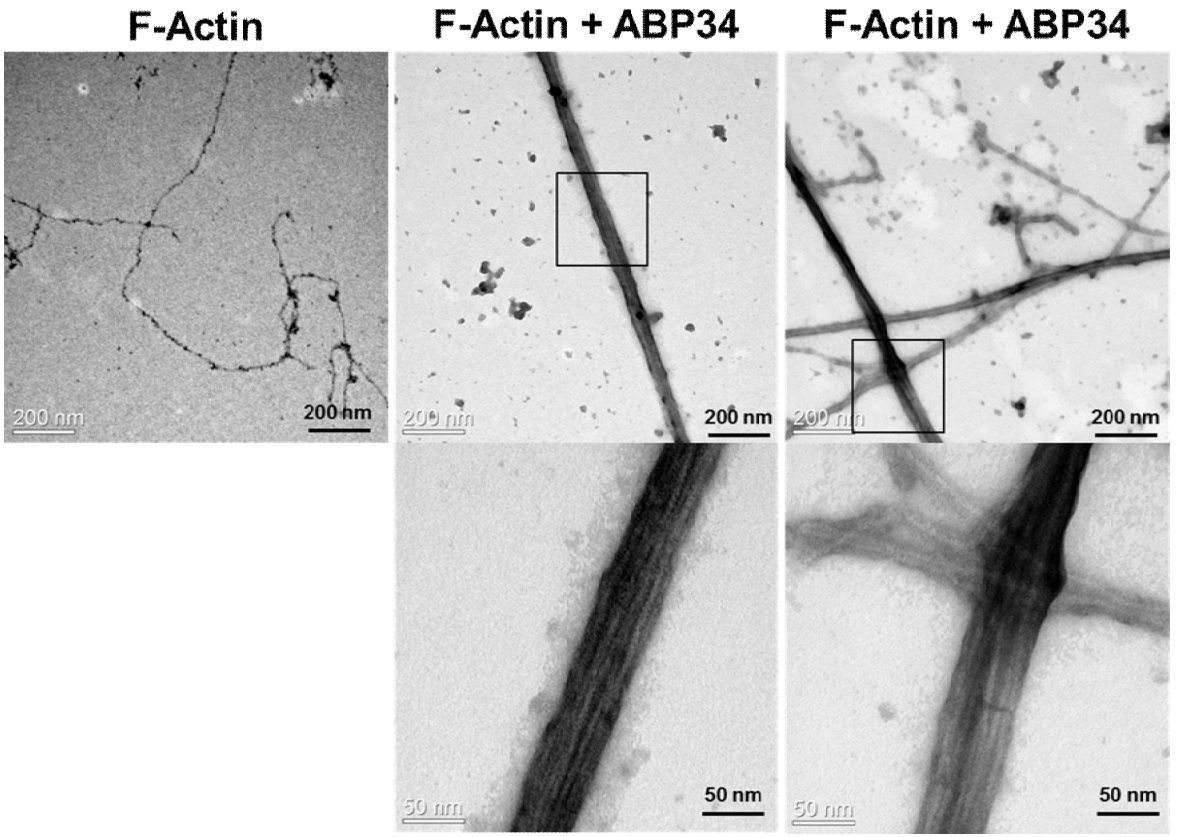

Fig. 21. Electron micrographs of negative stained F-actin and ABP34 F-actin complex. Transmission electron micrographs of F-actin and ABP34. Left: 5 μM F-actin, middle: 5 μM F-actin with 1 μM ABP34 (low magnitude), right: 5 μM F-actin with 1 μM ABP34 (high magnitude). F-actin bundles are formed in the presence of ABP34 (middle, right). Scale bars represent 200 nm and 50 nm, respectively.

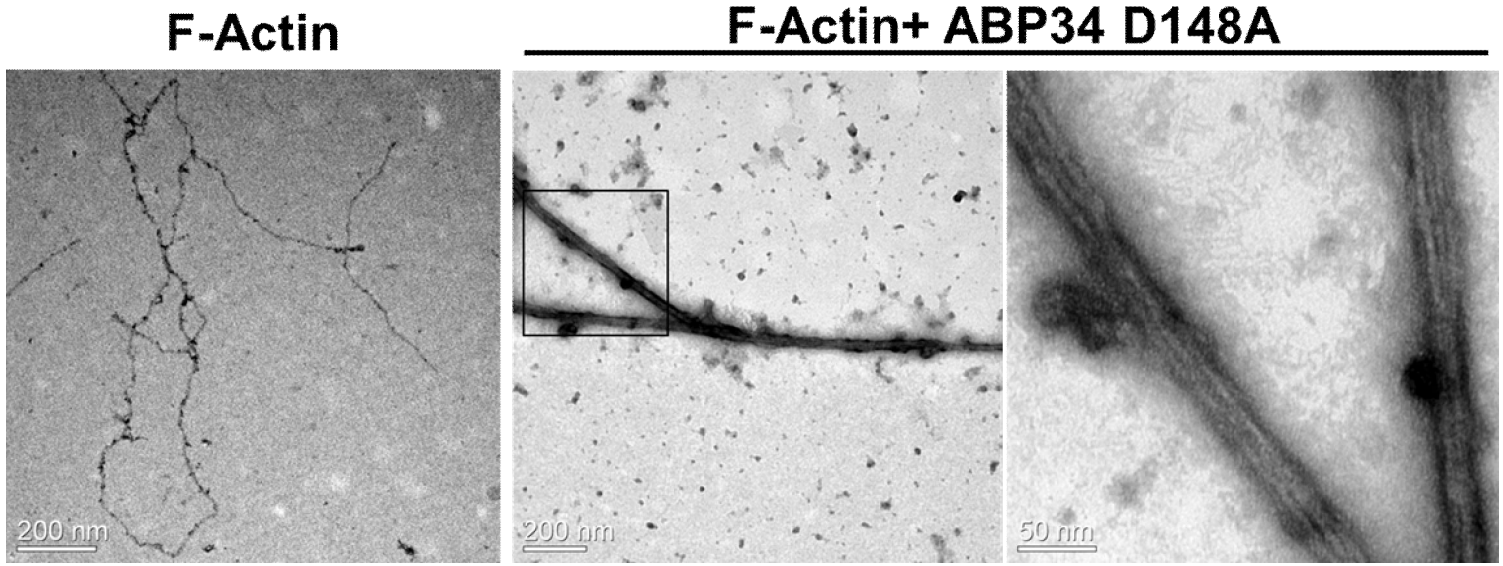

Fig. 22. Electron micrographs of negative stained F-actin and D148A ABP34 F-actin complex.

Transmission electron micrographs of F-actin and D148A ABP34. Left: 5 μM F-actin, middle: 5 μM F-actin with 1 μM D148A ABP34 (low magnitude), right: 5 μM F-actin with 1 μM D148A ABP34 (high magnitude). F-actin bundles are formed in the presence of ABP34 (middle and right panels). Scale bars represent 200 nm and 50 nm, respectively.

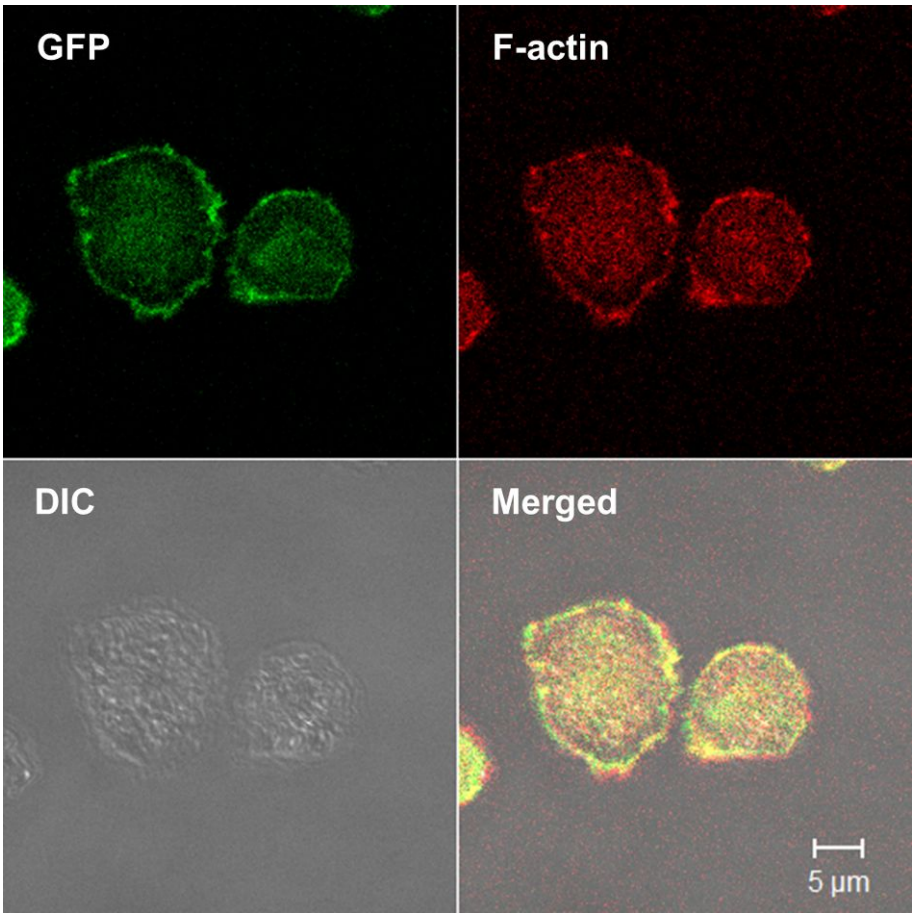

Fig. 23. Localization of actin bundling protein ABP34 in *Dictyostelium discoideum*. Distribution of F-actin and ABP34 proteins *in vivo*. The cells expressing GFP-ABP34 were placed on glass coverslip in nutrient medium, allowed to adhere and fixed with cold methanol, stained for F-actin with TRITC-conjugated phalloidin (right top). Images of *Dictyostelium* cells expressing GFP-ABP34 were recorded with confocal laser-scanning microscope. GFP-ABP34 expressing cells (left top) exhibited the high concentrations of GFP-ABP34 in cortical region along with F-actin according to the merged image (right bottom). The scale bar represents 5 µm.

3. Crystal structure of ABP34

3.1. Crystallization of ABP34

ABP34 was crystallized by the micro batch under oil and hanging-drop vapour-diffusion crystallization method using optimized screening solutions. Droplets which contained 1 μl each of protein and reagent solution were pipet under a layer of oil. The drop was placed under a mixture of paraffin oil and silicon oil at 295K. The droplets containing 1 μl of protein sample (40 mg/ml) and an equal volume of precipitant solution containing 0.2 M Ammonium acetate, 0.1 M Tri-sodium citrate pH 5.6, 30% Polyethylene glycol 4000 were grown to final single crystals. Several hexagonal shaped of crystals were produced under the condition in two weeks (Fig. 24). Mutated ABP34 crystals, one of EF-hand amino acids were also produced. Crystals were frozen at 100 K for data collection. Crystals of the ABP34 diffracted to 1.89 Å resolution, and the structure was solved by Ca^{2+}/S-SAD phasing method.

3.2. Calcium/sulfur SAD phasing

To determine the crystal structure of ABP34, we tried the molecular replacement (MR) and experimental phasing using selenium multi-wavelength anomalous dispersion (Se-MAD). But, all trials are failed due to the lack of proper search model in PDB for MR or the poor diffraction quality of Se-Met derivative crystals for Se-MAD. Finally, motivated by the presence of 5 cysteines and 7 methionines in ABP34 monomer, sulfur SAD (S-SAD) phasing was attempted based on the anomalous signal of sulfur (Roeser *et al.*, 2005). A 2.3 Å resolution SAD data set (Table 3) was

collected at a wavelength of at 1.9 Å. The crystal of ABP34 belonged to the orthorhombic space group $P2_12_12_1$, with unit-cell parameters a = 78.878, b = 85.902, c = 136.891 Å. There are three molecules in the asymmetric unit, giving a Matthews coefficient (V_M) of 2.28 $Å^3$ Da^{-1} (Matthews, 1968) and a calculated solvent content of 46.14%. Anomalous signals, which were evaluated by <*d*″/sig>, a good indicator of the strength of the anomalous signal, were over the threshold (0.80) (Sheldrick, 2010) to the highest resolution shell (Fig. 27). S-SAD phasing generally requires high redundant data to accurately measure the subtle anomalous signal. Therefore, we rescaled the SAD data set of total 999 frames to evaluate the effect of multiplicity (Fig. 27). Despite the presence of a reasonable anomalous signal, the interpretable electron-density map can be calculated from the 1–500 frames data (data not shown).

The *AutoSol* program was used to find anomalous sulfur substructures and produced a phase set with a figure of merit (FOM) before and after density modification of 0.30 and 0.65, respectively. In fact, among the 34 heavy atom sites found by *HySS*, three sites turned out to be the calcium ions occupied in calcium-binding EF-hand motif of N-domain (Fig. 27). The lower occupancy of sulfur positions is an expression of the smaller dispersive signal of sulfur compared with calcium (*f*″ = 0.82 e^- versus *f*″ = 1.84 e^-) for the wavelength of 1.9 Å. Although the location of the relatively strong anomalous scatterers, calcium atoms (*f*" = 1.84), may facilitate the finding of sulfur atoms (*f*" = 0.82), the data evidently contained a meaningful anomalous scattering contribution originating from sulfur likely with the previous successful Ca^{2+}/S-SAD phasing cases (Roeser *et al.*, 2005; Koch *et al.*, 2010). This result is also in accordance with the report that the

location of Mn atoms facilitates the finding of sulfur atoms and the anomalous scattering of sulfur atoms contributes to SAD phasing (Ramagopal *et al.*, 2003). The experimental electron-density map was clearly interpretable and a model consisting of 749 residues among the total 885 amino acids with R_{work}/R_{free} of 0.236/0.288 was automatically built. The final model with R_{work}/R_{free} of 0.206/0.252 was built manually using the program COOT (Emsley and Cowtan, 2004) with 1.89-Å resolution native dataset and the iterative rounds of refinement were performed using the program REFMAC5 (Murshudov *et al.*, 2011) (Table 4).

3.3. Overall structure of ABP34

The structure of the ABP34 exhibits the two domains linked in a stable arrangement with the N-terminal and C-terminal domains make direct contact (Fig. 29). The structure of the *Dictyostelium discoideum* ABP34 has C-terminal actin binding domain and N-terminal domain which includes calcium binding motif and actin binding region.

The structure comprised of almost α-helices from N-terminal to C-terminal domain. The structure of the ABP34 construct contains 295 amino acid residues. The structure of the N-terminal domain is similar to those previously described in a number of EF-hand proteins conformations. The calcium regulation of ABP34 is important to regulation of actin crosslinking (Furukawa *et al.*, 2003). The ABP34 structure has one calcium binding region that is occupied by coordination of several amino acid residues and water molecules. The calcium ion binds on critical charged amino acids at the coordinating X, Y, Z and -X, -Y, -Z positions in ABP34 protein (Furukawa *et al.*, 2003). The calcium binding site in ABP34 is structurally

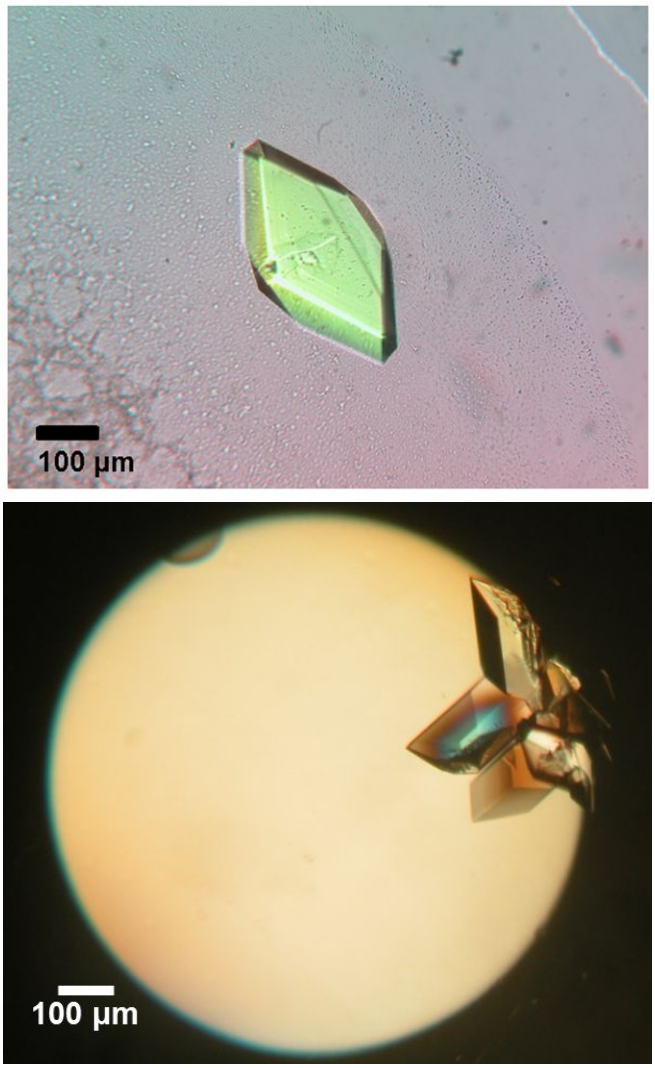

Fig. 24. Crystals of native ABP34. Rhombus-shaped crystals were produced using 0.2 M ammonium acetate, 0.1 M sodium citrate pH 5.6, 30% PEG 4K after three days. Crystal screening was conducted by hanging-drop vapor-diffusion (left) and micro batch oil (right) method using screening solutions. Droplets composed of 1 µl protein solution and equal volume of crystallization screening solution were incubated at 22°C.

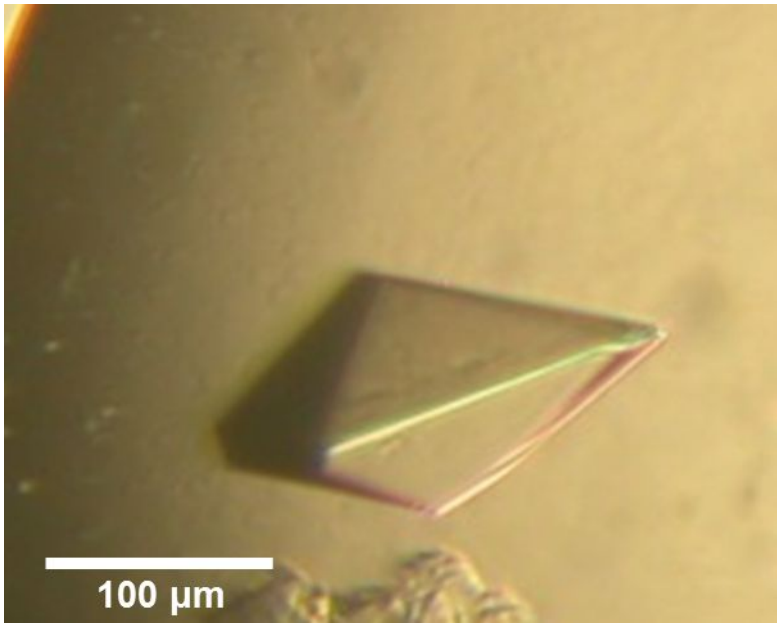

Fig. 25. Crystals of D148A ABP34. This crystal belongs to the orthorhombic crystal system, P212121. Crystals were produced using 0.2 M ammonium acetate, 0.1 M sodium citrate pH 5.6, 30% PEG 4K after three days at 22°C. Crystal screening was conducted by hanging-drop vapor-diffusion.

Table 3. Data collection statistics of ABP34.

	Ca^{2+}/S-SAD	Native
Wavelength (Å)	1.9075	1.1000
Total rotation range (°)	999	360
Space group	$P2_12_12_1$	$P2_12_12_1$
a, *b*, *c* (Å)	78.878, 85.902, 136.891	78.161, 85.244, 135.744
α, β, γ (°)	90, 90, 90	90, 90, 90
Mosaicity (°)	0.300	0.472
Resolution range (Å)	50.00 - 2.30	50.00 - 1.89
Total No. of reflections	1005649	696218
No. of unique reflections	40890	72226
Completeness (%)	96.9 (87.8)	98.9 (88.2)
Redundancy	24.6 (11.1)	9.6 (5.4)
$\langle I/\sigma(I)\rangle$	58.7 (4.3)	32.5 (2.9)
$R_{\text{r.i.m.}}$ (%)	6.6 (40.5)	8.2 (46.4)
Overall *B* factor from Wilson plot ($Å^2$)	33.6	21.9

$R_{\text{r.i.m.}}$ was estimated by multiplying the conventional R_{merge} value by the factor $[N/(N-1)]^{1/2}$, where N is the data multiplicity.

Table 4. Structure solution and refinement statistics of ABP34.

Resolution range (Å)	72.19 - 1.89 (1.94 - 1.89)
Completeness (%)	99.2 (94.6)
No. of reflections, working set	68586
No. of reflections, test set	3640
Final R_{cryst}	20.4
Final R_{free}	25.2
Cruickshank DPI	0.157
No. of non-H atoms	
Protein	6282
Calcium	3
Citrate	13
Water	383
Total	6681
R.m.s. deviations	
Bonds (Å)	0.017
Angles (°)	1.74
Average *B* factors (Å^2)	
Protein	34.9
Calcium	28.7
Citrate	50.6
Water	33
Ramachandran plot	
Most favoured (%)	97
Allowed (%)	2.8

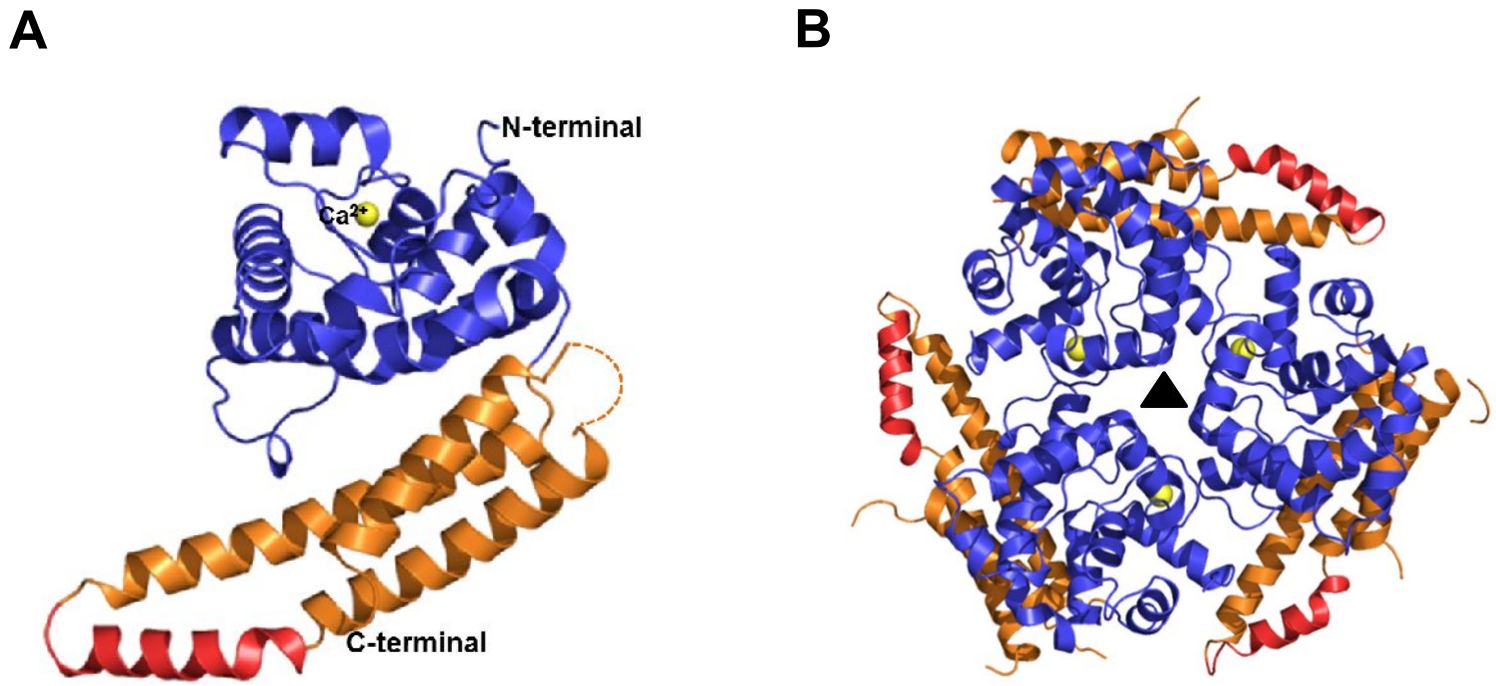

Fig. 26. Overall structure of ABP34. (A) The structure of ABP34 monomer with Ca^{2+} in EF-hand motif. N-terminal domain is colored by blue, C-terminal domain is colored by orange and 214 – 230 residues are colored by red. (B) The trimer of ABP34 in an asymmetric unit. Trifold symmetry is denoted as black triangle.

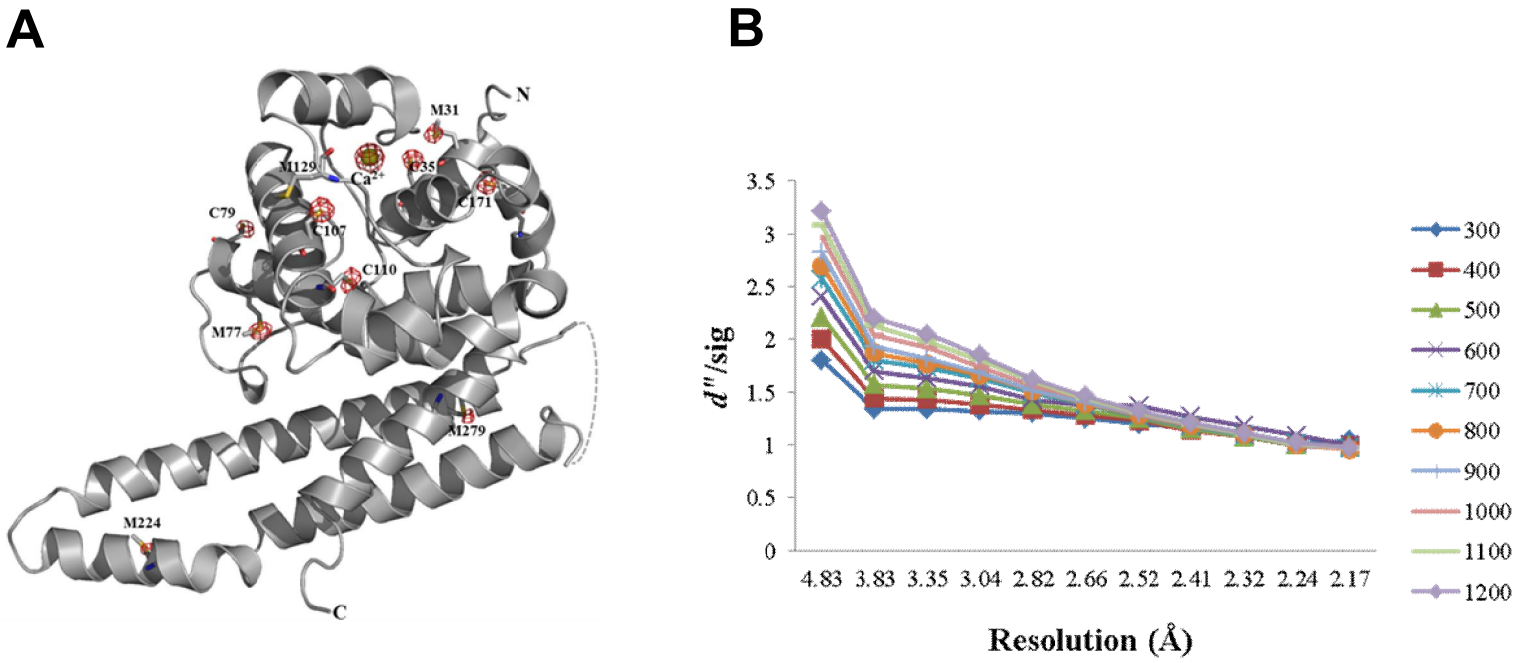

Fig. 27. Anomalous signals from sulfur and calcium. (A) The <*d*''/sig> plots from SHELXC as a function of resolution. (B) Anomalous Fourier maps (red mesh) at the 5σ level. Calcium ion and sulfur atoms from cysteine and methionine are represented by yellow sphere and stick, respectively.

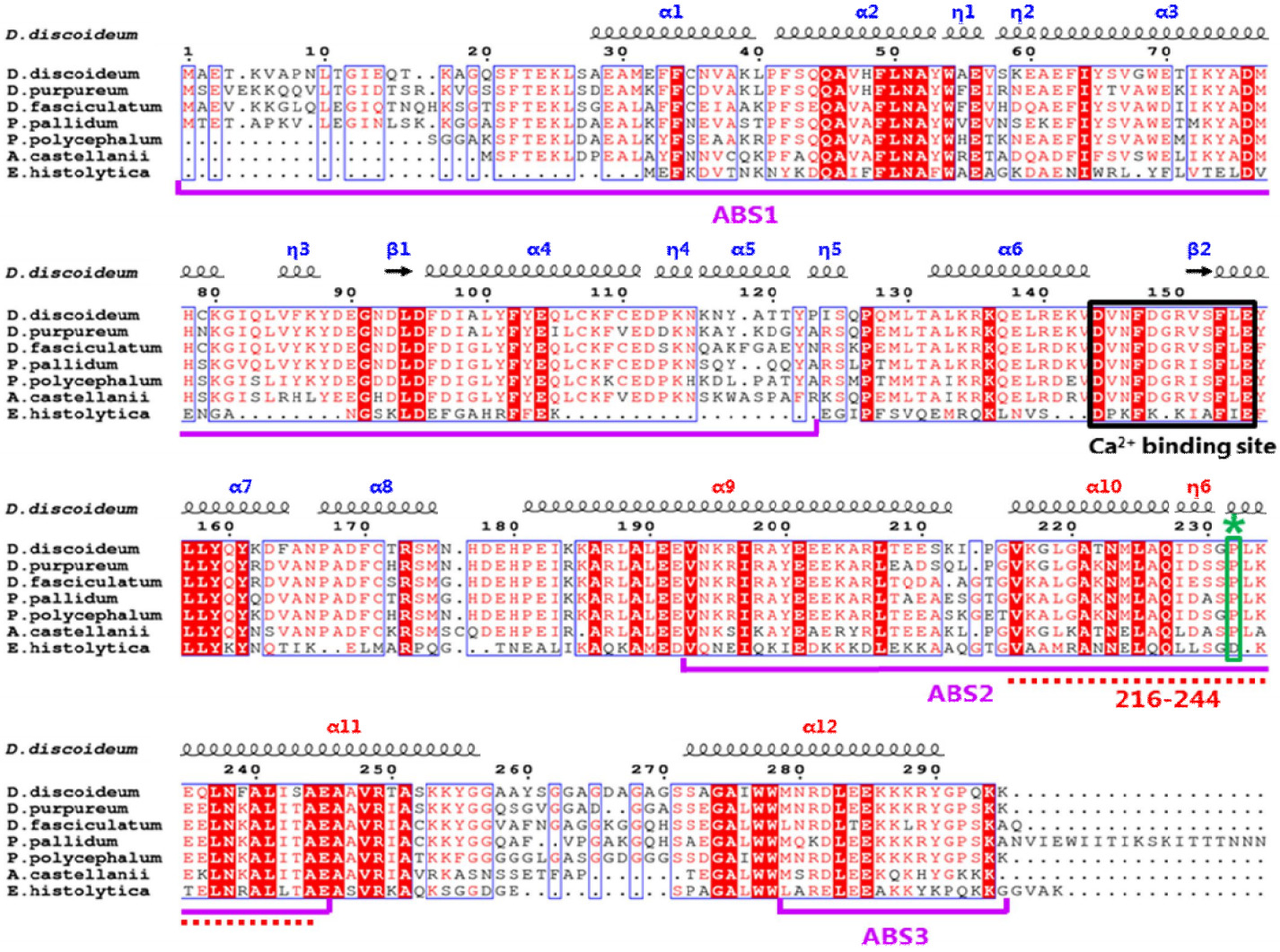
D.discoideum
α1
α2
η1
η2
α3
D.discoideum MAET.KVAPNLTGIEQT..KAGQSFTEKLSAEAMEFFCNVAKLPFSQQAVHFLNAYWAEVSKEAEFIYSVGWETIKYADM
D.purpureum MSEVEKKQQVLTGIDTSR.KVGSSFTEKLSDEAMKFFCDVAKLPFSQQAVHFLNAYWFEIRNEAEFIYTVAWEKIKYADM
D.fasciculatum MAEV.KKGLQLEGIQTNQHKSGTSFTEKLSGEALAFFCEIAAKPFSEQAVAFLNAYWFEVHDQAEFIYSVAWDIIKYADM
P.pallidum MTET.APKV.LEGINLSK.KGGASFTEKLDAEALKFFNEVASTPFSQQAVAFLNAYWVEVNSEKEFIYSVAWETMKYADM
P.polycephalum ...........SGGAKSFTEKLDAEALKYFSEAAKRPFSQQAVAFLNAYWHETKNEAEFIYSVAWEMIKYADM
A.castellanii .....MSFTEKLDPEALAYFNNVCQKPFAQQAVAFLNAYWRETADQADFIFSVSWELIKYADM
E.histolytica MEFKDVTNKNYKDQAIFFLNAFWAEAGKDAENIWRL.YFLVTELDV
ABS1
η3
β1
α4
η4
α5
η5
α6
β2
D.discoideum
D.discoideum HCKGIQLVFKYDEGNDLDFDIALYFYEQLCKFCEDPKNKNY.ATTYPISQPQMLTALKRKQELREKVDVNFDGRVSFLEY
D.purpureum HNKGIQLVYKYDEGNDLDFDIALYFYEILCKFVEDDKNKAY.KDGYARSQPEMLTALKRKQELREKVDVNFDGRVSFLEY
D.fasciculatum HCKGIQLVYKYDEGNDLDFDIGLYFYEQLCKFCEDSKNQAKFGAEYNRSKPEMLTALKRKQELRDKVDVNFDGRVSFLEF
P.pallidum HSKGVQLVYKYDEGNDLDFDIGLYFYEQLCKFCEDPKNSQY..QQYARSLPTMLTALKRKQELRDKVDVNFDGRISFLEY
P.polycephalum HSKGISLIYKYDEGDDLDFDIGLYFYEQLCKKCEDPKHKDL.PATYARSMPTMMTAIKRKQELRDEVDVNFDGRISFLEY
A.castellanii HSKGISLRHLYEEGHDLDFDIGLYFYEQLCKFVEDPKNSKWASPAFRKSQPEMLTAIKRKQELRDRVDVNFDGRVSFLEY
E.histolytica ENGA.....NGSKLDEFGAHRFFEK.....EGIPFSVQEMRQKLNVS...DPKFK.KIAFIEF
Ca²⁺ binding site
α7
α8
α9
α10
η6
D.discoideum
D.discoideum LLYQYKDFANPADFCTRSMN.HDEHPEIKKARLALEEVNKRIRAYEEEKARLTEESKI.PGVKGLGATNMLAQIDSGFLK
D.purpureum LLYQYRDVANPADFCHRSMN.HDEHPEIRKARLALEEVNKRIRAYEEEKARLEADSQL.PGVKGLGAKNMLAQIDSSFLK
D.fasciculatum LLYQYRDVANPADFCSRSMG.HDEHPEIKKARLALEEVNKRIRAYEEEKARLTQDA.AGTGVKALGAKNMLAQIESSFLK
P.pallidum LLYQYQDVANPADFCTRSMG.HDEHPEIKKARLALEEVNKRIRAYEEEKARLTAEAESGTGVKALGAKNMLAQIDASFLK
P.polycephalum LLYQYKDVANPADFCHRSMN.HDEHPEIRKARLALEEVNKRIRAYEEEKARLTEEASKGETVKALGAKNMLAQIDSGFLK
A.castellanii LLYQYNSVANPADFCKRSMSCQDEHPEIR.ARLALEEVNKSIKAYEAERYRLTEEAKL.PGVKGLKATNELAQLDASFLA
E.histolytica LLYKYNQTIK..ELMARPQG..TNEALIKAQKAMEDVQNEIQKIEDKKKDLEKKAAQGTGVAAMRANNELQQLLSGD.K
ABS2
216-244
α11
α12
D.discoideum
D.discoideum EQLNFALISAEAAVRTASKKYGGAAYSGGAGDAGAGSSAGAIWWMNRDLEEKKKRYGPQKK.....
D.purpureum EELNKALITAEAAVRIASKKYGGQSGVGGADG..GGASSEGALWWMNRDLEEKKKRYGPSKK.....
D.fasciculatum EELNKALITAEAAVRIACKKYGGVAFNGAGGKGGQHSSEGALWWLNRDLTEKKLRYGPSKAQ.....
P.pallidum EELNKALITAEAAVRIACKKYGGQAF..VPGAKGQHSAEGALWWMQKDLEEKKKRYGPSKANVIEWIITIKSKITTTNNN
P.polycephalum EELNKALITAEAAVRIATKKFGGGGGLGASGGDGGGSSDGAIWWMNRDLEEKKKRYGPSKK.....
A.castellanii EKLNKALITAEAAVRIAVRKASNSSETFAP.....TEGALWWMSRDLEEKQKHYGKKK.....
E.histolytica TELNRALLTAEASVRKAQKSGGDGE.....SPAGALWWLARELEEAKKYKPQKKGGVAK.....
ABS3

Fig. 28. Comparison of the deduced amino acid sequence of *Dictyostelium discoideum* ABP34. Structure-based multiple sequence alignment of ABP34 with the homologs in amoeba species. The secondary structure elements of *D. discoideum* ABP34 are shown above the alignment. Homologous regions are boxed, with identical amino-acid residues are colored as bold white letters on a red background and functionally equivalent residues are indicated as red letters. Residues belong to the Ca^{2+} binding site is highlighted with black box and the position of conserved actin binding residues is indicated by red dots. The proposed actin binding sites ABS1, ABS2 and ABS3 are under lined (magenta) and proline kink is marked with star and boxed in green. Full names of the strains are as follows *D. purpureum*, *Dictyostelium purpureum*; *D. fasciculatum*, *Dictyostelium fasciculatum*; *P. pallidum*, *Polysphondylium pallidum*; *P. polycephalum*, *Physarum polycephalum*; *A, castellanii*, *Acanthamoeba castellanii*; *E. histolytica*, *Entamoeba histolytica*.

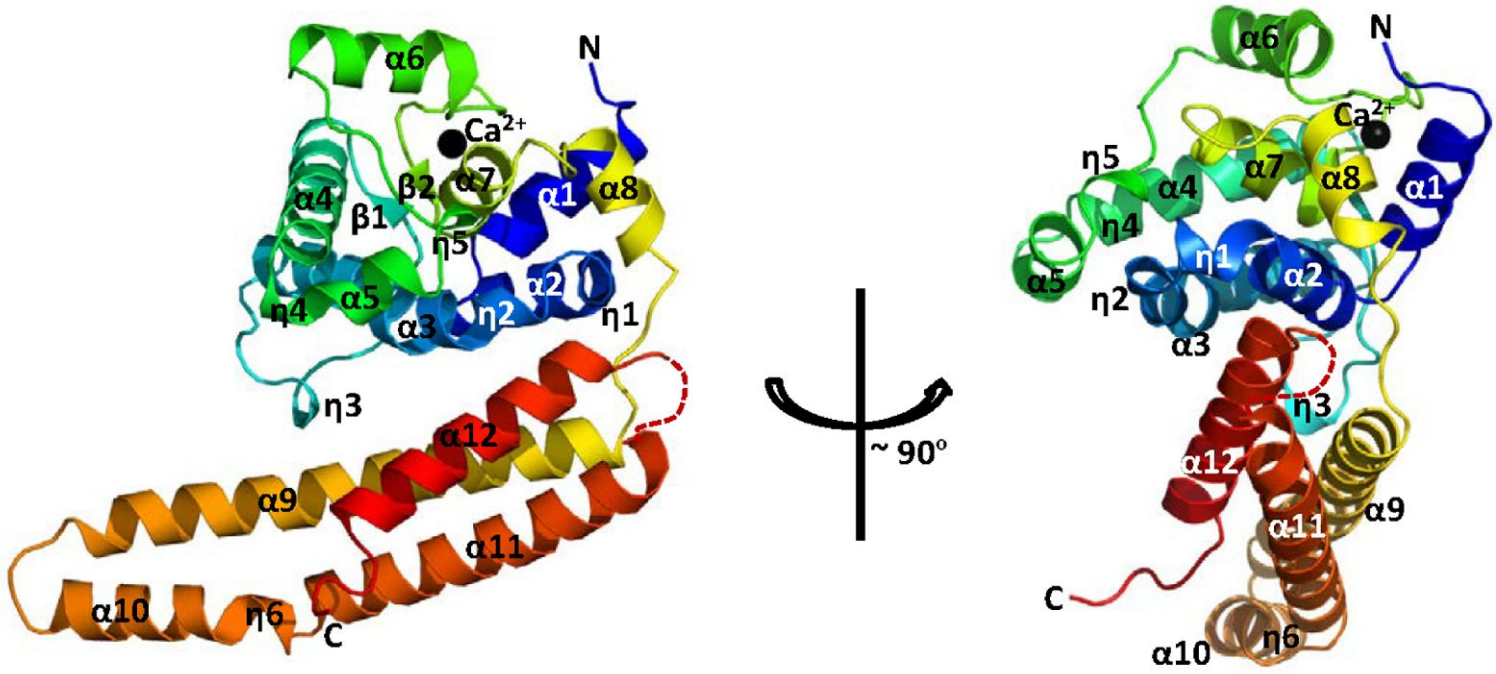

Fig. 29. Structure of ABP34. Cartoon representation of ABP34 monomer structure from front (left) and side (right) view. The molecule is colored progressively from blue at the N-terminus to red at the C-terminus. Secondary structures including helices and sheets are labelled. Calcium ion is highlighted with a black sphere and the disordered region (257–269) is shown as a dotted line.

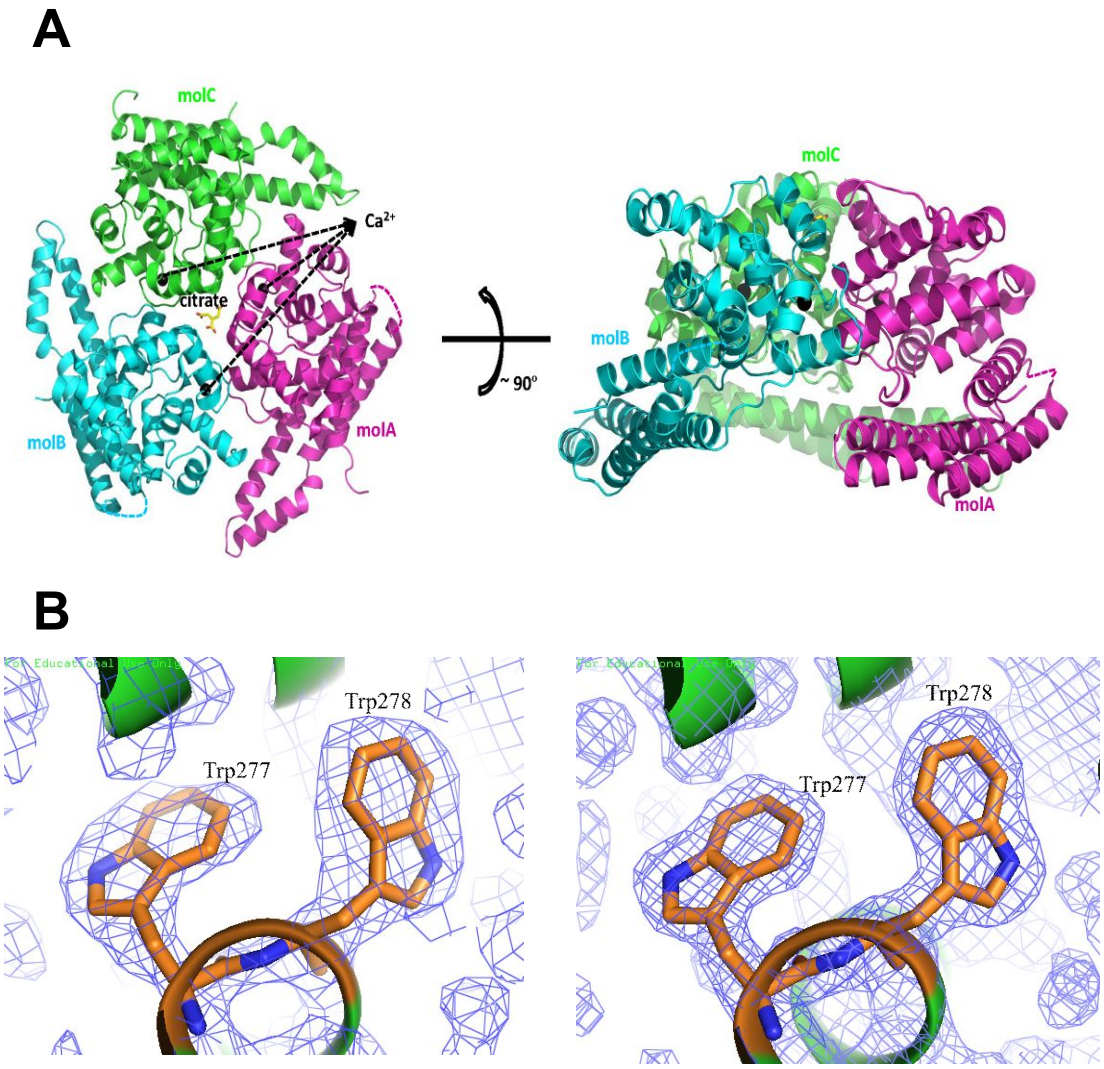

Fig. 30. Structure of ABP34. (A) Cartoon representation of three ABP34 molecules in the asymmetric unit. Molecule A, B and C are shown separately in different colors. One citrate molecule in the non-crystallographic three-fold symmetry axis is shown as stick (yellow). Calcium ions are highlighted with black spheres. A top view and a side view are shown on the left and on the right, respectively. (B) $2F_o$-F_c electron density maps showing the Trp277 and Trp278 residues of ABP34 (left, initial map; right, final map).

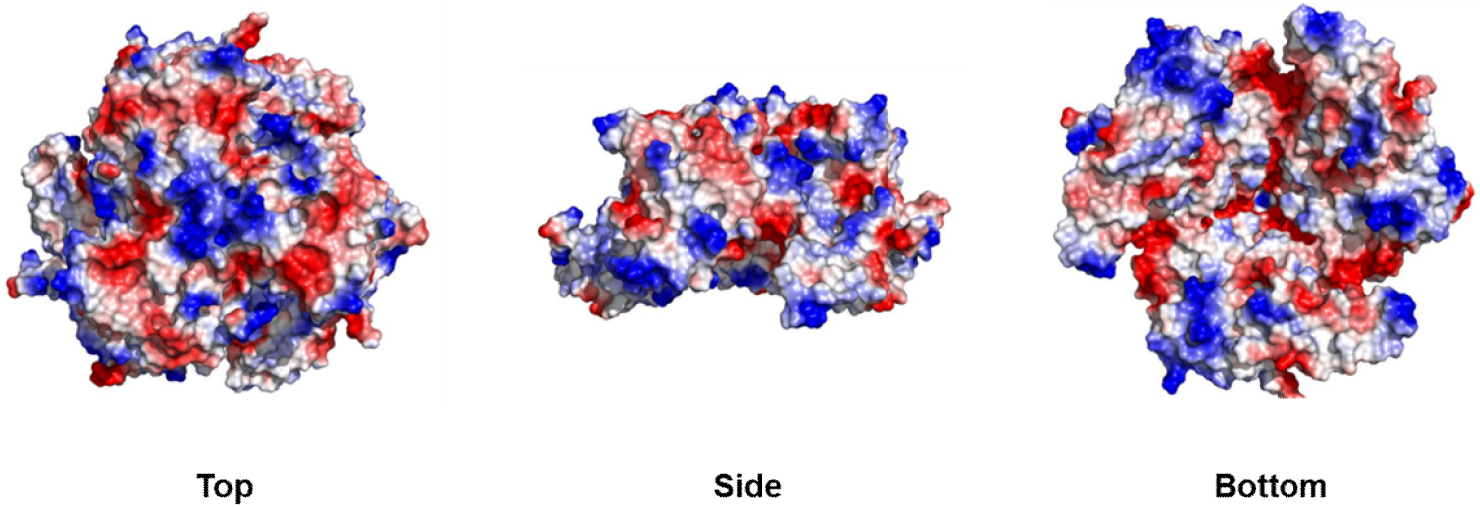

Fig. 31. Electrostatic surface charge model of ABP34.

The surface is colored according to charge; positive potential at the surface is indicated in blue, negative potential is indicated in red. The figure was prepared by PyMOL.

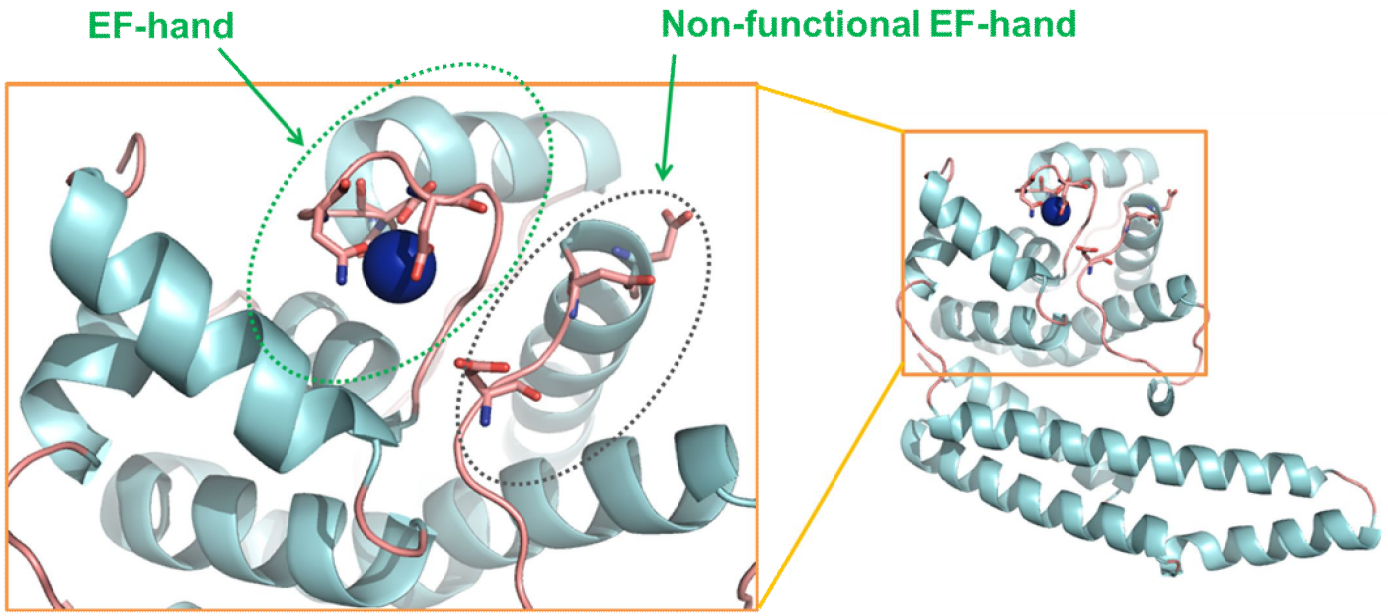

Fig. 32. Conformation of two putative EF-hand from N-terminal domain of ABP34. Cartoon diagram of EF-hand pair is highlighted in dots circles, respectively. The putative calcium ion binding residues are denoted as sticks. Calcium ion is indicated as blue sphere.

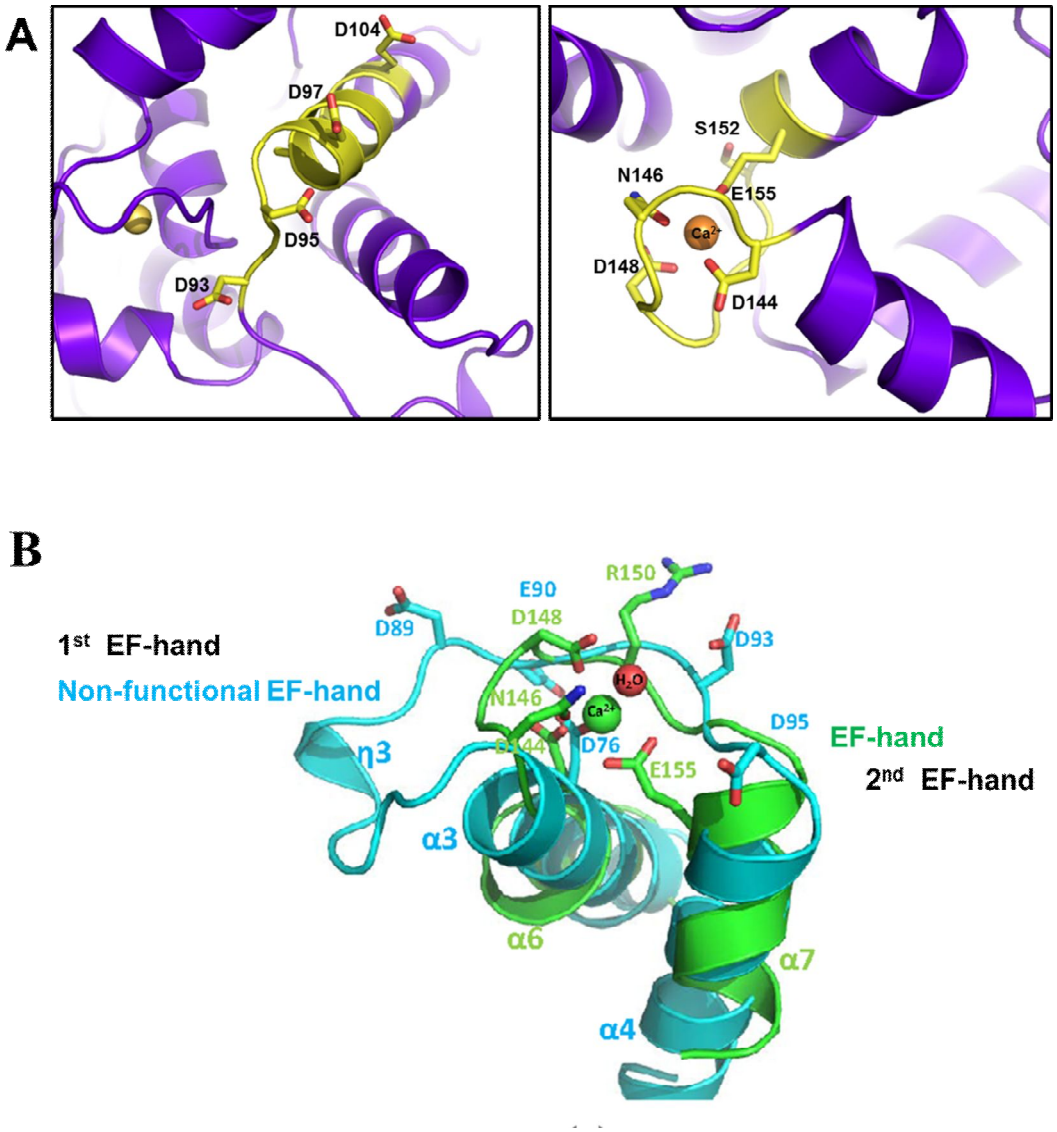

Fig. 33. Comparison of two putative EF-hand from N-terminal domain of ABP34. (A) Left panel is non functional putative EF-hand right panel is functional EF-hand; (B) Superimposed model of two putative EF-hand from N-terminal domain of ABP34.

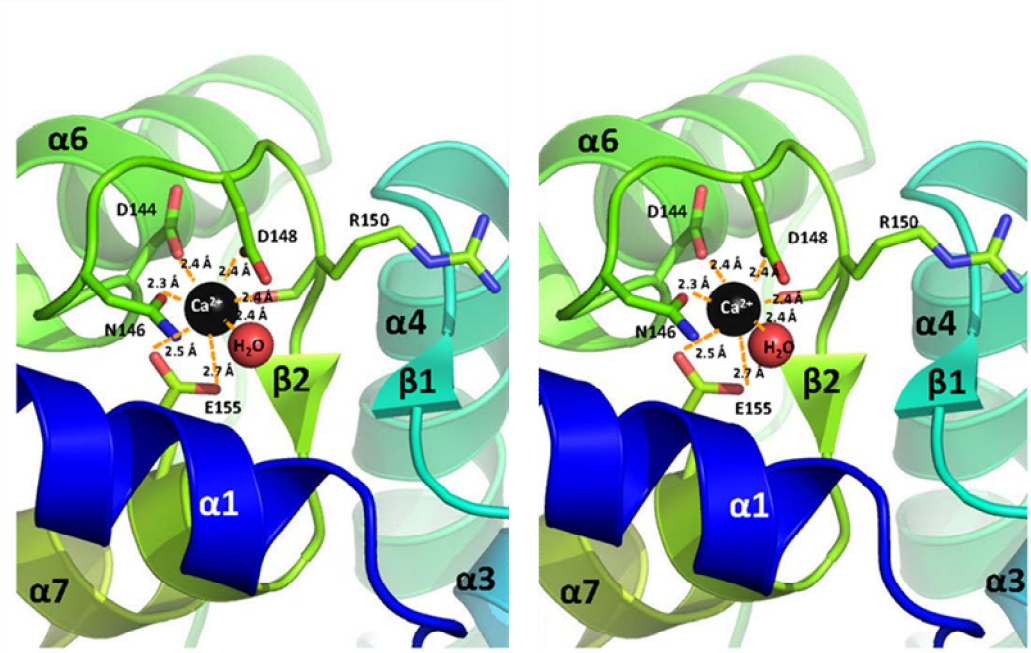

Fig. 34. Stereo view of the calcium binding domain. Stereo view of the calcium binding domain is represented by cartoon diagram. Critical amino-acid residues in EF-hand are all indicated in stick model. Ca^{2+} ion bound from the domain is stabilized by the Ca^{2+}-ligand interactions. Interaction residues and associated hydrogen bond (orange dots lines) between polar groups and a crystallographically observed water molecules is shown between E155 and R150. The side chain of this loop is provided by two aspartic acid residues and asparagine and arginine with carboxyl group of glutamic acid, creating a small binding site that more greatly favours binding of Ca^{2+} ion. The Ca^{2+} ion and the water ligand are represented by black and red spheres, respectively.

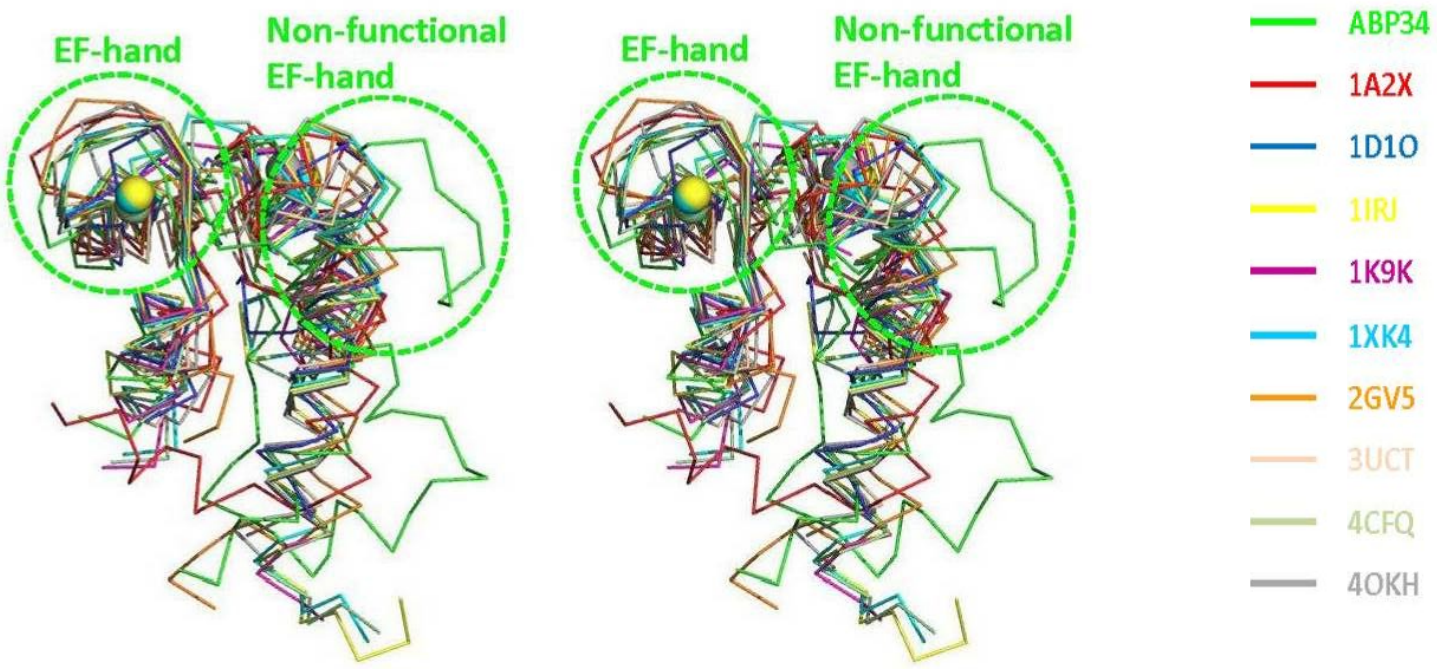

Fig. 35. Superimposed models of EF-hand from N-terminal domain of ABP34. Structural comparison (stereo) of the EF-hand in ABP34 N-domain with the top-scored *DALI* hits [calmodulin (3UCT), proteins S100A4 (4CFQ), cell division control protein 31 (2GV5), calgranulin A (1XK4), migration inhibitory factor-related protein 14 (1IRJ), calbindin D9K (1D1O), troponin C (1A2X), calpain-3 (4OKH)]. EF-hand pair of ABP34 is highlighted with green dots circles.

conserved with respect to EF-hand motif in other calcium binding proteins, each using glutamate located on the helix and an aspartate and adjacent carbonyl backbone. On the other hand, another putative EF hand region was appeared that structurally was unable to bind calcium ion, is not similar to actual EF hand region on ABP34. It is consistent with the prior studies (Maselli *et al.*, 2002; Furukawa *et al.*, 2003) that the first EF hand does not participate in calcium binding to the ABP34 protein.

The C-terminal domain residues of ABP34 are clearly defined in the electron density map. The domain is comprised of three helices which contribute to actin binding. The region of amino acid residues 193-254 is concerned to actin binding that composed of the first helix part 180-211 and linked to second helix 232-255, and third helix 273-290. The second and third helices are connected by amino acids 256-275 as linker between the the terminal basic region and the bulk of the polypeptide (Fechheimer *et al.*, 1991).

3.4. Interaction zone of ABP34

Intramolecular interaction within the Ca^{2+}-regulated ABP34 actin-bundling protein was found to contribute to the regulation of its actin-binding activity (Lim *et al.*, 1999). An inhibitory effect of the N-terminus on the strong actin binding site amino acids 193-254 (IZ-2) and amino acids 71-123 (IZ-1) was confirmed that loop and helix participate in intramolecular domain-domain interaction on the structure. In the detail, amino acid residues 85-89 (VFKYD) and 197-202 (IRAYEE) are revealed to the interaction. This supports that 71-123 (IZ-1) and 193-254 (IZ-2) are structurally possible to intramolecular interaction (Fig. 36, 37). The intramolecular interaction zone

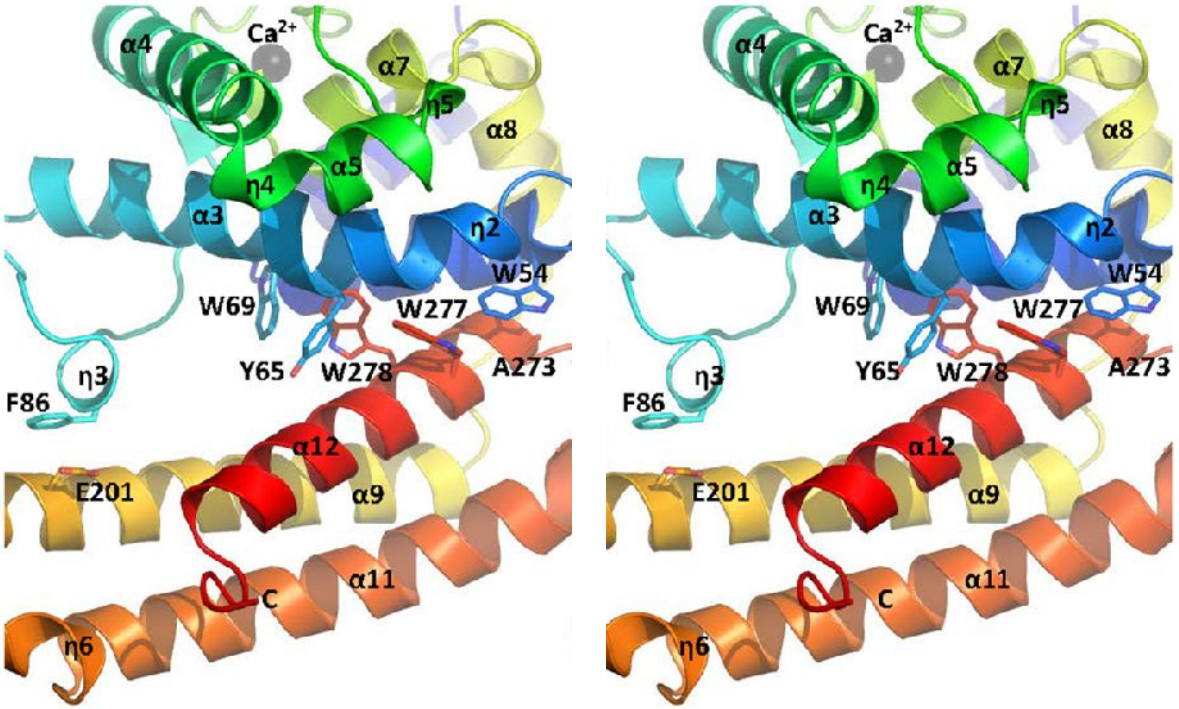

Fig. 36. Inter-domain interaction. Stereoviews of the inter-domain interactions between N-domain and C-domain. Side chains which are participated in the hydrophobic interactions. Secondary-structural elements are labelled on cartoon diagrams. Calcium ion is represented by black sphere.

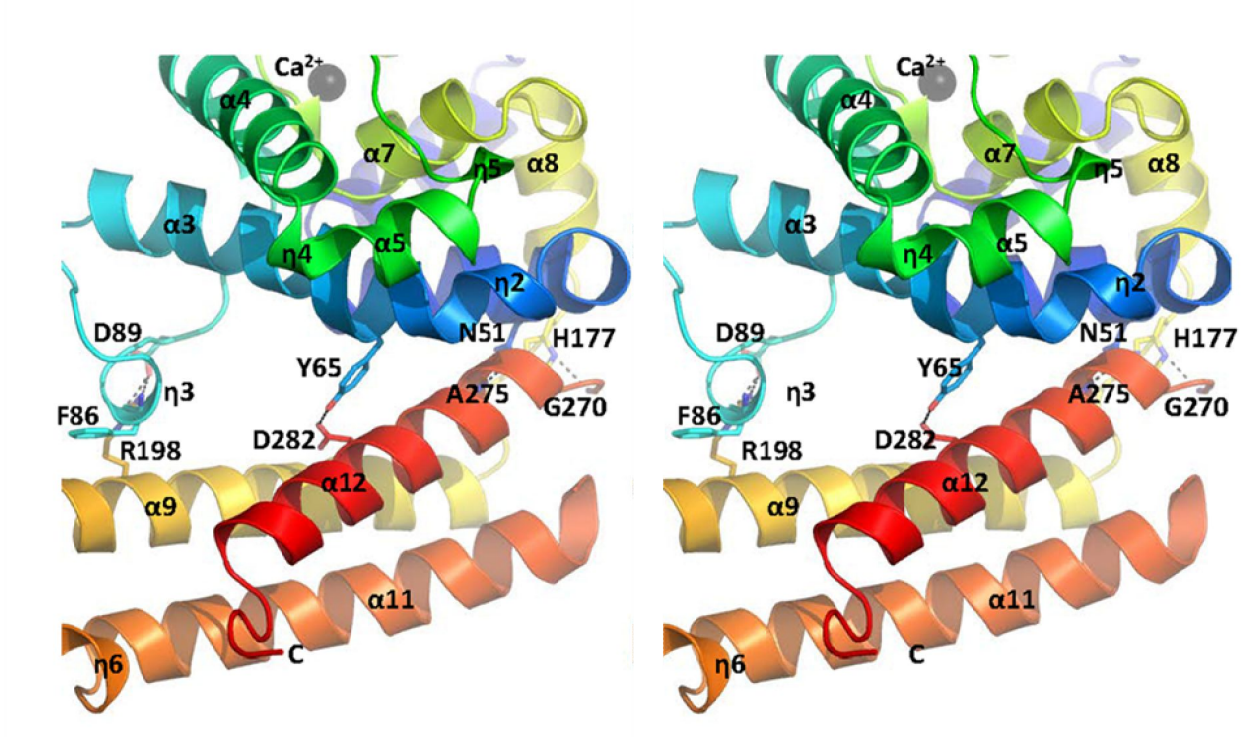

Fig. 37. Inter-domain interaction. Stereoviews of the inter-domain interactions between N-domain and C-domain. Side chains which are participated in the electrostatic interactions are denoted as sticks and the residue numbers are labelled. The electrostatic interactions are highlighted with black dotted lines.

is important for actin binding. But, structure of ABP34 provides new information that calcium ion was bound despite of intramolecular interaction. Additionally, ABP34 is able to crosslink F-actin into bundles with binding calcium ion in the ABP34 protein in vitro. It is different to previously model (Lim *et al.*, 1999) and provide new information in our ABP34 structure.

3.5. Sequence homology of actin binding region

ABP34 contains three specific regions involved in F-actin binding (Lim *et al.*, 1999). The main actin-binding site of ABP34 consists of 193 to 254 amino acid residues. Amino acid sequence analyses of the ABP34 protein show homology to other actin bundling protein, *Dictyostelium* α-actinin and ABP120 in partial amino acid sequence with residues 216 and 244 of ABP34. This conserved area is provided actin binding region in ABP34 structure (Fig. 38). This conserved area is responsible for binding to actin filaments in α-actinin and ABP120 (Bresnick *et al.*, 1990; Hartwig and Kwiatkowski, 1991). The residues of actin binding domains are concentrated hydrophobic and charged amino acids, the helix between actin binding regions. Acidic side chains of actin surface could react with the actin binding protein amino groups. Thus, comparison of actin binding structures of ABP34 with actin bundling protein suggests location of the actin-binding site.

3.6. Structure of ABP34 N-terminal domain

The EF-hand is almost always known to occur in pairs, creating an 11 Å distance between the two bound Ca^{2+} ions (Biekofsky and Feeney, 1998). Stacked with each other in a face-to-face manner, this pair forms a four-helix bundle with the amphipathic helices packed together to make a hydrophobic

core. Two EF-hands are further stabilized through the short antiparallel β-sheet formed between the pairs EF-loops (Grabarek, 2006). Even though the two EF-hands in the domain are related by an approximate 2-fold axis of symmetry that passes through the eighth position of the loop, they are not identical (Gifford *et al.*, 2007). In ABP34, EF-hand pair specific four-helix bundle is formed by α3, α4, α6 and α7 helices and maintained by hydrophobic core (Fig. 33, 34). Two short antiparallel β-sheets (β1, β2) further stabilize the EF-hand pair. But, the intervening loop between α3 and α4 is composed of 18 amino acids (80KGIQLVFKYDEG-NDLDFD97) with one 3_{10}-helix (η3) and β1 sheet. This loop also lost the proper composition of Ca^{2+} coordinating ligands. As a result, putative EF-hand (α3–α4) in ABP34 is not an actual Ca^{2+} binding site and this is in accordance with the previous reports that this putative EF-hand of ABP34 cannot accommodate the calcium ion (Maselli *et al.*, 2002; Furukawa *et al.*, 2003) (Fig. 32, 33). Non-functional EF-hand is also reported in the case of SCPs (sarcoplasmic Ca^{2+} binding proteins) of the invertebrates Nereis diversicolor (a ragworm). In Nereis SCP, although EF2 is non-functional, owing to an extensive insertion, it is still paired with a functional EF1 and the two-fold symmetry is approximately preserved (Vijay-Kumar and Cook, 1992). The DALI search (Holm and Rosenström, 2010) using the N-domain (1–174) of ABP34 gave 23 hits covering nine unique proteins with a Z-score higher than 6.0. The top hit is calmodulin from Homo sapiens [PDB entry 3uct; Z-score of 7.2; r.m.s.d. of 1.9 Å over 69 Cα atoms; (Senguen and Grabarek, 2012)], followed by the representative EF-hand containing proteins (S100-A4, calgranulin A , S100-A6, calbindin, troponin C etc.) (Fig. 35, Table 5).

3.7. Structural homology of ABP34 C-terminal domain

We investigated the C-terminal actin binding region of ABP34 by DALI Server (Table 6). The search for structural homologs of C-terminal domain of ABP34 represented, the rod shaped helical structure of the cytoskeletal proteins α-spectrin, α-actinin, dystrophin, utrophin spectrin repeats and tubulin-specific chaperone A and tubulin binding cofactor A (Fig. 39). These proteins and domains are three-helix bundles or left-handed coiled-coil helical structures, like the ABP34 C-terminal domain. The structural homology arises not only because they are both coiled-coil structures, which obviously defined a particular fold that can be found in many proteins, but also because the length of the rod units is identical in ABP34 C-terminal domain and tubulin chaperon cofactor A and spectrin repeats (Guasch *et al.*, 2002). Especially, C-terminal helix of ABP34 has hydrophobic core of bundled folding formation, resemble to other actin binding proteins. It is likely that three helix bundled domain stabilizes conformation of the actin binding proteins. Furthermore, as in the ABP34 C-terminal domain and tubulin binding cofactor A family, the second helix is distorted (Fig. 39). The structure is a monomer with a rod-like shape and consists of a three α-helix bundle with the second helix kinked by a proline break, offering a convex surface at one face of the protein.

3.8. F-actin binding model

To gain insights into the F-actin binding mode of ABP34, molecular docking between F-actin and ABP34 was performed using *PatchDock* server (Schneidman-Duhovny *et al.*, 2005). The ABP34 monomer was docked into F-actin structure [PDB code : 3G37 (Murakami *et al.*, 2010)], and molecular

docking was attempted based on the shape-complementary-principles algorithm in *PatchDock* server. After extensive rounds of modeling, we obtained a proper model showing that ABP34 binds to the side of actin filament and the residues 216–244 in ABS2 fit into a pocket between actin subdomains 1 and 2, with a buried surface of actin (Fig. 40). Actin subdomain 1 (residues 1–32, 70–144 and 338–372) is a preferred target domain for many actin binding proteins (Djinovic-Carugo and Carugo, 2010). Filamin binds all actin isoforms, and the binding sites on actin have been shown to reside at actin subdomain 1 (Mejean *et al.*, 1992). Moreover, the binding interface between actin and α-actinin is located in actin subdomain 1 near Thr103 (Mimura and Asano, 1987). These sites are also found in other actin-binding proteins, including myosin, tropomyosin and caldesmon (McGough, 1998). As mentioned in section 3.5, the conserved residues 216–244 in ABS2 of ABP34 are crucial for strong actin binding and mostly hydrophobic, which is the force driving the interaction with actin filaments (Franzot *et al.*, 2005). In addition, in cells, diverse actin cross-linkers or bundlers interact with the actin filaments by side-binding sequences likely with α-actinin (Crevenna *et al.*, 2015). This conserved region is an archetypical binding site for a broad family of actin-binding proteins that bind to the side of actin filaments in spectrin superfamily, which includes α-actinin and ABP120 (Bresnick *et al.*, 1991; Vandekerckhove and Vancompernolle, 1992; Franzot *et al.*, 2005). Consequently, the residues 216–244 of ABP34 may bind to the side of subdomain 1 in an actin filament through hydrophobic interaction between the surface residues on ABS2 and, similarly to several other actin-bundling proteins.

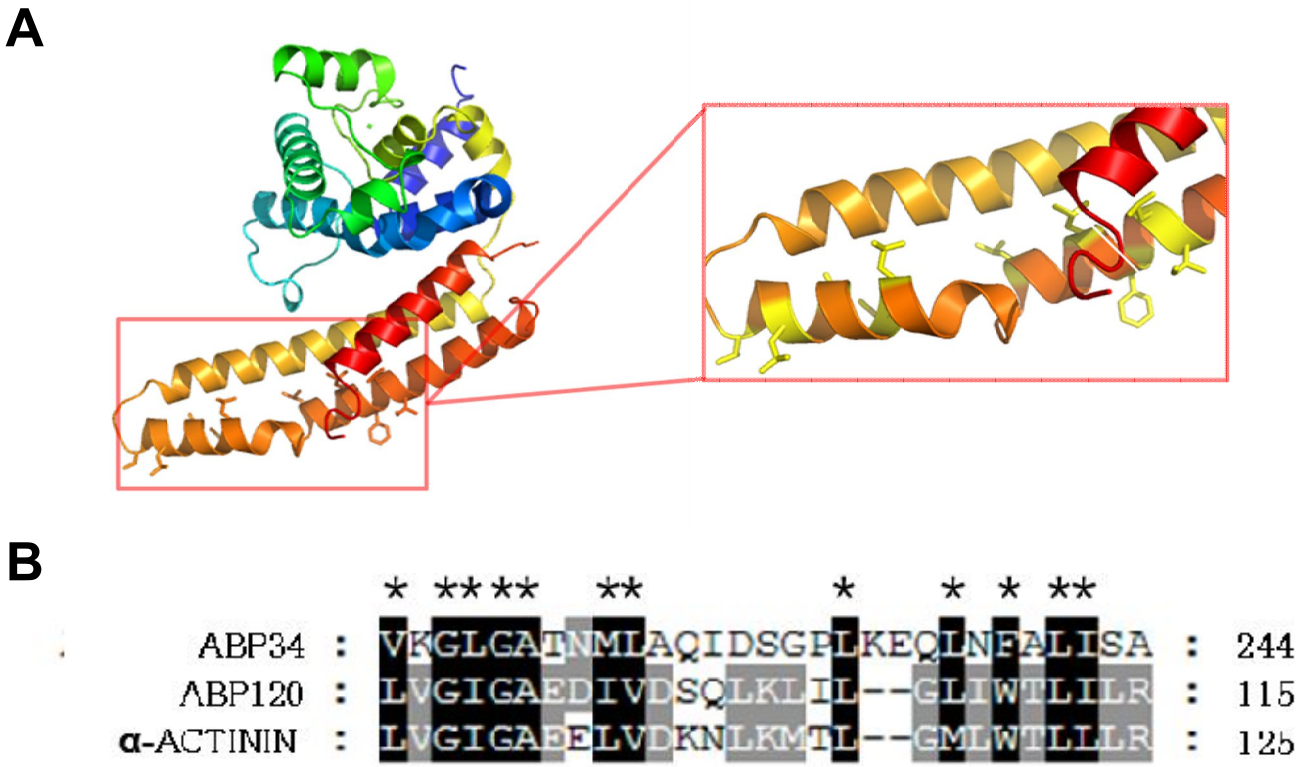

Fig. 38. Sequence conservation of actin binding region of ABP34. (A) Cartoon diagram of ABP34 C-domain. Conserved residues in A are shown as sticks and labelled. (B) Multiple sequence alignment of the strong actin binding region (216–244) in C-domain of ABP34 with the actin binding regions in α-actinin and ABP120. Conserved residues are highlighted in black boxed letters and marked with asterisks.

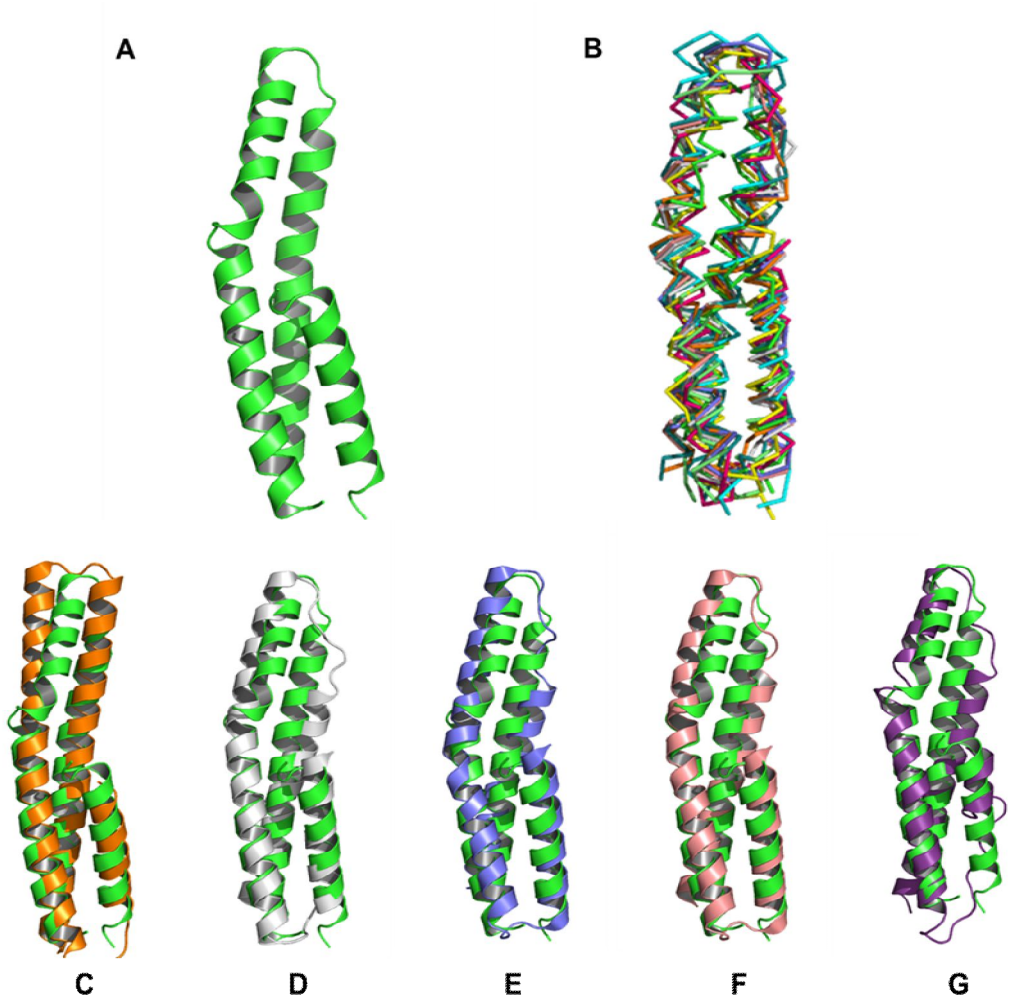

Fig. 39. Comparision of C-terminal structure of ABP34. (A) Cartoon representations of C-terminal structure of ABP34, (B) Structure superimposition of the C-terminal of ABP34. Structural comparisons of ABP34 C-domain (green) with the top-scored DALI hits. (C) Tubulin-specific chaperon A (orange), (D) α-spectrin repeat 16 (gray), (E) Utrophin spectrin repeat (blue), (F) Dystrophin spectrin repeat 1 (pink), (G) α-actinin 3 spectrin repeat 1 (purple). The differences in the actin binding region and the connecting loop are presented by red dotted ellipses.

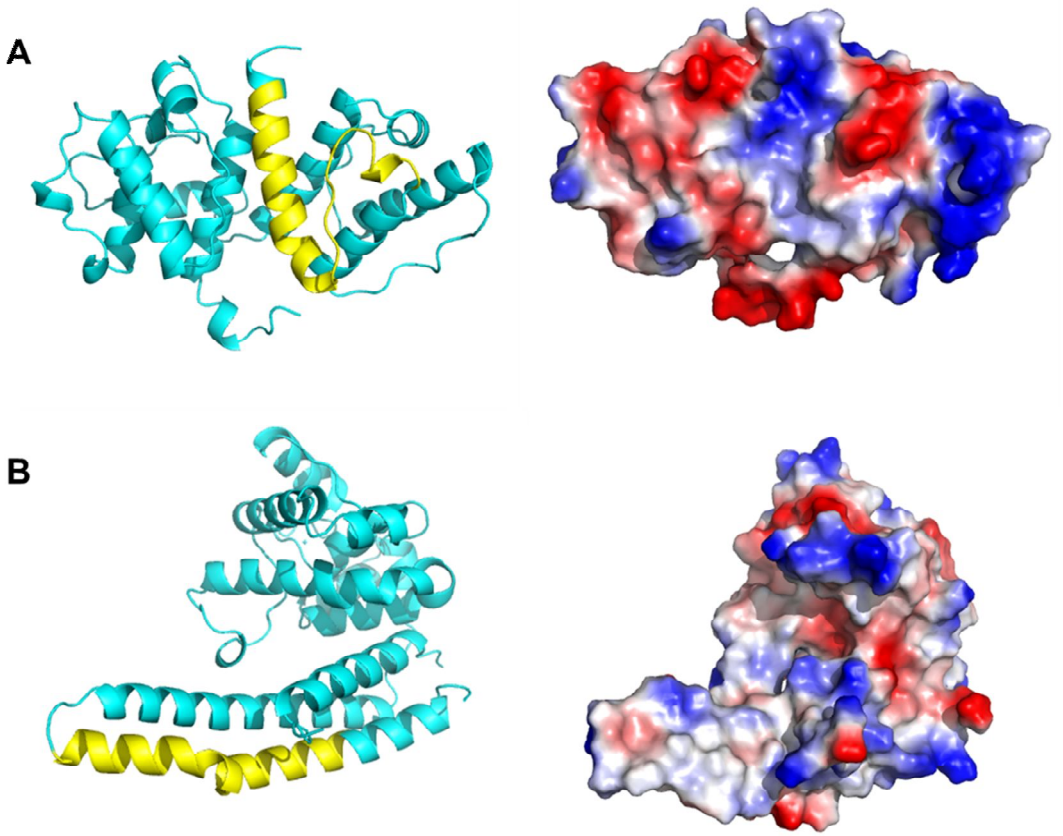

Fig. 40. Human α-actinin and ABP34 structure of actin binding domain. (A) is cartoon diagrame of human α-actinin structure (left), right is electrostatic surface charge model of human α-actinin; (B) is cartoon diagrame of ABP34 (left), right is electrostatic surface charge model of ABP34. The actin binding regions are coloured by yellow.

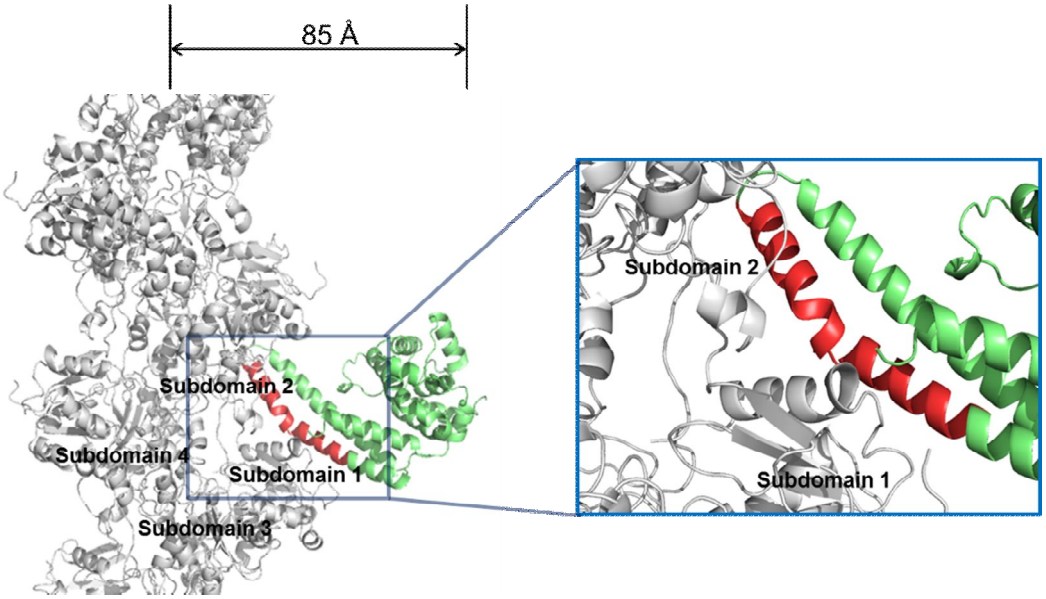

Fig. 41. Complex model of F-actin with ABP34.

Cartoon diagram of F-actin binding model. ABP34 monomer is docked into F-actin using *PatchDock* server. ABP34 (green) is located in the surface between subdomain 1 and subdomain 2 of an actin monomer (yellow) in F-actin (gray). The strong actin binding region (216–244) is coloured by red and in the enlarged panel, the residues 216–244 are shown as sticks.

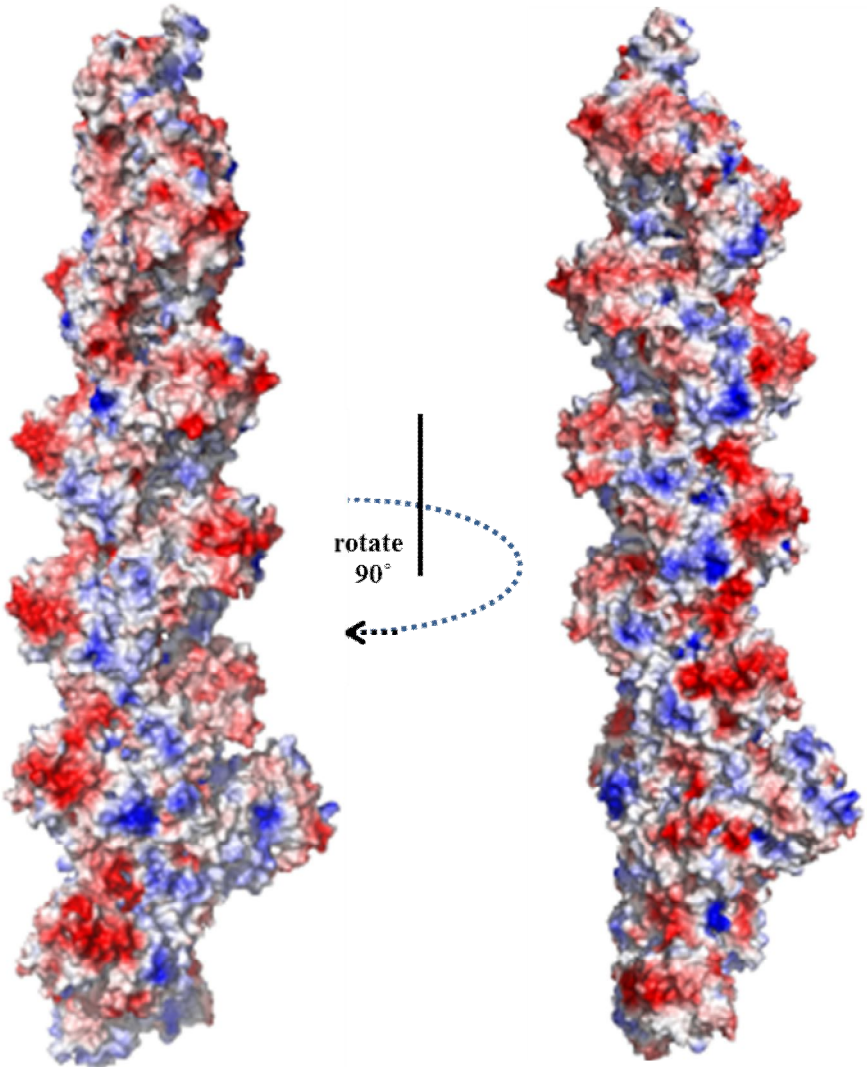

Fig. 42. Electrostatic potential surface diagram of complex model of actin filament with ABP34. The surface is colored according to charge; positive potential at the surface is indicated in blue, negative potential is indicated in red. ABP34 monomer is docked into F-actin using PatchDock server (left) and clockwise 90˚ rotation view (right). The figure was prepared by PyMOL.

Table 5. DALI server results with full-length ABP34.

PDB code	Protein	Z-score	R.m.s.d.s	Length aligned
3HAI-A	human pacsin1 F-BAR	8.3	2.6	74
2F1M-A	Acriflavine resistance protein A	8.3	9.5	84
3MXZ-A	Tubulin-specific chaperone A	8.2	2.6	83
3TUL-B	Cell invasion protein sipB	8.2	6.6	95
3HAJ-B	human pacsin2 F-BAR	7.8	13.1	114
3INN-A	Membrane fusion protein (MFP) heavy metal cation efflux ZneB (CzcB-like)	7.7	2.8	64
2V0O-A	FCH domain only protein 2	7.6	2.6	74
3LLL-B	Protein kinase C and casein kinase substrate in neurons protein 2	7.6	13.7	114
1WP1-A	Outer membrane protein oprM	7.4	2.9	75
2FB5-A	hypothetical Membrane Spanning Protein	7.4	3.4	73
4CQI-A	Tubulin-binding cofactor A	7.4	3.2	91
2FB5-C	hypothetical Membrane Spanning Protein	7.4	3.4	73
3Q4H-B	Pe family protein	7.3	3	74
1KU9-A	hypothetical protein MJ223	7.1	2.8	64
1SER-B	seryl-transfer RNA synthetase	7	2.6	69
2IC6-B	Nucleocapsid protein	7	3.7	74

Table 6. DALI server results with ABP34 N-domain.

PDB code	Protein	Z-score	R.m.s.d.s	Length aligned
3UCT-B	Calmodulin	7.2	1.9	69
4CFQ-A	Protein S100-A4	6.3	3	78
2GV5-B	Cell division control protein 31	6.3	2.3	72
1XK4-H	Calgranulin A	6.2	3	78
1K9K-A	Molecule: S100-A6	6.2	2.8	75
1IRJ-B	Migration inhibitory factor-realted protein 14	6.2	2.7	76
1D1O-A	Calbindin D9K	6.2	2	70
1A2X-A	Troponin C	6.1	2.8	76
4OKH-C	Calpain-3	6.1	3.1	84

Table 7. DALI server results with ABP34 C-domain.

PDB code	Protein	Z-score	R.m.s.d.s	Length aligned
4CQI-A	Tubulin-Binding Cofactor A	8.9	3.6	87
1HX1-B	Heat shock 70 kDa protein 8	8.5	2.5	90
4R61-A	gp41-based construct covNHR3-ABC	8.3	2.9	94
3LDQ-B	Heat shock cognate 71 kDa protein	8.3	2.8	90
1CUN-C	α-Spectrin	8.2	3.1	90
3MXZ-A	Tubulin-specific chaperone A	8.1	2.8	85
3FZF-B	Heat shock cognate 71 kDa protein	8.1	2.8	90

IV. DISCUSSION

The ABP34 is an abundant actin cross-linking protein unique to *Dictyostelium*. The protein localizes at the leading and trailing edges of locomoting cells, filopods, phagocytic cups and cell-to-cell contact sites (Furukawa *et al.*, 2003). To evaluate the role of ABP34 during development and growth, mutant strains that ABP34 overexpressed and its expression level was inhibited by RNA interference in *Dictyostelium*. In the presence study, we identified the *abpB* RNAi cells grew more slowly in axenic medium and showed decrease cell size. During developmental, they showed fast rate culmination and final fruiting body was also small size. But, ABP34 overexpressed cells similar to wild type. GFP fusion proteins are used for this study of the in vivo dynamics of actin binding proteins. ABP34 was associated with the actin cytoskeleton of cells during growth. Under dark condition, they showed a short period slugger migration stage and fast formed fruiting body. These results suggerst that *Dictyostelium* actin bundling protein ABP34 may be important for growth and developmental process, especially migrating slug to fruting body by regulating actin cytoskeleton. In these results, ABP34 protein was concentrated attatched agar surface of prespore region in the slug. This can be understood that movement of cell in the upperpart of the prespore zone is indistinguishable from cell movement on a solid substrate. The cytoskeleton is extended and the retracting rear where it is disassembled. In the slug, a cell would essentially only make contact with the non-moving parts of neighbouring cells, linking their own internal cytoskeleton to that of neighbouring cells via transmembrane adhesion molecules (Weijer, 1999). Notably, previous work frequently reported on the inability of cytoskeletal mutant, particularly of those lacking actin cross-linking or bundling proteins such as α-actinin,

ABP120, the cortexillin or formin to proceed through late development (Witke *et al.*, 1992; Rivero *et al.*, 1999; Shu *et al.*, 2012; Junemann *et al.*, 2013). Double mutant lacking the actin bundling proteins cortexillin I and II, which was shown to be blocked in differentiation and development at the mound stage (Shu *et al.*, 2012). These result defined actin bundling proteins as a critical player in development and and particularly in terminal differentiation.

Previously, biochemical studies have shown that ABP34 has three actin-binding sites, one Ca^{2+}-binding EF hand and intramolecular interaction zones that are important for regulation of actin binding by an N-terminal inhibitory domain (Lim *et al.*, 1999; Lim *et al.*, 1999). In this work, we further characterized the biochemical information of ABP34 which reported new structural features with calcium binding and actin bundling activity of ABP34 protein. The ABP34 recombinant proteins were analyzed using X-ray crystallography and electron microscopy and sedimentation assay.

ABP34 is monomeric stable molecule in vitro when it presence alone.

The ABP34 protein has an apparent subunit molecular weight of 34 kDa as visualized by SDS-PAGE and a native molecular mass of 32,836 Da as determined by gel filtration. Thus, ABP34 is monomeric protein in solution. Although considerable effort has been tried to gel filatration chromatography in various condition of buffer, but we could not find any difference. Moreover, electron microscopy was performed, but the protein is too small to resolve clearly by electron microscopy so its length and shape cannot be directly identified. But previously, Stokes radius of the ABP34 determined by calibration of the columns was 2.7 nm and these indicate that the protein

has an asymmetric shape, assuming a prolate ellipsoid shape (Fechheimer and Taylor, 1984; Furukawa and Fechheimer, 1990). The measurements lead to calculated axial ratio of 3.5 and 5 nm, and lengths of 5.1 and 6.3 nm for the hydrated and anhydrated forms, respectively (Furukawa and Fechheimer, 1990). This value is similar to that of 3.6 nm and 6.2 nm, measured for the width and height of ABP34 protein, respectively on our crystal structure. All of the available evidences support a monomeric structure of the native protein, in addition consideration of the molecular dimensions of the ABP34 protein and the filament bundle suggest that the asymmetric monomer is large enough to span the required distance (Furukawa and Fechheimer, 1990). It was confirmed our result that crystal structure of ABP34 showed asymmetric shape molecule.

ABP34 is calcium regulating protein.

We have examined influence of secondary structure that could explain possibility of conformational change of ABP34 in presence of micro molar calcium and EGTA. Moreover, chromatographic analysis also performed at many conditions of ABP34 with buffer, but ABP34 protein was not significantly affected by changes of extra buffer conditions. This hypothesis is supported by change in free calcium ion concentration that has no detectable effect on the quaternary structure of the ABP34 protein (Fechheimer and Taylor, 1984). Thus, the ABP34 molecule exists as stable monomer when it presences alone, although that binding to F-actin, the significance of ABP34 dimerization or whether it is required for actin bundling activity is unknown (Fechheimer and Taylor, 1984).

Ca^{2+} binding site of ABP34 is highly conserved in the structure of most

calcium binding proteins. The interaction of the ABP34 with actin was highly dependent on the free calcium ion concentration. The ABP34 actin binding protein is known to bind and cross-link actin filament into bundling at low concentration (1×10^{-8} M) of free calcium, but the activity is significantly inhibited in the presence of a free calcium ion concentration of high calcium concentration (2×10^{-8} M) by sedimentation, viscometry, electron microscopy (Fechheimer and Taylor, 1984; Fechheimer, 1987; Lim and Fechheimer, 1997). This result indicates that a change in free Ca^{2+} may regulate the actin interaction under physiological conditions. The free calcium ion concentration regulates gelation in mixtures of actin and the ABP34 in vitro by controlling the number of cross links between the filaments (Fechheimer and Taylor, 1984; Fechheimer, 1987).

Functinal and Non- functional EF-hand in ABP34

The regulatory EF-hand protein is the ability to change their conformation upon binding Ca^{2+}, thus acquiring different interactive properties. In the high calcium concentration, the N-domain nonfunctional EF-hand and calcium bound EF-hand of ABP34 could undergo a conformational change that inhibit F-actin binding by the ABS2 from the other polypeptide chain. Because inter domain interaction of ABP34 could be possible this binding by exposing the ABS in both C-domain and N-domain. The mechanism by which Ca^{2+} causes the “opening” in CaM and other Ca^{2+}-sensor proteins adopt the open conformation because the geometric strain caused by binding Ca^{2+} in the closed domain conformation is energetically more costly than the exposure of hydrophobic side-chains in the open conformation. Undoubtedly, the energy balance plays an important

role by linking the domain opening to the Ca^{2+} and target binding (Grabarek, 2006). Herzberg et al. proposed that Ca^{2+}-binding causes a transition from the closed to the open domain conformation, in which the exposed hydrophobic pocket serves as a target interaction site (Herzberg *et al.*, 1986; Grabarek, 2006). ABP34 also may be "open conformation" caused by binding Ca^{2+} in N-domain nonfunctional EF-hand thereby exposure of hydrophobic side-chain between two domains that possibly inhibit F-actin binding. Structural studies have shown that the regulatory domains of skeletal and cardiac troponin C (sNTnC and cNTnC) undergo different conformational changes upon Ca^{2+} binding; sNTnC "opens" with a large exposure of the hydrophobic surface, while cNTnC retains a "closed" conformation similar to that in the apo state (McKay *et al.*, 2000). In addition to its role in regulating the interaction of plectin1a (P1a) and integrin β4, Kostan et al showed that Ca^{2+}-CaM also prevents plectin ABD from binding to F-actin (Kostan *et al.*, 2009). The binding of Ca^{2+}-CaM to the N-terminal extension of P1a is involved in disruption of the plectin/integrin β4 and plectin/F-actin complexes by shunting integrin β4 and F-actin, without directly competing for the binding site (Song *et al.*, 2015). At low cytosolic calcium concentrations, the P1a/integrin α6β4 complex is maintained in hemidesmosomes (HD) (Green and Jones, 1996). Increased cytosolic calcium concentration, during differentiation or wound healing, leads to activation of CaM (Ca^{2+}-CaM). CaM in its active form binds to the structurally disordered N-term tail of P1a via its N-terminal lobe. CaM binding leads to the folding of the N-term tail of P1a into an α-helix. The steric clash caused by CaM bound to the α-helix results in shunting of integrin 4 from the complex, contributing to HD disassembly (Song *et al.*,

2015). In ABP34, in which site nonfunctional EF1 does not bind Ca^{2+}, the N-terminal domain remains closed with C-domain by interdoamin interaction, upon Ca^{2+} binding to the single active functional EF2. In the original crystal structure of ABP34 and Ca^{2+} is bound only to the N-domain one EF2, which presents a close conformation with an intact, solvent-not exposed hydrophobic pocket in inter-domain interaction region. Since ABP34 is buried in the closed conformation, the ABS1, ABS2 and ABS3 in N-domain and C-domain ABP34 are expected to arrange upon binding to actin filaments. Thus, the Ca^{2+}-free N-terminal domain also has a closed conformation in which all helices are tightly packed against each other. But, increased cytosolic calcium concentration, It may be open, leads to activation of non-functional EF-hand (Ca^{2+}-EF1). EF1 in its active form binds to the structurally disordered C-terminal ABS of ABP34 via its N-terminal inter-domain region. Ca^{2+}-EF1 binding leads to the open of the C-terminal and N-terminal inter-domain region. The steric clash possibly caused by Ca^{2+} bound to the α-helix results in shunting of ABP34 from the F-actin complex, contributing to F-actin bundle disassembly. Finally, it is proposed that non-functional EF1 putative calcium binding loop of N-domain is an important determinant of the conformational change and regulation of F-actin bundling by extra calcium concentration as calmodulin like domain of α-actinin and calmodulin regulated other proteins.

ABP34 interacts with actin filaments and forms actin bundle

Formation of bundles of actin filaments in the ABP34 protein was confirmed by sedimentation analysis and electron microscopy. The ABP34 binds to actin in an apparent molecular ratio of 1:20, but variation of bundle

formation ratio is existed of reaction time and filament length distribution (Fechheimer and Taylor, 1984; Furukawa and Fechheimer, 1996). Typically the F-actin binding saturated at one ABP34 protein molecule per 10-20 actin monomers in a filament (Lim and Fechheimer, 1997)). It is different to other actin bundling proteins in the saturation level of interaction with actin. fimbrin, fascin, and α-actinin protein exhibit saturable binding at a level of one actin binding protein to 3, 5, and 7 actin monomers in filaments, respectively (Bryan and Kane, 1978; Fechheimer, 1987; Meyer and Aebi, 1990). Thus, the ABP34 is expected to bind tightly to actin in the cells and to leave a large fraction of the actin filaments available for interaction with other macromolecules (Fechheimer, 1987).

Parallel actin bundles form the core structure of cellular protrusions such as filopodia, microvilli. These structures are tightly packed, noncontractile bundles cross-linked by a class of F-actin bundling proteins, such as fascin and fimbrin, that determine ~12 nm spacing between actin filaments (Volkmann *et al.*, 2001), and the involvement of such proteins is essential for structure formation. Bundling proteins such as fascin, the ABP34 proteins have short rigid conformation molecules lacking the flexibility. The cross-linking proteins such as filamin and spectrin are long, flexible macromolecules, while the ABP34 bundling proteins are shorter and presumably less flexible (Fechheimer and Furukawa, 1993). The center to center spacing of actin filaments in bundles of actin and the 30 kDa proteins is 10.2 nm after correction both of the perspective of viewing filaments (Furukawa and Fechheimer, 1990). This value is similar to that of 10-12 nm observed for the center to center spacing of actin filaments in both native and reconstituted cross-linked bundles of actin with villin and fimbrin.

Estimates of the diameter of the actin filament indicate that mass extends as far as a single filament diameter of 10 nm. Thus the space to be traversed by the cross-linking protein may as short as 1 to 2 nm and could be accommodated by a rod–shape molecule 6 nm in length. Thus, this protein is present in the cross-link as an asymmetric monomer. In consideration of the molecular dimensions of the ABP34 protein and of the filament bundle suggest that the asymmetric monomer is large enough to span the required distance (Furukawa and Fechheimer, 1990).

The structure of C-terminal region of ABP34

A search for structural homologs of C-terminal domain of ABP34 represented, the rod shaped helical structure of the cytoskeletal proteins α-spectrin, α-actinin, dystrophin, utrophin spectrin repeats and tubulin-specific chaperone A and tubulin binding cofactor A. These proteins and domains are three-helix bundles or left-handed coiled-coil helical structures, like the ABP34 C-terminal domain (Guasch *et al.*, 2002). The spectrin repeat is a domain composed of three α-helices (Muthu *et al.*, 2012). A number of aromatic residues in the hydrophobic core of the domain are typically conserved (Djinovic-Carugo *et al.*, 2002). But the spectrin-like repeats utrophin and α-actinin rod domain exhibited no measurable actin binding activity when expressed in the absence of the amino-terminal domain (Djinovic-Carugo *et al.*, 2002; Rybakova and Ervasti, 2005)). Interestingly, only a limited portion of the dystrophin rod domain is directly involved in binding F-actin. The actin binding rod domain is highly sensitive to ionic strength, suggests that a cluster of basic repeats in the dystrophin rod domain binds actin through electrostatic interactions (Amann *et al.*, 1998). Thus, as

is the case for dystrophin, electrostatic interactions may contribute to the actin binding activity of other proteins. Moreover, typical spectrin repeat has three conserved helices. The surface of each helix in the repeat unit has conserved charged and nonpolar residues that are important not only for stabilizing the repeat through intramolecular interactions but also for interactions with other proteins and cytoplasmic structures (Otey and Carpen, 2004; Virel and Backman, 2007).

27 amino acids of ABP34 C-terminal regions

Sequence alignments of the ABP34 protein with other protein, partial actin binding sequence has little sequence homology to the ABP34 in actin binding site amino acids. The homology is meaningful prediction of specific conserved regions as actin binding sites in α-actinin and ABP-120 proteins. These amino acids is essential for actin binding ABP-120 with 27-mer region in *Dictyostelium* α-actinin (Noegel *et al.*, 1987), chicken pectoralis α-actinin (Arimura *et al.*, 1988), human ABP/filamin (Gorlin *et al.*, 1990), human dystrophin (Koenig *et al.*, 1988), chicken dystrophin (Lemaire *et al.*, 1988), and *Drosophila* β-spectrin (Byers, 1989). The 27 amino acids is hydrophobic character that for the actin crosslinking proteins, binding occurs through hydrophobic interactions (Bresnick *et al.*, 1990). And the main actin binding residues surrounding concentrate to hydrophobic and charged amino acids, helix of C-terminal ABP34. From the structure of terminal domain of ABP34 protein play critical role in formation of filament bundle. Additionally, absence of terminal domain in 27kDa fragment of ABP34 does not bundle the actin filament (Fechheimer and Furukawa, 1993).

The conserved hydrophobic 27 amino acids of α-actinin are located in

last α-helix of the calponin homology (CH), linker loops that connect the two CH domains in α-actinin structure (Lee *et al.*, 2008). ABP34 has not CH domain but conserved 27 amino acid region is crucial for binding region. This conservation is probably significant, since the overall sequence identity between the actin binding proteins are solvent exposed from part of the actin-binding interface. Analysis of conservation of solvent-exposed amino acid residues implicated in actin binding sites (ABS1, ABS2 and ABS3) or close to them shows conserved hydrophobic patches on ABS2. The conservation at the amino acid level is in line with the fact that actin is one of the most conserverd proteins in nature, imposing therefore evolutionary pressure on the actin-binding sites of the interaction protein that the force driving the interaction with actin filaments is at least partly hydrophobic (Sjöblom *et al.*, 2008). Thus, there is no structural homology between α-actinin and ABP34, the conserved 27 amino acids of actin binding region plays a central role in actin interactions.

F-Actin binding model of ABP34 protein

The positioning of actin binding sites experiments with defined segment of recombinant protein reveal three actin binding sites located at amino acids 1-123, 193-254, and 279-295 (Lim *et al.*, 1999). The strongest of these sites, located at amino acids 193-254, is necessary and sufficient for co-sediment with F-actin in vitro (Lim *et al.*, 1999). In the model of ABP34 with actin, ABP34 was bound to actin molecules by one of the C-terminal helix, residues 216-230, which region is included in the strong actin-binding site, 193-254, in ABP34 protein. The helix corresponding to actin binding in the ABP34 structure fits into a pocket between actin subdomains 1 and 2, with a

buried surface of actin. Thus, the estimated binding site of ABP34 structurally protruded for easily actin binding.

Additionally, between the diverse cross-linkers or bundlers interact with the actin filament by side-binding sequences which include α-actinin (Crevenna *et al.*, 2015). The conservation of the sequence in a number of actin cross-linking proteins, the 27 amino acid sequence is an archetypical binding site for a broad family of actin binding proteins that bind to the sides of actin filaments (Bresnick *et al.*, 1991; Vandekerckhove and Vancompernolle, 1992). It is structurally conceivable description that bundling protein binds to side of filaments. ABP34 is also actin bundling protein like several proteins that would bind to the side of actin filaments. The hydrophobic residues mediate binding to the side of actin filaments, whereas the charged residues permit binding to divalent ion via actin binding proteins. Therefore, the residues 216-244 of ABP34 may bind to side of actin filament subdomain 1 which occur hydrophobic interaction by surface residues on actin binding domain like several other actin-bundling proteins. In addition, actin subdomain 1 (residues 1-32, 70-144 and 338-372) is the preferred target domain for many actin binding proteins (Djinovic-Carugo and Carugo, 2010). These sites overlap with those of several actin-binding proteins (McGough, 1998). Thus conformational accessibility and sequence homology can easily account for F-actin binding. Therefore, different cytoskeletal proteins can simultaneously interact with actin filaments affects the structure of actin bundles and their mechanical properties and may be of great importance in formation of different elements of cytoskeleton (Gusev, 2001). Consequently, surface composition and sequence conservation of actin binding proteins suggest the specific actin-binding motif for functional

relationships with actin bundling in the ABP34 protein.

Structural and functional relationship of ABP34

ABP34 is calcium regulated F-actin bundling protein in *D. discoideum*. The F-actin binding and bundling activities of recombinant ABP34 were verified by co-sedimentation assay and transmission electron microscopy data, respectively. The co-localization of ABP34 and actin in cells was also confirmed through fluorescence microscopy. The ABP34 adopts a two-domain structure with an EF-hand containing an N-domain and a strong actin-binding C-domain. The EF-hand is occupied by a calcium ion with pentagonal bipyramidal coordination likely with the canonical EF-hand. The residues 216–244 in the C-domain are part of the strongest actin-binding sites (193–254) and have conserved sequences with the actin-binding region of α-actinin and ABP120. The second helical region of C-domain is implicated in actin binding. The F-actin binding model suggests that ABP34 may bind to the side of actin between actin subdomains 1 and 2 through hydrophobic interactions. The inter-domain interactions participate in the connection between calcium binding (EF-hand in the N-domain) and actin binding (ABS2 in the C-domain). Interaction with calcium ion appears to compact form in the ABP34 structure. ABP34 organize bundles of actin filament in vitro and folded monomer for intact protein. Actin filament bundling may be monomeric state of ABP34. Thus, ABP34 could form more effective bundling short actin filament space by regulating cortical actin filament, thereby controlling the cell size and the proper localization of cytoskeleton component. Moreover these effective bundling may lead by Ca^{2+} binding structure of ABP34. This explanation is supported by the

observation that the difference in localizationof ABP34 and F-actin at the trailing edge of moving cells is not observed in cells expressing the calcium-insensitive ABP34 calcium binding site deletion mutant (ΔEF2) protein (Furukawa *et al.*, 2003). Further, the trailing edge of cells expressing ABP34 ΔEF2 was sometimes extended and contained large aggregates of actin filaments that appeared to have been released from the posterior cortex but not yet disassembled. The decrease in the ABP34 at rear of the cell could be a result of calcium induced release from actin. These results suggest that the calcium-insensitive ABP34 ΔEF2 protein is not readily disassociated from actin at the rear of the cell, remains bound to F-actin in the tail and inhibits depolymerization of actin at the rear (Furukawa *et al.*, 2003).

Thus the interpretation consistent with all of the data available at this time is that the cross-link is a monomer of the ABP34 by tightly binding of Ca^{2+}. Each cross-link contains one molecule of ABP34 by two main actin binding sites for actin and terminal actin binding sites of ABP34 may allow flexibility in the orientation of the interaction with several actin filaments and effective bundling by Ca^{2+} binding. To elucidate the detailed mechanism through which ABP34 achieves F-actin bundling in a calcium-regulated manner, it is essential to obtain the crystal structures of Ca^{2+}-free and actin complex of ABP34. Further study for mutagensesis of possible actin binding sites from structure should be followed for identifying actin bundling mechanism of ABP34.

V. REFERENCES

Adams, P. D., Afonine, P. V., Bunkoczi, G., Chen, V. B., Davis, I. W., Echols, N., Headd, J. J., Hung, L. W., Kapral, G. J., Grosse-Kunstleve, R. W., McCoy, A. J., Moriarty, N. W., Oeffner, R., Read, R. J., Richardson, D. C., Richardson, J. S., Terwilliger, T. C. and Zwart, P. H. (2010). PHENIX: a comprehensive Python-based system for macromolecular structure solution. *Acta Crystallogr D Biol Crystallogr* **66**, 213-221.

Amann, K. J, Renley, B. A. and Ervasti, J. M. (1998). A cluster of basic repeats in the dystrophin rod domain binds F-actin through an electrostatic interaction. *Journal of Biological Chemistry* **273**, 28419-28423.

Annesley, S. J. and Fisher, P. R. (2009). *Dictyostelium discoideum*--a model for many reasons. *Mol Cell Biochem* **329**, 73-91.

Arimura, C., Suzuki, T., Yanagisawa, M., Imamura, M., Hamada, Y. and Masaki, T. (1988). Primary structure of chicken skeletal muscle and fibroblast α-actinins deduced from cDNA sequences. *European Journal of Biochemistry* **177**, 649-655.

Aubry, L. and Firtel, R. (1999). Integration of signaling networks that regulate *Dictyostelium* differentiation. *Annu Rev Cell Dev Biol* **15**, 469-517.

Bennett, H. and Condeelis, J. (1988). Isolation of an immunoreactive analogue of brain fodrin that is associated with the cell cortex of *Dictyostelium* amoebae. *Cell Motil Cytoskeleton* **11**, 303-317.

Biekofsky, R. R. and Feeney, J. (1998). Cooperative cyclic interactions involved in metal binding to pairs of sites in EF-hand proteins. *FEBS letters* **439**, 101-106.

Bonner, J. and Williams, J. (1994). Inhibition of cAMP-dependent protein kinase in *Dictyostelium* prestalk cells impairs slug migration and phototaxis. *Dev Biol* **164**, 325-327.

Bremer, A. and Aebi, U. (1992). The structure of the F-actin filament and the actin molecule. *Curr Opin Cell Biol* **4**, 20-26.

Bresnick, A. R., Janmey, P. A. and Condeelis, J. (1991). Evidence that a 27-residue sequence is the actin-binding site of ABP-120. *J Biol Chem* **266**, 12989-12993.

Bresnick, A. R., Warren, V. and Condeelis, J. (1990). Identification of a short sequence essential for actin binding by *Dictyostelium* ABP-120. *J Biol Chem* **265**, 9236-9240.

Bretscher, A., Osborn, M., Wehland, J. and Weber, K. (1981). Villin associates with specific microfilamentous structures as seen by immunofluorescence microscopy on tissue sections and cells microinjected with villin. *Exp Cell Res* **135**, 213-219.

Bretscher, A. and Weber, K. (1979). Villin: the major microfilament-associated protein of the intestinal microvillus. *Proc Natl Acad Sci U S A* **76**, 2321-2325.

Brier, J., Fechheimer, M., Swanson, J. and Taylor, D. L. (1983). Abundance, relative gelation activity, and distribution of the 95,000-dalton actin-binding protein from *Dictyostelium discoideum*. *J Cell Biol* **97**, 178-185.

Brink, M., Gerisch, G., Isenberg, G., Noegel, A. A., Segall, J. E., Wallraff, E. and Schleicher, M. (1990). A *Dictyostelium* mutant lacking an F-actin cross-linking protein, the 120-kD gelation factor. *J Cell Biol* **111**, 1477-1489.

Bryan, J. and Kane, R. E. (1978). Separation and interaction of the major components of sea urchin actin gel. *Journal of molecular biology* **125**, 207-224.

Carboni, J. M. and Condeelis, J. S. (1985). Ligand-induced changes in the location of actin, myosin, 95K (alpha-actinin), and 120K protein in amebae of *Dictyostelium discoideum*. *J Cell Biol* **100**, 1884-1893.

Cocucci, S. M. and Sussman, M. (1970). RNA in cytoplasmic and nuclear fractions of cellular slime mold amebas. *The Journal of cell biology* **45**, 399-407.

Condeelis, J. (1993). Life at the leading edge: the formation of cell protrusions.

Annu Rev Cell Biol **9**, 411-444.

Condeelis, J., Vahey, M., Carboni, J. M., DeMey, J. and Ogihara, S. (1984). Properties of the 120,000- and 95,000-dalton actin-binding proteins from *Dictyostelium discoideum* and their possible functions in assembling the cytoplasmic matrix. *J Cell Biol* **99**, 119s-126s.

Choi, C. H. (2004). Roles of Glutaredoxin 1 in Development of *Dictyostelium discoideum*. *Seoul National University* Ph.D. Thesis.

Cox, D., Condeelis, J., Wessels, D., Soll, D., Kern, H. and Knecht, D. A. (1992). Targeted disruption of the ABP-120 gene leads to cells with altered motility. *J Cell Biol* **116**, 943-955.

Crevenna, A. H., Arciniega, M., Dupont, A., Mizuno, N., Kowalska, K., Lange, O. F., Wedlich-Soldner, R. and Lamb, D. C. (2015). Side-binding proteins modulate actin filament dynamics. *Elife* **4**.

Devreotes, P. N. and Zigmond, S. H. (1988). Chemotaxis in eukaryotic cells: a focus on leukocytes and *Dictyostelium*. *Annu Rev Cell Biol* **4**, 649-686.

Djinovic-Carugo, K. and Carugo, O. (2010). Structural portrait of filamin interaction mechanisms. *Curr Protein Pept Sci* **11**, 639-650.

Djinovic-Carugo, K., Gautel, M., Ylänne, J. and Young, P. (2002). The spectrin repeat: a structural platform for cytoskeletal protein assemblies. *FEBS letters* **513**, 119-123.

Dormann, D. and Weijer, C. J. (2001). Propagating chemoattractant waves coordinate periodic cell movement in *Dictyostelium* slugs. *Development* **128**, 4535-4543.

Egelman, E. H., Francis, N. and DeRosier, D. J. (1982). F-actin is a helix with a random variable twist. *Nature* **298**, 131-135.

Eichinger, L., Koppel, B., Noegel, A. A., Schleicher, M., Schliwa, M., Weijer, K.,

Witke, W. and Janmey, P. A. (1996). Mechanical perturbation elicits a phenotypic difference between *Dictyostelium* wild-type cells and cytoskeletal mutants. *Biophys J* **70**, 1054-1060.

Eichinger, L., Lee, S. S. and Schleicher, M. (1999). *Dictyostelium* as model system for studies of the actin cytoskeleton by molecular genetics. *Microsc Res Tech* **47**, 124-134.

Eichinger, L. and Noegel, A. A. (2005). Comparative genomics of *Dictyostelium discoideum* and *Entamoeba histolytica*. *Curr Opin Microbiol* **8**, 606-611.

Emsley, P. and Cowtan, K. (2004). Coot: model-building tools for molecular graphics. *Acta Crystallogr D Biol Crystallogr* **60**, 2126-2132.

Faix, J., Steinmetz, M., Boves, H., Kammerer, R. A., Lottspeich, F., Mintert, U., Murphy, J., Stock, A., Aebi, U. and Gerisch, G. (1996). Cortexillins, major determinants of cell shape and size, are actin-bundling proteins with a parallel coiled-coil tail. *Cell* **86**, 631-642.

Fechheimer, M. (1987). The *Dictyostelium discoideum* 30,000-dalton protein is an actin filament-bundling protein that is selectively present in filopodia. *J Cell Biol* **104**, 1539-1551.

Fechheimer, M. and Furukawa, R. (1991). Preparation of 30,000-Da actin cross-linking protein from *Dictyostelium discoideum*. *Methods Enzymol* **196**, 84-91.

Fechheimer, M. and Furukawa, R. (1993). A 27,000-D core of the *Dictyostelium* 34,000-D protein retains Ca^{2+}-regulated actin cross-linking but lacks bundling activity. *J Cell Biol* **120**, 1169-1176.

Fechheimer, M., Ingalls, H. M., Furukawa, R. and Luna, E. J. (1994). Association of the *Dictyostelium* 30 kDa actin bundling protein with contact regions. *J Cell Sci* **107 (Pt 9)**, 2393-2401.

Fechheimer, M., Murdock, D., Carney, M. and Glover, C. V. (1991). Isolation

and sequencing of cDNA clones encoding the *Dictyostelium discoideum* 30,000-dalton actin-bundling protein. *J Biol Chem* **266**, 2883-2889.

Fechheimer, M. and Taylor, D. L. (1984). Isolation and characterization of a 30,000-dalton calcium-sensitive actin cross-linking protein from *Dictyostelium discoideum*. *J Biol Chem* **259**, 4514-4520.

Fechheimer, M. and Taylor, D. L. (1987). Introduction of exogenous molecules into the cytoplasm of *Dictyostelium discoideum* amoebae by controlled sonication. *Methods Cell Biol* **28**, 179-190.

Feng, Y. and Walsh, C. A. (2004). The many faces of filamin: a versatile molecular scaffold for cell motility and signalling. *Nat Cell Biol* **6**, 1034-1038.

Fire, A., Xu, S., Montgomery, M. K., Kostas, S. A., Driver, S. E. and Mello, C. C. (1998). Potent and specific genetic interference by double-stranded RNA in *Caenorhabditis elegans*. *nature* **391**, 806-811.

Fisher, P. R. (1997). Genetics of phototaxis in a model eukaryote, *Dictyostelium discoideum*. *Bioessays* **19**, 397-407.

Franzot, G., Sjoblom, B., Gautel, M. and Djinovic Carugo, K. (2005). The crystal structure of the actin binding domain from alpha-actinin in its closed conformation: structural insight into phospholipid regulation of alpha-actinin. *J Mol Biol* **348**, 151-165.

Friedberg, F. and Rivero, F. (2010). Single and multiple CH (calponin homology) domain containing multidomain proteins in *Dictyostelium discoideum*: an inventory. *Mol Biol Rep* **37**, 2853-2862.

Furukawa, R. and Fechheimer, M. (1994). Differential localization of alpha-actinin and the 30 kD actin-bundling protein in the cleavage furrow, phagocytic cup, and contractile vacuole of *Dictyostelium discoideum*. *Cell Motil Cytoskeleton* **29**, 46-56.

Furukawa, R. and Fechheimer, M. (1996). Role of the *Dictyostelium* 30 kDa protein in actin bundle formation. *Biochemistry* **35**, 7224-7232.

Furukawa, R., Maselli, A., Thomson, S. A., Lim, R. W., Stokes, J. V. and Fechheimer, M. (2003). Calcium regulation of actin crosslinking is important for function of the actin cytoskeleton in *Dictyostelium*. *J Cell Sci* **116**, 187-196.

Furukawa, R. and Fechheimer, M. (1990). Localization, expression, evolutionary conservation, and structure of the 30,000 dalton actin bundling protein of *Dictyostelium discoideum*. *Developmental Genetics* **11**, 362-368.

Gerisch, G., Albrecht, R., De Hostos, E., Wallraff, E., Heizer, C., Kreitmeier, M. and Muller-Taubenberger, A. (1993). Actin-associated proteins in motility and chemotaxis of *Dictyostelium* cells. *Symp Soc Exp Biol* **47**, 297-315.

Gifford, J. L., Walsh, M. P. and Vogel, H. J. (2007). Structures and metal-ion-binding properties of the Ca^{2+}-binding helix-loop-helix EF-hand motifs. *Biochem J* **405**, 199-221.

Gorlin, J. B., Yamin, R., Egan, S., Stewart, M., Stossel, T. P., Kwiatkowski, D. J. and Hartwig, J. H. (1990). Human endothelial actin-binding protein (ABP-280, nonmuscle filamin): a molecular leaf spring. *The Journal of Cell Biology* **111**, 1089-1105.

Grabarek, Z. (2006). Structural basis for diversity of the EF-hand calcium-binding proteins. *J Mol Biol* **359**, 509-525.

Green, K. J and Jones, J. C. (1996). Desmosomes and hemidesmosomes: structure and function of molecular components. *The FASEB Journal* **10**, 871-881.

Grosse-Kunstleve, R. W. and Adams, P. D. (2003). Substructure search procedures for macromolecular structures. *Acta Crystallogr D Biol Crystallogr* **59**, 1966-1973.

Guasch, A., Aloria, K., Perez, R., Avila, J., Zabala, J. C. and Coll, M. (2002).

Three-dimensional structure of human tubulin chaperone cofactor A. *J Mol Biol* **318**, 1139-1149.

Gusev, N. B. (2001). Some properties of caldesmon and calponin and the participation of these proteins in regulation of smooth muscle contraction and cytoskeleton formation. *Biochemistry (Mosc)* **66**, 1112-1121.

Hanahan, D. (1983). Studies on transformation of *Escherichia coli* with plasmids. *Journal of molecular biology* **166**, 557-580.

Hartwig, J. H. and Kwiatkowski, D. J. (1991). Actin-binding proteins. *Curr Opin Cell Biol* **3**, 87-97.

Heidel, A. J., Lawal, H. M., Felder, M., Schilde, C., Helps, N. R., Tunggal, B., Rivero, F., John, U., Schleicher, M., Eichinger, L., Platzer, M., Noegel, A. A., Schaap, P. and Glockner, G. (2011). Phylogeny-wide analysis of social amoeba genomes highlights ancient origins for complex intercellular communication. *Genome Res* **21**, 1882-1891.

Herzberg, O., Moult, J. and James, M. N. (1986). A model for the Ca^{2+}-induced conformational transition of troponin C. A trigger for muscle contraction. *J Biol Chem* **261**, 2638-2644.

Hock, R. S. and Condeelis, J. S. (1987). Isolation of a 240-kilodalton actin-binding protein from *Dictyostelium discoideum*. *J Biol Chem* **262**, 394-400.

Holm, L. and Rosenström, P. (2010). Dali server: conservation mapping in 3D. *Nucleic acids research* **38**, W545-W549.

Jeong, S. Y., Choi, C. H., Kim, J. S., Park, S. J. and Kang, S. O. (2006). Thioredoxin reductase is required for growth and regulates entry into culmination of *Dictyostelium discoideum*. *Mol Microbiol* **61**, 1443-1456.

Johns, J. A., Brock, A. M. and Pardee, J. D. (1988). Colocalization of F-actin and 34-kilodalton actin bundling protein in *dictyostelium* amoebae and cultured

fibroblasts. *Cell motility and the cytoskeleton* **9**, 205-218.

Junemann, A., Winterhoff, M., Nordholz, B., Rottner, K., Eichinger, L., Gräf, R. and Faix, J. (2013). ForC lacks canonical formin activity but bundles actin filaments and is required for multicellular development of *Dictyostelium* cells. *European journal of cell biology* **92**, 201-212.

Kamath, R. S, Martinez-Campos, M., Zipperlen, P., Fraser, A. G. and Ahringer, J. (2001). Effectiveness of specific RNA-mediated interference through ingested double-stranded RNA in *Caenorhabditis elegans*. *Genome Biol* **2**, 0002.0001-0002.0010.

Kay, R. R. (1997). *Dictyostelium* development: lower STATs. *Curr Biol* **7**, R723-725.

Kim, J. S. (2011). Roles of the homeodomain-containing protein Hbx4 in *Dictyostelium discoideum*. *Seoul National University* Ph.D. Thesis.

Kim, J. S., Seo, J. H., Yim, H. S. and Kang, S. O. (2011). Homeoprotein Hbx4 represses the expression of the adhesion molecule DdCAD-1 governing cytokinesis and development. *FEBS Lett* **585**, 1864-1872.

Koch, M., Diez, J., Wagner, A. and Fritz, G. (2010). Crystallization and calcium/sulfur SAD phasing of the human EF-hand protein S100A2. *Acta Crystallogr Sect F Struct Biol Cryst Commun* **66**, 1032-1036.

Koenig, M., Monaco, A. P. and Kunkel, L. M. (1988). The complete sequence of dystrophin predicts a rod-shaped cytoskeletal protein. *Cell* **53**, 219-228.

Korenbaum, E. and Rivero, F. (2002). Calponin homology domains at a glance. *J Cell Sci* **115**, 3543-3545.

Kostan, J., Gregor, M., Walko, G. and Wiche, G. (2009). Plectin isoform-dependent regulation of keratin-integrin α6β4 anchorage via Ca^{2+}/calmodulin. *J Biol Chem* **284**, 18525-18536.

Kuspa, A. and Loomis, W. F. (2006). The Genome of *Dictyostelium discoideum*. *Methods Mol Biol* **346**, 15-30.

Lee, S. H., Weins, A., Hayes, D. B., Pollak, M. R. and Dominguez, R. (2008). Crystal structure of the actin-binding domain of α-actinin-4 Lys255Glu mutant implicated in focal segmental glomerulosclerosis. *Journal of molecular biology* **376**, 317-324.

Lemaire, C, Heilig, RLMJ and Mandel, JL (1988). The chicken dystrophin cDNA: striking conservation of the C-terminal coding and 3'untranslated regions between man and chicken. *The EMBO journal* **7**, 4157.

Lim, R. W. and Fechheimer, M. (1997). Overexpression, purification, and characterization of recombinant *Dictyostelium discoideum* calcium-regulated 34,000-dalton F-actin bundling protein from *Escherichia coli*. *Protein Expr Purif* **9**, 182-190.

Lim, R. W., Furukawa, R., Eagle, S., Cartwright, R. C. and Fechheimer, M. (1999). Three distinct F-actin binding sites in the *Dictyostelium discoideum* 34,000 dalton actin bundling protein. *Biochemistry* **38**, 800-812.

Lim, R. W., Furukawa, R. and Fechheimer, M. (1999). Evidence of intramolecular regulation of the *Dictyostelium discoideum* 34,000 Da F-actin-bundling protein. *Biochemistry* **38**, 16323-16332.

Lowry, O. H., Rosebrough, N. J., Farr, A. L. and Randall, R. J. (1951). Protein measurement with the Folin phenol reagent. *J Biol Chem* **193**, 265-275.

Mann, S. K., Richardson, D. L., Lee, S., Kimmel, A. R. and Firtel, R. A. (1994). Expression of cAMP-dependent protein kinase in prespore cells is sufficient to induce spore cell differentiation in *Dictyostelium*. *Proc Natl Acad Sci U S A* **91**, 10561-10565.

Martens, H., Novotny, J., Oberstrass, J., Steck, T. L., Postlethwait, P. and Nellen, W. (2002). RNAi in *Dictyostelium*: the role of RNA-directed RNA

polymerases and double-stranded RNase. *Molecular biology of the cell* **13**, 445-453.

Maselli, A. G., Davis, R., Furukawa, R. and Fechheimer, M. (2002). Formation of Hirano bodies in *Dictyostelium* and mammalian cells induced by expression of a modified form of an actin-crosslinking protein. *J Cell Sci* **115**, 1939-1949.

Matsudaira, P. (1991). Modular organization of actin crosslinking proteins. *Trends Biochem Sci* **16**, 87-92.

Matthews, B. W. (1968). Solvent content of protein crystals. *Journal of molecular biology* **33**, 491-497.

McCoy, A. J., Grosse-Kunstleve, R. W., Adams, P. D., Winn, M. D., Storoni, L. C. and Read, R. J. (2007). Phaser crystallographic software. *J Appl Crystallogr* **40**, 658-674.

McGough, A. (1998). F-actin-binding proteins. *Curr Opin Struct Biol* **8**, 166-176.

McKay, R. T., Saltibus, L. F., Li, M. X. and Sykes, B. D. (2000). Energetics of the induced structural change in a Ca^{2+} regulatory protein: Ca^{2+} and troponin I peptide binding to the E41A mutant of the N-domain of skeletal troponin C. *Biochemistry* **39**, 12731-12738.

McRobbie, S. J. and Newell, P. C. (1985). Effects of cytochalasin B on cell movements and chemoattractant-elicited actin changes of *Dictyostelium*. *Exp Cell Res* **160**, 275-286.

Mejean, C., Lebart, M. C., Boyer, M., Roustan, C. and Benyamin, Y. (1992). Localization and identification of actin structures involved in the filamin-actin interaction. *Eur J Biochem* **209**, 555-562.

Meyer, R. K. and Aebi, U. (1990). Bundling of actin filaments by alpha-actinin depends on its molecular length. *The Journal of cell biology* **110**, 2013-2024.

Mimura, N. and Asano, A. (1987). Further characterization of a conserved actin-binding 27-kDa fragment of actinogelin and alpha-actinins and mapping of their

binding sites on the actin molecule by chemical cross-linking. *J Biol Chem* **262**, 4717-4723.

Muller-Taubenberger, A., Kortholt, A. and Eichinger, L. (2013). Simple system--substantial share: the use of *Dictyostelium* in cell biology and molecular medicine. *Eur J Cell Biol* **92**, 45-53.

Murakami, K., Yasunaga, T., Noguchi, T. Q., Gomibuchi, Y., Ngo, K. X., Uyeda, T. Q. and Wakabayashi, T. (2010). Structural basis for actin assembly, activation of ATP hydrolysis, and delayed phosphate release. *Cell* **143**, 275-287.

Murshudov, G. N., Skubak, P., Lebedev, A. A., Pannu, N. S., Steiner, R. A., Nicholls, R. A., Winn, M. D., Long, F. and Vagin, A. A. (2011). REFMAC5 for the refinement of macromolecular crystal structures. *Acta Crystallogr D Biol Crystallogr* **67**, 355-367.

Muthu, M., Richardson, K. A. and Sutherland-Smith, A. J. (2012). The crystal structures of dystrophin and utrophin spectrin repeats: implications for domain boundaries. *PLoS One* **7**, e40066.

Noegel, A. A., Leiting, B., Witke, W., Gurniak, C., Harloff, C., Hartmann, H., Wiesmuller, E. and Schleicher, M. (1989). Biological roles of actin-binding proteins in *Dictyostelium discoideum* examined using genetic techniques. *Cell Motil Cytoskeleton* **14**, 69-74.

Noegel, A. A. and Luna, J. E. (1995). The *Dictyostelium* cytoskeleton. *Experientia* **51**, 1135-1143.

Noegel, A., Witke, W. and Schleicher, M. (1987). Calcium-sensitive non-muscle alpha-actinin contains EF-hand structures and highly conserved regions. *FEBS Lett* **221**, 391-396.

Otey, C. A. and Carpen, O. (2004). α-actinin revisited: A fresh look at an old player. *Cell motility and the cytoskeleton* **58**, 104-111.

Otto, G. P. and Kessin, R. H. (2001). The intriguing biology of *Dictyostelium discoideum*. Meeting report: International *Dictyostelium* Conference 2001. *Protist* **152**, 243-248.

Otwinowski, Z. and Minor, W. (1997). Processing of X-ray diffraction data collected in oscillation mode. *Macromolecular Crystallography, Pt A* **276**, 307-326.

Pang, K. M., Lynes, M. A. and Knecht, D. A. (1999). Variables controlling the expression level of exogenous genes in *Dictyostelium*. *Plasmid* **41**, 187-197.

Pikzack, C., Prassler, J., Furukawa, R., Fechheimer, M. and Rivero, F. (2005). Role of calcium-dependent actin-bundling proteins: characterization of *Dictyostelium* mutants lacking fimbrin and the 34-kilodalton protein. *Cell Motil Cytoskeleton* **62**, 210-231.

Podolski, J. L. and Steck, T. L. (1990). Length distribution of F-actin in *Dictyostelium discoideum*. *J Biol Chem* **265**, 1312-1318.

Pollard, T. D., Almo, S., Quirk, S., Vinson, V. and Lattman, E. E. (1994). Structure of actin binding proteins: insights about function at atomic resolution. *Annu Rev Cell Biol* **10**, 207-249.

Pollard, T. D. and Cooper, J. A. (1986). Actin and actin-binding proteins. A critical evaluation of mechanisms and functions. *Annu Rev Biochem* **55**, 987-1035.

Pollard, T. D. and Cooper, J. A. (2009). Actin, a central player in cell shape and movement. *Science* **326**, 1208-1212.

Ponte, E., Rivero, F., Fechheimer, M., Noegel, A. and Bozzaro, S. (2000). Severe developmental defects in *Dictyostelium* null mutants for actin-binding proteins. *Mech Dev* **91**, 153-161.

Prassler, J., Stocker, S., Marriott, G., Heidecker, M., Kellermann, J. and Gerisch, G. (1997). Interaction of a *Dictyostelium* member of the plastin/fimbrin family with actin filaments and actin-myosin complexes. *Mol Biol Cell* **8**, 83-95.

Ramagopal, U. A., Dauter, M. and Dauter, Z. (2003). SAD manganese in two crystal forms of glucose isomerase. *Acta Crystallogr D Biol Crystallogr* **59**, 868-875.

Raper, K. B. (1935). *Dictyostelium discoideum*, a new species of slime mold from decaying forest leaves. *J. Agr. Res* **50**, 135-147.

Rivero, F., Albrecht, R., Dislich, H., Bracco, E., Graciotti, L., Bozzaro, S. and Noegel, A. A. (1999). RacF1, a novel member of the Rho protein family in *Dictyostelium discoideum*, associates transiently with cell contact areas, macropinosomes, and phagosomes. *Mol Biol Cell* **10**, 1205-1219.

Rivero, F., Furukawa, R., Fechheimer, M. and Noegel, A. A. (1999). Three actin cross-linking proteins, the 34 kDa actin-bundling protein, alpha-actinin and gelation factor (ABP-120), have both unique and redundant roles in the growth and development of Dictyostelium. *J Cell Sci* **112 (Pt 16)**, 2737-2751.

Rivero, F., Furukawa, R., Noegel, A. A. and Fechheimer, M. (1996). *Dictyostelium discoideum* cells lacking the 34,000-dalton actin-binding protein can grow, locomote, and develop, but exhibit defects in regulation of cell structure and movement: a case of partial redundancy. *J Cell Biol* **135**, 965-980.

Rivero, F., Koppel, B., Peracino, B., Bozzaro, S., Siegert, F., Weijer, C. J., Schleicher, M., Albrecht, R. and Noegel, A. A. (1996). The role of the cortical cytoskeleton: F-actin crosslinking proteins protect against osmotic stress, ensure cell size, cell shape and motility, and contribute to phagocytosis and development. *J Cell Sci* **109 (Pt 11)**, 2679-2691.

Rivero, F., Kuspa, A., Brokamp, R., Matzner, M. and Noegel, A. A. (1998). Interaptin, an actin-binding protein of the alpha-actinin superfamily in *Dictyostelium discoideum*, is developmentally and cAMP-regulated and associates with intracellular membrane compartments. *J Cell Biol* **142**, 735-750.

Roeser, D., Dickmanns, A., Gasow, K. and Rudolph, M. G. (2005). *De novo* calcium/sulfur SAD phasing of the human formylglycine-generating enzyme using

in-house data. *Acta Crystallogr D Biol Crystallogr* **61**, 1057-1066.

Root, P. A., Prince, A. and Gundersen, R. E. (1999). Aggregation of *Dictyostelium discoideum* is dependent on myristoylation and membrane localization of the G protein alpha-subunit, G alpha 2. *J Cell Biochem* **74**, 301-311.

Rybakova, I. N. and Ervasti, J. M. (2005). Identification of spectrin-like repeats required for high affinity utrophin-actin interaction. *Journal of Biological Chemistry* **280**, 23018-23023.

Sambrook, J. and Gething, M. J. (1989). Protein structure. Chaperones, paperones. *Nature* **342**, 224-225.

Saran, S., Meima, M. E., Alvarez-Curto, E., Weening, K. E., Rozen, D. E. and Schaap, P. (2002). cAMP signaling in *Dictyostelium*. Complexity of cAMP synthesis, degradation and detection. *J Muscle Res Cell Motil* **23**, 793-802.

Schlatterer, C., Knoll, G. and Malchow, D. (1992). Intracellular calcium during chemotaxis of *Dictyostelium discoideum*: a new fura-2 derivative avoids sequestration of the indicator and allows long-term calcium measurements. *Eur J Cell Biol* **58**, 172-181.

Schleicher, M. and Noegel, A. A. (1992). Dynamics of the *Dictyostelium* cytoskeleton during chemotaxis. *New Biol* **4**, 461-472.

Schleicher, M., Noegel, A., Schwarz, T., Wallraff, E., Brink, M., Faix, J., Gerisch, G. and Isenberg, G. (1988). A *Dictyostelium* mutant with severe defects in alpha-actinin: its characterization using cDNA probes and monoclonal antibodies. *J Cell Sci* **90 (Pt 1)**, 59-71.

Schneidman-Duhovny, D., Inbar, Y., Nussinov, R. and Wolfson, H. J. (2005). PatchDock and SymmDock: servers for rigid and symmetric docking. *Nucleic Acids Res* **33**, W363-367.

Senguen, F. T. and Grabarek, Z. (2012). X-ray structures of magnesium and

manganese complexes with the N-terminal domain of calmodulin: insights into the mechanism and specificity of metal ion binding to an EF-hand. *Biochemistry* **51**, 6182-6194.

Sheldrick, G. M. (2010). Experimental phasing with SHELXC/D/E: combining chain tracing with density modification. *Acta Crystallographica Section D: Biological Crystallography* **66**, 479-485.

Shu, S., Liu, X., Kriebel, P. W., Daniels, M. P. and Korn, E. D. (2012). Actin cross-linking proteins cortexillin I and II are required for cAMP signaling during *Dictyostelium* chemotaxis and development. *Molecular biology of the cell* **23**, 390-400.

Sjöblom, B., Salmazo, A. and Djinović-Carugo, K. (2008). α-Actinin structure and regulation. *Cellular and molecular life sciences* **65**, 2688-2701.

Soll, D. R., Yarger, J. and Mirick, M. (1976). Stationary phase and the cell cycle of *Dictyostelium discoideum* in liquid nutrient medium. *Journal of cell science* **20**, 513-523.

Song, J. G., Kostan, J., Drepper, F., Knapp, B., de Almeida Ribeiro, E., Jr., Konarev, P. V., Grishkovskaya, I., Wiche, G., Gregor, M., Svergun, D. I., Warscheid, B. and Djinovic-Carugo, K. (2015). Structural insights into Ca2+-calmodulin regulation of Plectin 1a-integrin beta4 interaction in hemidesmosomes. *Structure* **23**, 558-570.

Stendahl, O. I., Hartwig, J. H., Brotschi, E. A. and Stossel, T. P. (1980). Distribution of actin-binding protein and myosin in macrophages during spreading and phagocytosis. *J Cell Biol* **84**, 215-224.

Stossel, T. P., Chaponnier, C., Ezzell, R. M., Hartwig, J. H., Janmey, P. A., Kwiatkowski, D. J., Lind, S. E., Smith, D. B., Southwick, F. S., Yin, H. L. and Zaner, K. S. (1985). Nonmuscle actin-binding proteins. *Annu Rev Cell Biol* **1**, 353-402.

Stossel, T. P., Condeelis, J., Cooley, L., Hartwig, J. H., Noegel, A., Schleicher, M. and Shapiro, S. S. (2001). Filamins as integrators of cell mechanics and signalling. *Nat Rev Mol Cell Biol* **2**, 138-145.

Studier, F. W. (1991). Use of bacteriophage T7 lysozyme to improve an inducible T7 expression system. *Journal of Molecular Biology* **219**, 37-44.

Sucgang, R., Kuo, A., Tian, X., Salerno, W., Parikh, A., Feasley, C. L., Dalin, E., Tu, H., Huang, E., Barry, K., Lindquist, E., Shapiro, H., Bruce, D., Schmutz, J., Salamov, A., Fey, P., Gaudet, P., Anjard, C., Babu, M. M., Basu, S., Bushmanova, Y., van der Wel, H., Katoh-Kurasawa, M., Dinh, C., Coutinho, P. M., Saito, T., Elias, M., Schaap, P., Kay, R. R., Henrissat, B., Eichinger, L., Rivero, F., Putnam, N. H., West, C. M., Loomis, W. F., Chisholm, R. L., Shaulsky, G., Strassmann, J. E., Queller, D. C., Kuspa, A. and Grigoriev, I. V. (2011). Comparative genomics of the social amoebae *Dictyostelium discoideum* and *Dictyostelium purpureum*. *Genome Biol* **12**, R20.

Sussman, M. (1987). Cultivation and synchronous morphogenesis of *Dictyostelium* under controlled experimental conditions. *Methods in cell biology* **28**, 9.

Terwilliger, T. C. (2002). Automated structure solution, density modification and model building. *Acta Crystallogr D Biol Crystallogr* **58**, 1937-1940.

Terwilliger, T. C., Adams, P. D., Read, R. J., McCoy, A. J., Moriarty, N. W., Grosse-Kunstleve, R. W., Afonine, P. V., Zwart, P. H. and Hung, L. W. (2009). Decision-making in structure solution using Bayesian estimates of map quality: the PHENIX AutoSol wizard. *Acta Crystallogr D Biol Crystallogr* **65**, 582-601.

Titus, M. A., Warrick, H. M. and Spudich, J. A. (1989). Multiple actin-based motor genes in *Dictyostelium*. *Cell Regul* **1**, 55-63.

Van Driessche, N., Shaw, C., Katoh, M., Morio, T., Sucgang, R., Ibarra, M., Kuwayama, H., Saito, T., Urushihara, H., Maeda, M., Takeuchi, I., Ochiai, H., Eaton, W., Tollett, J., Halter, J., Kuspa, A., Tanaka, Y. and Shaulsky, G. (2002). A transcriptional profile of multicellular development in *Dictyostelium discoideum*.

Development **129**, 1543-1552.

Vandekerckhove, J. and Vancompernolle, K. (1992). Structural relationships of actin-binding proteins. *Curr Opin Cell Biol* **4**, 36-42.

Vijay-Kumar, S. and Cook, W. J. (1992). Structure of a sarcoplasmic calcium-binding protein from *Nereis diversicolor* refined at 2· 0 Å resolution. *Journal of molecular biology* **224**, 413-426.

Virel, A. and Backman, L. (2007). A comparative and phylogenetic analysis of the α-actinin rod domain. *Molecular biology and evolution* **24**, 2254-2265.

Volkmann, N., DeRosier, D., Matsudaira, P. and Hanein, D. (2001). An atomic model of actin filaments cross-linked by fimbrin and its implications for bundle assembly and function. *The Journal of cell biology* **153**, 947-956.

Wang, Z., Morris, J. C., Drew, M. E. and Englund, P. T. (2000). Inhibition of *Trypanosoma brucei* gene expression by RNA interference using an integratable vector with opposing T7 promoters. *Journal of Biological Chemistry* **275**, 40174-40179.

Winder, S. J. (2003). Structural insights into actin-binding, branching and bundling proteins. *Curr Opin Cell Biol* **15**, 14-22.

Witke, W., Hofmann, A., Koppel, B., Schleicher, M. and Noegel, A. A. (1993). The Ca^{2+}-binding domains in non-muscle type alpha-actinin: biochemical and genetic analysis. *J Cell Biol* **121**, 599-606.

Witke, W., Schleicher, M. and Noegel, A. A. (1992). Redundancy in the microfilament system: abnormal development of *Dictyostelium* cells lacking two F-actin cross-linking proteins. *Cell* **68**, 53-62.

국문초록

*Dictyostelium discoideum*의 34 kDa 액틴 결합 단백질인 ABP34는 칼슘에 의해 조절되는 액틴 결합 단백질 중에 하나로 낮은 농도의 칼슘이온에서 액틴 미세섬유를 다발로 형성하는데 관여한다. *Dictyostelium* amoeba에서 ABP34 단백질은 주로 filopodia에서 액틴 미세섬유의 다발을 형성 하는데 역할을 한다. *D. discoideum* 에서 이 액틴 다발형성 단백질의 세포 내 기능을 알아 보기 위해 RNA 저해 (ABP34 RNAi) 균주를 제작 하였다. ABP34 RNAi 균주는 느리게 성장하였고 세포 크기도 감소되어 있음을 확인하였다. 분화 과정 동안에는 분화 속도가 빠르게 진행되었고 결실체의 크기 또한 작아져 있었다. 어두운 상태에서 분화를 하였을 때에도 짧은 slug 기간을 보였고 결실체를 빠르게 형성하였다. ABP34를 형광현미경으로 관찰한 결과 세포 성장과 분화 과정 동안 액틴 세포골격에 결합 되어 있음을 알 수 있었다.

ABP34의 특성을 이해하기 위해 *Escherichia coli*에서 재조합 단백질을 대량 발현하여 분리하였고 결정화 하였다. Gel filtration 크로마토그래피로 ABP34가 용액 상태에서 단일체의 구조로 존재하는 것을 확인하였고 분자량은 32,836 Da 으로 측정되었다. X-선 회절을 이용하여 칼슘 이온이 결합 되어있는 1.89 Å 해상도의 결정 구조를 밝혔고 또한 이 단백질이 액틴 미세섬유와 결합하여 액틴 다발을 형성하는 활성을 가지는 것을 확인하였다. 처음으로 밝혀진 ABP34의 구조는 전체적으로 두 domain의 구조로 칼슘이 결합하는 N-domain과 액틴 결합에 관여하는 C-domain으로 이루어져 있었다. N-domain의 EF-hand는 전하를

띄는 아미노산 잔기에 칼슘이 결합되어 있다. C-domain의 세개의 나선은 다발 모양으로 몇개의 밝혀진 세포골격을 구성하는 단백질들의 일부와 닮은 구조임을 알 수 있었다. 이 C-domain 중에 가장 강한 액틴 결합부위(193-254)의 일부인 216-244 아미노산 잔기는 액틴 결합 단백질인 α-actinin 과 ABP120의 액틴 결합부위와 함께 보존된 서열을 가지고 있다. ABP34의 C-domain의 구조를 통해서 소수성 아미노산과 양전하를 띄는 아미노산으로 이루어진 액틴 결합부위에 해당하는 부분이 표면에 노출되어 있음을 알 수 있었다. C-domain의 보존된 216-244 아미노산 잔기는 액틴의 subdomain 1 과 subdomain 2 사이에 소수성 상호작용을 통해 액틴의 측면에 결합할 것임을 F-액틴과 모델을 통해서 가능성을 제시 하였다. 따라서 C-domain의 구조는 액틴 결합에 중요한 구조라고 생각된다. 또한 ABP34에 칼슘이 결합되어있는 EF-hand와 F-액틴의 결합부위가 있는 C-domain이 두 domain 사이에 상호 작용을 통해 액틴에 결합할 것을 예측하였다. 따라서 이 ABP34의 구조는 세포골격 단백질 구조 중에서 새로운 형태임을 밝혔고 이것은 액틴 결합을 통해 다발형성을 연구하는데 있어 가치있는 구조적 관점을 제공할 것이다. 또한 이 연구를 통해 *Dictyostelium* 액틴 다발형성 단백질 ABP34가 성장과 분화 과정 동안 액틴 미세섬유와 결합하여 기능을 하고 특히 slug의 이동에서부터 결실체를 형성하기까지 액틴 다발형성을 통해 세포골격 형성에 중요한 역할을 할것으로 생각된다.

주요어: ABP34, 액틴 다발형성 단백질, X-ray 결정 구조, EF-hand, RNAi, *Dictyostelium discoideum*